2009 (Heisei 21)

Doctoral Thesis

MINIATURIZED PIEZOELECTRICALLY DRIVEN UNCONSTRAINED VALVES FOR ROBOTIC APPLICATIONS

Ritsumeikan University Graduate School of

Science and Engineering

Doctoral Program in Science and Engineering

Department of Robotics

JIEN SUMADI

ABSTRACT

MINIATURIZED PIEZOELECTRICALLY DRIVEN

UNCONSTRAINED VALVES FOR ROBOTIC APPLICATIONS

JIEN SUMADI

Advisor: Prof. SHINICHI HIRAI

Pneumatic actuators have many promising features that make them attractive for robotic use, including light in weight and having high compliance and force-to-weight ratio. The growing demand for an increased power-to-weight ratio in pneumatic robots drives trends in miniaturization in component production. These trends have been hindered by the lack of ultra-precision assembly and the limited availability of mini solenoid valves. An unconstrained valve driven by a piezoelectric actuator (PEA) is thus proposed for its simplicity and high miniaturization potential. In this thesis, the realization of miniaturized unconstrained valves is discussed, which covers valve design towards miniaturization and implementation in robotics. The miniaturization design of a pneumatic valve with unconstrained poppet - orifice mechanism was considered as an advantageous breakthrough to eliminate the assembling complexity and to avoid the effect of positioning distortion due to temperature changes. Firstly, we presented an analysis and simulation model of an unconstrained poppet valve, which includes the mechatronic part of a PEA, Hertzian model, dynamics of poppet motion, and airflow through an orifice. An overall valve model based on the dynamics of a bouncing poppet were built and verified experimentally for valves with different piezoelectric dimensions. Secondly, we studied individual design parameters in detail referencing experimental results. The simulation model can therefore be used to understand the behavior of unconstrained poppet valves. Flow generation drops together with valve miniaturization, illustrating the tradeoff between output flow and size limitations. The energy conversion inefficiency in PEA is improved by using an LC tuner with 400% increase over the conventional approaches. Thirdly, using unconstrained valves for pneumatic control has the advantage over solenoid on-off valves of compactness made possible by the unconstrained structure and PEA use, enabling inherent PCM-emulation. Application tests of pressure control for artificial muscle and speed control for pneumatic cylinder were verified by experiments.

Acknowledgments

With a deep gratitude, I would like to thank Prof. Shinichi Hirai for his supervision of my doctoral work and motivation throughout scientific journals and international conferences in addition to all the other help he has given me during my time at Ritsumeikan University. He helped rearrange many of the ideas presented here, and meticulously corrected my writing and gave constant encouragement. In particular, thanks are due to Prof. Sadao Kawamura, who gave useful criticism and advice on the control of pneumatic actuators. Ms. Mari Hatanaka helped secure the funding for conferences and dealt extremely efficiently with the administrative side throughout my study period.

My sincere gratitude are due to Prof. Tohru Watanabe for his constant supervision and advice throughout Master and Doctoral course study. He has been contributing much in securing employment, industry-related projects, and financial support. He shared a lot of tutors and discussions on electromagnetic motors and control.

I would also like to thank the members of Machining Center, MEMS Micro Center, and Sugiyama Laboratory. They have been a great partner to work with and I wish to thank them all for their help and advice building our miniaturized valves.

This thesis is based on three years of research funded by Toray Engineering, Co., Ltd. During the course of the research I have been helped by many individuals and I would like to especially thank Kenshin Honda for his generous donations of assistance.

My sincere thanks are due to the official referees, Prof. Sadao Kawamura, and Prof. Toshiyuki Toriyama, for their detailed review, constructive criticism and excellent advice during the preparation of this thesis.

Lastly, I would like to thank all my friends in Hirai Laboratory, especially Zhongkui Wang, Yujiro Yamazaki and Kazuki Namima, who have been there for me and made my life more colorful. Also sincere thanks to my fellow research buddy, Hiroshi Takayama, Yoichiro Ogawa, Masahiko Ito, and Masayuki Tatsumi, for their inspiration, support, and great help with the experimental works.

Contents

List of Figures

List of Tables

Nomenclature

α	Multiplier for valve charging / discharge process (α taken as 1 while discharging for isothermal, and $\alpha = \beta$ for adiabatic charging process)
β	Ratio of discharge time divided by the charging time
$\triangle\tau$	Infinitesimally short time of instantaneous impact
$\ddot{\delta}$	Acceleration of penetration
δ_{max}	Maximum indentation
ΔQ	Change in internal energy
Δt	One sampling period
ΔU_{PI}	Magnitude of input to a closed-loop digital PI control
δ	Penetration between a poppet and a piezoelectric actuator
$\dot{\delta}$	Indentation rate
$\dot{\delta}_0$	Initial rate of indentation
$\dot{q}$	Total current flowing into piezoelectric actuator
$\dot{q}_p$	Current transduced from the mechanical side as a result of interaction with the externally applied load
$\dot{y}$	Elongation rate of piezoelectric actuator
$\dot{m}_1$	Air mass flow at the valve inlet
$\dot{m}_2$	Valve outlet mass flow from the orifice
$\dot{q}$	Total current flow through piezoelectric actuator
ϵ_{33}^T	Dielectric constant of piezoelectric actuator
η	Viscosity of piezoelectric actuator

κ	Specific heat ratio ($\kappa = 1.4$ for air)
μ	Hysteresis damping coefficient
μ_0	Magnetic permeability of a solenoid
ν	Poisson's ratio of valve base resembling a diaphragm
ω	Angular driving frequency ($\omega = 2\pi f$)
$\overline{u}_f$	Fluid velocity
$\overline{u}_p$	Poppet velocity under pressure drag
ρ	Mass density of piezoelectric actuator
ρ_f	Fluid density
ρ_{air}	Mass density of air
τ	Valve response time
υ_p	Poisson's ratio of piezoelectric actuator
υ_s	Poisson's ratio of poppet
A	Cross-sectional area of piezoelectric actuator (or a single electrode surface area)
a	Distance from the projection of the poppet centerpoint at the initial condition to a point on the orifice plate
A_{12}	Cross-sectional area of air supply inlet to pneumatic cylinder
A_{23}	Cross-sectional area of cylinder exhaust port
A_{eff}	Effective valve area
A_{max}	Fully opened valve area (maximum opening area)
A_o	Partially opened valve area
A_{p2}	Cross-sectional area of pneumatic cylinder
a_p	Acceleration of piezoelectric actuator
b	Aperture between the poppet and orifice plate
C	Total capacitance of multi-layered piezoelectric actuator

c	Distance from the center of poppet to the edge of orifice
C_D	Drag coefficient
C_d	Discharge coefficient of unconstrained valve
c_o	Initial values of damping
c_{poff}	Incremental constant of damping related to pressure changes
c_p	Damping coefficient of piezoelectric actuator
c_t	Total damping of unconstrained valve (PEA & valve body)
c_{voff}	Incremental constant of damping related to voltage changes
cu	Velocity-dependent damping force of pneumatic cylinder
d	Diameter of a solenoid
d_s	Distance between electrodes of a piezoelectric actuator
E	Elasticity modulus of piezoelectric actuator
e	Coefficient of restitution
E_b	Young's modulus of valve base
e_n	Tracking error at n sampling time
E_p	Young's modulus associated with piezoelectric actuator
E_s	Young's modulus associated with poppet
F	Average time required to fill or exhaust a constant volume V_h
f	Driving frequency of unconstrained valve
F_c	Penetrating contact force
F_{drag}	Pressure drag force
F_{dyn}	Dynamic force generated by piezoelectric actuator
F_e	Externally applied force to a piezoelectric actuator
f_f	Friction force working at pneumatic cylinder
F_{pc}	Load acting on pneumatic cylinder

F_p	Force internally generated from piezo effect
F_{sol}	Pulling force of a solenoid
F_{so}	Spring preload force of pneumatic cylinder
G	Mechanical operator that governs the mechanical relationship between F_p and y
g	Gravitational acceleration
h	Poppet bouncing height
I	Supply current to a solenoid
i	Average current flow through piezoelectric actuator
K	Coefficient that depends on material properties, Young's modulus and Poisson's ratio
k_0	Initial values of stiffness
k_{poff}	Incremental constant of stiffness related to pressure changes
K_p	Proportional gain
k_p	Stiffness of piezoelectric actuator
k_t	Total stiffness of unconstrained valve (PEA & valve body)
k_{valve}	Valve constant
k_{voff}	Incremental constant of stiffness related to voltage changes
L	Length of piezoelectric actuator
L_{coil}	Inductance of external coil connected in series with a piezoelectric actuator
m_{eff}	Effective piezoelectric actuator mass
m_p	Mass of piezoelectric actuator
m_s	Mass of poppet
m_t	Total mass of unconstrained valve (PEA & valve body)
N	Number of turns in a solenoid
p	Air pressure

p_0	Initial pressure value
P_1	Supply pressure to pneumatic cylinder
P_2	Pressure at the internal chamber of pneumatic cylinder
P_3	Ambient pressure surrounding pneumatic cylinder
P_{IN}	Input pressure to the valve
p_{in}	Upstream pressure
P_{OUT}	Valve outlet pressure
p_{out}	Downstream pressure
P_s	Pressure inside the valve body
Q	Flow rate output of an unconstrained valve
q_p	Charge transduced from the mechanical side of piezoelectric actuator
R	Molar gas constant ($R = 0.287$ kJ/kgK)
R_b	Distance from the center of valve base to the edge
r_i	Radius of the circle of poppet intersection with the orifice plate
r_o	Radius of orifice
r_s	Radius of poppet
T	Ambient room temperature
t	Time elapsed
T_1	Ambient temperature outside pneumatic cylinder
T_2	Temperature at internal cylinder chamber
t_b	Valve base thickness
T_{em}	Transformer ratio of piezoelectric transducer
T_i	Integral gain
u_2	Velocity of cylinder rod
U_{p-p}	Peak-to-peak voltage applied to piezoelectric actuator

V_h Hollow valve volume

V_{IN} Input voltage to a piezoelectric actuator

$V_p^{(-)}$ Approach velocity of piezoelectric actuator before impact

$V_s^{(+)}$ Velocity of poppet after impact

$V_s^{(-)}$ Approach velocity of poppet before impact

W_{12} Supply weight flow rate to the cylinder

W_{23} Exhaust weight flow rate from the cylinder

w_o Estimated displacement amplification of valve base

W_s Poppet weight

X Displacement of pneumatic cylinder

Y Admittance of a piezoelectric actuator

y Internal stroke of piezoelectric actuator

Z Total impedance of piezoelectric actuator

z Pressure drop ratio ($z = p_{out}/p_{in}$)

Z_c Impedance of the non-resonant part of a piezoelectric actuator

Z_r Impedance of the resonant part of a piezoelectric actuator

Chapter 1

Introduction

1.1 Pneumatic Actuation in Mechatronics

Pneumatic actuator has found its applications in mechatronics more recently [1], such as pneumatic nutation motors, a micro pneumatic tube actuator for assisting colonscope insertion, a pneumatic rubber actuator for compliant robots, and an intelligent pneumatic cylinder. In robotic fields there is a recent trend towards building human motion support systems to assist the physically disabled during rehabilitation and for exercises [2, 3, 4]. These mechanical systems are generally known as so-called wearable robots which demand a high power to weight ratio to be fairly light when attached to human. The actuators for this type of machine have to be elastic, flexible for human to be able to move easily and more importantly safe. Suitable candidates for this human support system are pneumatic actuators like the McKibben actuator [5], the bellows manipulator [6], the pneumatic balloon [7], and Hexahedron Rubber Actuators [8].

Wearable robots or robotic manipulators are currently deployed in proximity with humans, where the interaction between human and robot must be inherently safe. The safety issue primarily involves mitigating impact load from unexpected collisions between robot and human. Robots that employ compliant actuators are inherently safe since they do not produce the large impact loads associated with high impedance designs. Compliant manipulation requires the manipulator to have accurate position tracking and soft collision while making contact with an uncertain environment, whether the uncertainty is with regard to position of the constraint obstacles, or stiffness of the environment. Pneumatic actuators, by contrast, has natural impedances with mechanical compliance that make them attractive for compliant control, where force are controlled by manipulating the air pressure and compliance is provided by the compressibility of air [9].

Typical robot actuators such as hydraulic and electric motor that has

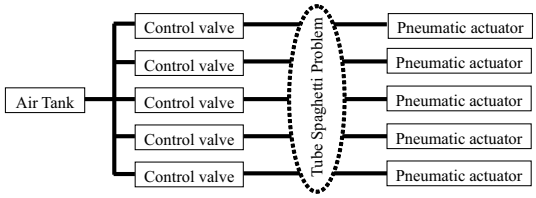

Figure 1.1: Tube spaghetii problem found in pneumatic actuators

high stiffness are suitable for tasks requiring high accuracy position control, as noted in [9]. The stiffness of an electric motor/gearhead combination is well-suited for accurate positioning tasks, however, it is a mismatch for kinematically constrained interaction tasks. For tasks requiring force control, such as interaction, it is logical to look to pneumatic actuators that are compliant. In terms of robot design, the heavy and bulky motors present practical challenges due to the low force-to-weight ratio of electrical motors, contributing to increase the weight and inertia of the system. Addressing these limitations, Shin, *et. al.* [10] replace the heavy electrical actuators with pneumatic actuators, which enable the system to be smaller and lighter.

The pneumatic wearable robot has an ever increasing number of pneumatic actuators and valves. The total system weight is strongly related to the weight of control valves since pneumatic actuators are relatively light. Because weight and size are essential aspects for safety in robot design, commercial pressure regulators, which are bulky and heavy, cannot be used because they will increase the inertia of the robots [10]. The pressure regulator can be located separately from the robots to improve the actuator performance, however, long tubes and fittings would be necessary. In particular, a long tube between the actuator and valve is impractical as it yields the "tube spaghetti problem" leading to the complexity of the design (Fig. 1.1). These two problems, valve weight and tube spaghetti, pose difficulties in constructing practical wearable robots. One method to alleviate these is to integrate the actuator with a miniaturized valve. An additional advantage of reducing the distance between actuator and valve is increased control response time.

In general, a pneumatic control valve comes complete with a sensor, control circuit, and an on-off operated mechanism. Major technological advances in the field of micro electro mechanical systems (MEMS) and large scale integration (LSI) brought new opportunities to miniaturize pneumatic valves through the development of a MEMS micro pressure sensor and microprocessor. Electrifying the pneumatic valve with microprocessors creates a digital valve that provides an interface between digital electronics and pneumatic systems. Unlike analog valves, a digital valve can operate

directly from microprocessor signals without the requirement for a built-in controller thus making the control valves compact. One challenge that remains now is lack of a smaller mechanical on-off latching structure.

The application of microprocessors to fluid power interface valves was first carried out more than two decades ago, and it was shown to provide a number of advantages for fluid power systems, except for the originally high cost of microprocessors [11]. Now, however, microprocessors have become cheap, and so all the benefits of microprocessors can be utilized for the development of electropneumatic valves. There is a great deal of interest in integrating the versatility of microprocessors into pneumatic valves along with the efforts to miniaturize valves. The work reported by Akagi and Dohta [12] with regard to small-sized multiport pressure control valves is an example. They built an additional interface to connect the controller unit with the valve arrays.

Commercially available pneumatic control valves can supply sufficient flow rate for a wearable robot to work properly, however, we are confounded by the dilemma of unacceptable weight that will be discussed in Section 1.2. This section presents an overview of the currently available conventional solenoid valves. Section 1.3 describes the contemporary microvalves produced by MEMS technology. Microvalves actually used to control micro pneumatic actuators [13, 14] are limited by a low output flow. Section 1.4 introduces a novel concept that has been proposed to make the best use of the limited capabilities of conventional machining to realize production of miniaturized valves by eliminating the constraints of the poppet valve, *i.e.*, the so-called unconstrained valves [15]. An unconstrained structure makes the valve assembly processes easier, making it practical for miniaturization to the micro scale. In-depth information about unconstrained valves will be covered throughout the rest of the sections.

1.2 Solenoid On-Off Valves

According to [16], pneumatic control valves have three major types, *i.e.*, pressure control valves, flow control valves, and directional control valves. Pressure control valves are required to reduce the pressure when it is too high for the operation involved, and to provide relatively constant pressure when the line pressure varies. Flow control valves are used to control the speed of a pneumatic cylinder, allowing free, full flow in one direction and an adjustable flow in the other direction. Directional control valves have a function to direct or prevent flow through selected passages, which are commonly available in spool, poppet, and disc types.

Research on pneumatic valves can be roughly classified into two groups, *i.e.*, development of precise position control of servo valves [17], and on-off

valves [18, 19]. They share the same purpose in application, *i.e.*, to enhance the control of the nonlinear dynamic behavior of overall pneumatic systems. Servo valves are expensive and their internal structures have a high degree of complexity. In contrast, pressure control using on-off valves is relatively inexpensive and has a higher frequency bandwidth than that using servo valves [19]. Thus, the decision of whether to use servo or on-off valves is made taking cost, size, and application requirements into consideration.

There are various methods of operating the wide variety of control valves, where the main valve actuation is called operators. Operators serve two major functions: to actuate a valve or return it to its normal position after it has been actuated. In general, valve operators are categorized as follows [16]:

- Manual operators : hand or foot.
- Mechanical operators : cam roller, link clevis, and mechanical lever.
- Solenoid operators: direct-acting and pilot-operated.
- Pilot operators: direct-pilot, low-pressure pilot, bleed-pilot, and differential-pilot.
- Return operators.

Most of the commercially available pneumatic valves are actuated by solenoids. A direct-acting solenoid is one which is directly connected to the valve, directly opening or closing the valve ports, depending on whether the solenoid id energized or de-energized. Valve operation is not dependent on the air pressure or flow rate. On the other hand, a pilot-operated solenoid is essentially a compact, direct-acting solenoid valve that controls a pilot air pressure in order to actuate a piston or diaphragm that mechanically opens or closes the valve. The pilot air may be obtained through an internal passage in the valve, or it may be supplied from an external source. In most cases, solenoids require high current to supply sufficient force to the valve especially for the direct-acting solenoids. The pulling force of a solenoid depends on several factors such as supply current, number of turns in the coil, and material of the core, as calculated by $F_{sol} = \mu_0 d N^2 I^2$. Despite difficulties in solenoid miniaturization, commercially available solenoid-actuated miniaturized valves have been developed [20], but further miniaturization to micro size has been quite difficult as the force generated by an electromagnetic actuator scales down at the cube of its length.

Because of the almost limitless variety of usages, space requirements and functions for pneumatic valves, there is no common method for their mounting. Two most common types are direct and sub-base mounting,

however, this does not infer limitations with respect to other possible designs and arrangement combinations for different mounting types. Valve mounting actually occupies a large portion of space compared to the valve itself, which is a common case in miniaturized valves. Direct mounting as an integral part of the valve body and the valve operating mechanism makes the valve more compact and low cost. Sub-base mounting is bulky and added valve cost, however, it permits the user to remove or replace the valve when required without disconnecting the tubing.

1.3 Microvalves

MEMS-based microvalves are roughly classified into two major categories: active and passive microvalves [21], as shown in Fig. 1.2. The active microvalves have three subgroups: (1) mechanical, (2) non-mechanical, and (3) external. Mechanical active microvalves are defined as valves that are accomplished using the MEMS-based bulk or surface micromachining technologies, where mechanically moveable membranes are coupled to magnetic, electric, piezoelectric, or thermal actuation methods. Non-mechanical active microvalves are valves that are operated by the use of smart materials. These non-mechanical active microvalves may hold movable membranes which are actuated due to their functionalized smart materials such as phase change or rheological materials. External active microvalves are valves actuated by the aid of external systems such as built-in modular or pneumatic means. In addition, passive microvalves are sometimes regarded as a part of micropumps.

Today, the robotics requirements for microfluidic systems continue to force an evolution and revolution in valve design for miniaturization. Smaller device size, higher pressures, biocompatibility, response, and the microtechnology are all contributing to the valve design in microscale. Since passive valves are not directly used for actuator control and are usually a part of micropumps, this thesis only lists the active microvalves categorized by their actuation principle as [21, 22]:

- Pneumatic microvalves
  Advantages : simple actuation concept.
  Disadvantages: not suitable for compact applications (need of an external pressure source) and slow response time.

- Thermopneumatic microvalves
  Disadvantages: complexity of using liquid for actuation that increases the cost and lowers the repeatability of the valve.

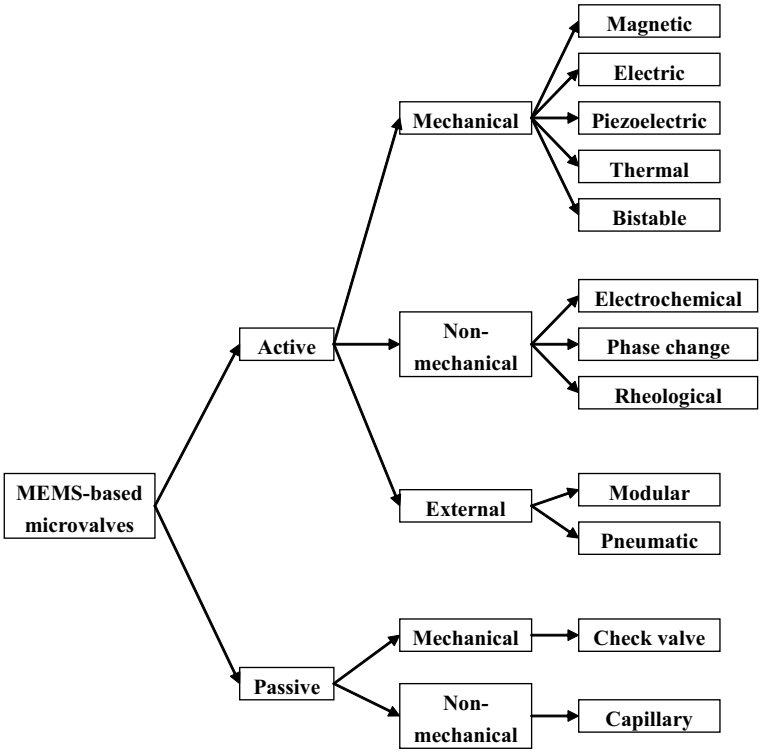

Figure 1.2: Classification of microvalves as defined in [21]

- Thermomechanical microvalves
  Advantages: high force and large stroke.
  Disadvantages: high power consumption and slow response.

- Piezoelectric microvalves
  Advantages: high speed, large force and commercial availability.
  Disadvantages: small displacement and high drive voltage.

- Electrostatic microvalves
  Advantages: fast response.
  Disadvantages: high drive voltage and small displacement.

- Electromagnetic microvalves
  Advantages: large deflection, can be integrated in silicon for compact design.
  Disadvantages: low efficiency due to heat loss in the coil.

- Electrochemical / chemical microvalves
  Advantages: suited for conventional microtechnologies such as photolithography, low operation voltage (power-saving applications).
  Disadvantages: swelling behavior and long response time.

- Capillary force microvalves
  Advantages: simple concept (no moving parts involved).
  Disadvantages: limited use for a check-valve and is not used directly in microvalves.

Based on the flow control methods, active microvalves are classified into two ways:

- Analog : in the analog or proportional mode, the valve actuator varies the gap between the valve seat and valve opening to change the flow rate.

- Digital : in the digital mode, the valve have two states: fully open and fully closed. A digital active microvalve can be driven in pulse-width-modulation (PWM) mode to achieve proportional flow control as in analog valves. In the PWM mode, the open time is controlled to vary the net flow proportional to the opening time.

According to [22], one of the key functional elements in an active microvalve is the actuator, where design and dimensioning of the actuator depends on the application requirements such as closing pressure or response time. Design of the valve spring and valve seat is important to allow the valve to have a leakage-free operation. Digital valves in the pulse-width-modulation mode can achieve the same performance as analog microvalves while they can minimize power consumption because the actuator is only needed for switching valve position. Microvalves with different actuation methods are compared in Table 1.1 for their maximum pressure, output flow, and power consumption. Since shape memory alloy (SMA) actuators have high force and large stroke, microvalves driven by a SMA actuator have the highest flow among the microvalves, followed by electromagnetic and thermopneumatic actuations. However, low operation bandwidth caused from the conversion of thermal energy and the large size are disadvantages of SMA actuators. In summary, the primary advantages of silicon microvalves over solenoid valves are order-of-magnitude decreases in both size and weight even though it is correlated to a drop in output flow.

Table 1.1: Microvalves with different actuation

Types of microvalves	Size (mm)	Max. Pressure (kPa)	Flow rate (mL/min)	Power
Electromagnetic [23]	10x10x4.33	200	2000	0.3 A
Piezoelectric [24]	13x13	50	70	300 V
Bimetallic [25]	23x17x0.6	1035	1000	1.03 W
Thermopneumatic [26]		207	1600	0.5 W
SMA [25]	13x51x33	550	6000	0.29 W
SMA [27]	3x3x5	250	360	0.22 W

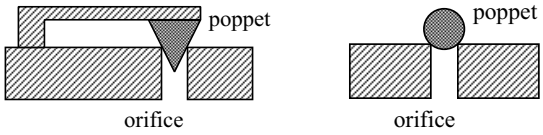

(a) Constrained valve (b) Unconstrained valve

Figure 1.3: Basic notion of an unconstrained valve

1.4 Unconstrained Valves

Most available commercial valves are of the constrained type, where accurate positioning of the poppet and valve seat is required to prevent leakage. Fig. 1.3(a) shows that a poppet constrained to a beam seats firmly on an orifice, requiring an absolute positioning accuracy of ≤ 100 μm. In microscale production, it becomes practically difficult to assemble such tiny parts to such extremely high precisions, ranging from 50 nm to 100 μm. In addition, any temperature change may strongly affect positioning distortion, especially for micro or miniaturized valves. One way to avoid those problems is to do away with the constraints, as shown in Fig. 1.3(b). In this thesis, we introduce an on-off control valve with vibrational actuation principle driven by a piezoelectric actuator where the poppet is structurally unconstrained [15]. The term "unconstrained valve" refers to a valve with no mechanical linkage between the poppet and valve seat. In principle, a valve with unconstrained structure is proposed in order to be miniaturized. A piezoelectric actuator was adopted because it has high flow power to weight ratios and a high potential to be downsized. In addition, the recent development of a robotic assistant system for use in high-field MRI scanners required fully MR-compatible operation [28]; the proposed piezoelectric valve is the valve of choice to fulfill the requirements of the MR-compatible controller.

1.4.1 Actuator Selection for Pneumatic Valves

Conventional pneumatic valves based on solenoid or mechanical actuation tends to be large and heavy. Smart actuators currently in use along with

Table 1.2: Comparison of smart actuators [29]

Material	Actuation	Advantages	Disadvantages
Piezoelectrics	Electric current	Fast response time	Low displacement
Electrostrictors	Electric current	Higher displacement	Non-linear response, high cost
Magnetostrictors	Magnetic/electric field		Magnetostriction
SMA	Temperature change	High strain response	Low response
Electroactive polymers	Electric field / pH change	A significant change in dimension or geometry	Requirement for electrolytic fluid
Electrorheological or magnetorheological fluids	Electric/magnetic field	Suitable for damping applications	

some new materials under research have become more popular for miniaturization for valve components due to their high power density, high efficiency, lightweight, and compactness [29]. Table 1.2 gives the list of major smart materials that have greater functionality and improved performance for the development of miniaturized valves.

In [30], it is considered that piezoelectricity, among the smart materials, is the best suited for valve miniaturization. PEAs can be generally divided into three types, *i.e.*, bender, bulk, and stack type. The bender type typically has large stroke and small force, whereas bulk type has higher output force but low amplification. A stacked-type PEA, however, can generate higher force and stroke compared to the bulk PEA although the elongation is about an order of tenth micrometers at maximum. Since both a large force and stroke are required for valve application, a stacked type PEA is considered the most suitable among the three types. Although there are many methods of stroke amplification had been proposed to amplify the output displacement mechanically, they are not appropriate for valve miniaturization due to space limitation.

Piezoelectrically driven pneumatic valves are compared in Table 1.3 between MEMS microvalves and unconstrained valves, which revealed that unconstrained valves have much higher output flow. MEMS microvalves are originally intended for dispensing micro fluidics, not for actuator control such as in robotics, with flow rate ranging from μL to mL. The disadvantage of piezoelectric actuation is the low displacement that consequently limits the output flow. Since the output flow is linearly proportional to input voltage, a high voltage is necessary in microvalves to obtain high output flow. The proposed unconstrained valves, in contrary, are driven by impact force from a PEA that realizes a periodic bouncing motion of the poppet to allow wider opening area of the orifice. This suggests that unconstrained poppet-orifice structure is indispensable for a piezoelectric valve to have a high output flow.

Table 1.3: Piezoelectrically driven pneumatic valves

Valves	Size (mm)	Pressure (kPa)	Flow Rate (L/min)	Power Consumption	Leakage	Number of ports
Unconstrained valves	10x20x21	0 - 500	10.5L/min@500kPa	900 mW	< 0.9L/min	3-way
Piezoelectric microvalves						
MCAs [31]	ϕ20x20	0 - 500	9.13sccm@500kPa	100 V	3.03e-8Pam^3/cm^2	2-way
Micro piezo [24]	13x13	0 - 50	70sccm@50kPa	100-200 V	unknown	2-way
Stack type PEA [32]	8x10x10	0 - 50	95μL/min@50kPa	100 V	unknown	2/3-way
Stack type PEA [33]	20x20x9	0 - 75	85mL/min@75kPa	100 V	0.1mL/min	2-way
Piezoelectric disc [34]	16x16x3	0 - 241	600mL/min@241kPa	unknown	low leak	2-way

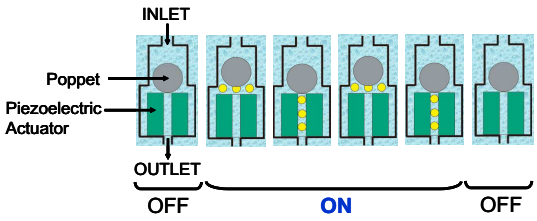

Figure 1.4: Unconstrained valve activated by vibration generated by a piezoelectric actuator for bounce

1.4.2 Operation of Piezoelectrically-driven Unconstrained Valves

Unconstrained valve refers to a valve whose poppet and valve seat are not mechanically linked. Because the poppet is unconstrained, the valve shuts off automatically when air pressure enters from the inlet port. Instead of a beam in a valve with constraints, air pressure securely positions the poppet over the orifice, closing the valve normally. The poppet seals the valve seat securely without exerting voltage. Even with the poppet and beam not linked, this alternative nonconstraint works well. Unconstrained valves use a PEA to generate vibration and a metal/glass ball blocking airflow. Preliminary vibration and impact effectively open an aperture between the poppet and orifice, with the PEA shooting the poppet off. Dynamic force from harmonic PEA movement impacts on the poppet, giving it the regular bounce, shown in Fig. 1.4. Based on the actuation principle, unconstrained valves have only on or off states thus it is classified as a digital valve. However, the frequency-control feature of an unconstrained valve can be used for flow control, making them a digital/analog converter valve.

1.4.3 Related Works

Different actuations of unconstrained valves have been investigated in several research works, such as PZT vibrator [35] and a vibration motor [12].

The purpose of both studies is to develop a lightweight and compact control valve that is useful for control of pneumatic actuators. Hirooka, *et. al* used their flow control valve for speed control to avoid the stopping shock of pneumatic cylinders at the stroke ends [35]. The report by Akagi, *et. al* shows that the tested valve is suitable as a wearable control valve because of their relatively large output flow with low weight / size [12]. In addition, the power consumption of the newly developed valve using vibration motor is reduced to approximately one half compared to the commercial valves.

The flow control valve in [35] consists of an orifice plate which has plural orifices and a PZT vibrator adhered on the orifice plate and metal particles. The orifice plate has about 10 to 20 orifices of 0.5 mm diameter. The valve is driven at resonance mode that can be used as a variable speed controller for pneumatic cylinders. The main moving part is the orifice plate, where the acceleration of the orifice parts is the most essential (Fig. 1.5(a)). This flow control valve works successfully at pressure up to 0.7 MPa and has a maximum flow rate of 61.45 L/min.

In [12], the valve consists of a vibration motor and a check valve made of a steel ball and an orifice inside a flexible tube. The valve is a normally closed valve similar to a check valve. As vibration is applied to the valve, the valve is activated as the steel ball moves away from the orifice. This type of valve is energized by forces working in horizontal direction (Fig. 1.5(b)), unlike the proposed unconstrained valve which is applied with impact force in vertical direction. It is said that this method is more effective because it is possible to open the valve with smaller force. The working principle of this valve is that when the vibration motor is rotating, the tube connected to the vibration motor is oscillated, making the ball rotate along the inner wall of the tube. If a continuous vibration is applied, the valve will generate a constant output flow. The valve prototype has maximum flow rate 9 L/min at 0.5 MPa. The total size of the tested valve is 20 mm in length, 5 mm in width, and 10 mm in height, with total mass of only 2 g.

1.5 Aim of The Thesis

The limitation for using pneumatic actuation in robotics is the weight and size of control valves, which need to be miniaturized. Although microvalves have been readily available and the current commercial solenoid valves are becoming more compact, there is still a gap between the two types of valves (Fig. 1.6). Microvalves are small but the flow rate is too low, while the commercially available solenoid valves have a high output flow but somewhat too large for use in robotics. This thesis focuses on the proposed unconstrained valves intended for miniaturization to achieve a valve with less weight/size and high output flow (Fig. 1.6). This thesis focuses on the

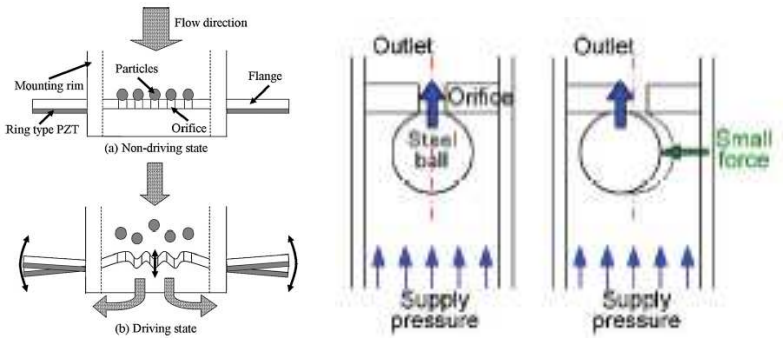

(a) (b)

Figure 1.5: Various concepts of unconstrained valves. (a) Working principle of flow control valve driven by PZT vibrator [35], and (b) Small-sized flexible control valve using vibration motor [12].

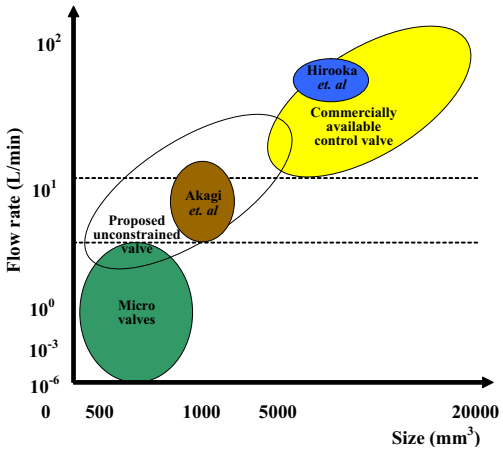

Figure 1.6: State-of-the-art pneumatic valves

study for the valve design with the main topics of analysis and simulation of unconstrained valves, selection of actuators, design of miniaturized unconstrained valves, and testing of unconstrained valves for applications in robotics. The current state-of-the-art smart materials have been implemented more widely than their conventional counterparts electric motors [29], as they have a high energy density, large bandwidth, simple packaging, lower maintenance costs, and improved system performance. This thesis particularly focuses on piezoelectricity for the feasibility of valve miniaturization.

The goal of this thesis is to study the unconstrained mechanism of pneumatic valves driven by piezoelectric actuators as an attempt to use smart material for miniaturization. This thesis particularly discusses the design parameters of an unconstrained valve towards miniaturization, modeling of

an overall unconstrained valve, and evaluation of the effectiveness of unconstrained valves for use in pneumatic control for robotics. The approaches we proceed with are to collect data for each design parameters from experimental tests, and to build an analytical model of unconstrained valves mainly based on the obtained data. The simulation model is then used to estimate the feasibility of miniaturization, attempting to predict the size limit for miniaturization. This work may thus serve as a general guide for miniaturizing unconstrained valve design. Finally, the miniaturized unconstrained valves is then implemented for the control of pneumatic actuators to test the valve performance in comparison to the standard solenoid valves, concluding the advantages and disadvantages of unconstrained valves.

1.6 Thesis Organization

Chapter 1 is the introduction to this thesis, and provides an overview of the background of this thesis. The research objective and thesis organization are also provided. Chapter 2 provides the experimental results and simulation model of an unconstrained valve. The valve input/output characteristics for each design parameter are described. Chapter 3 describes the valve design towards miniaturization. The selection of design parameters and flow tendency of a miniaturized unconstrained valve are summarized. Chapter 4 discusses the application features of unconstrained valves, comparing the size and control functions of conventional solenoid valves and unconstrained valves. Chapter 5 examines the current literature in the fields of pressure control for pneumatic robots. The motivation for this work is also presented. Chapter 6 examines the PCM-emulation control using unconstrained valves for speed control of pneumatic cylinders. A compact system using unconstrained valves in comparison to solenoid valves is detailed in this chapter. Chapter 7 states the conclusions drawn from our work and suggests possible directions for future research.

Chapter 2

Simulation Model of Unconstrained Pneumatic Valves

2.1 Introduction

There have been a number of technical papers regarding the development, modeling, and physical analysis of piezoelectrically driven micro valves. For example, a two-stage electrohydraulic servovalve with nozzle-flapper pilot system, controlled by stack-type piezoelectric elements, has been analyzed and experimentally tested [36]. In addition, a single-stage piezoelectric direct drive servovalve with higher bandwidth than conventional two-stage valves has been described [37], as has the design, simulation, and characterization of a bulk micromachined piezoelectric valve for fuel cell applications [38]. A pneumatic valve, consisting of a bimorph-type piezoelectric actuator, poppet valve, and pressure regulator, has been analyzed theoretically and experimentally [39], while a micromachined piezovalve using the buckling effect of silicon diaphragm for flow control system applications has been tested experimentally [31]. An active silicon microvalve with piezoelectric membrane actuators has been simulated and studied including the modeling and analysis of the deflection/pressure behavior of the membrane and flow through the valve [40]. A mathematical model of a pressure control servo valve system activated by a piezoactuator-driven flapper has been proposed [41]. The experimental results and flow characteristics of a pneumatic on-off control valve driven by impulse force of a multilayer PZT actuator has been described including the modeling and analysis of the motion of the snapped flapper and the hammering characteristics of the PZT actuator [42]. All of these valves have a constraint imposed on a poppet, as well as an orifice, therefore requiring tedious assembly for miniaturization. Herein, we pro-

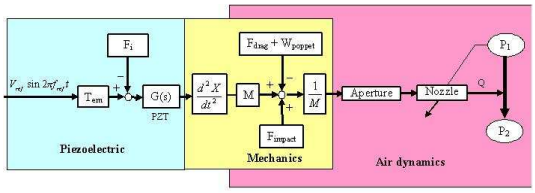

Figure 2.1: Dynamic model of unconstrained poppet valve

pose a piezoelectrically driven on-off poppet valve with an unconstrained structure to ease the valve assembling process, a valve especially designed for miniaturization.

This chapter describes the analysis and experimental testing of a piezoelectrically driven unconstrained pneumatic poppet valve for the study of miniaturization. A dynamic formulation based on mechatronics integration, involving piezoelectricity, pneumatics, and mechanical devices, is presented to explain the relationship between design parameters of the unconstrained valve and its performance.

2.2 Modeling of Unconstrained On-Off Valve

2.2.1 Overview of Unconstrained Valve Model

A nonlinear dynamic model of an unconstrained poppet valve can be formulated, considering its mechatronics structure and integration of piezoelectricity, pneumatic, and mechanical devices, using the notation shown in Fig. 2.1. The dynamic behavior of each internal device was modeled as necessary in order to obtain an acceptable valve model. This formulation was based on several physical parameters involving piezoelectric, mechanics and air dynamics, with assumption that the mechanical behavior is dominant than the pneumatic aspect. The detail about the overall valve model is based on the dynamics of a bouncing poppet that can be arranged as shown in Fig. 2.2. This dynamic model can be used to calculate the outlet flow rate of an unconstrained poppet valve, especially to predict the feasibility of miniaturization of an unconstrained poppet valve.

The inputs to the model are the input pressure P_{IN} and the harmonic waveform input signal with amplitude V_{IN} and frequency f, which correlate with the required flow rate output Q. The force F_p is the generated force from a piezoelectric actuator (PEA). The externally applied force to the PEA is represented as F_e, which has two components, the penetrating contact force F_c and the pressure drag force F_{drag}. The contact force is modeled by Hertzian contact, which directly affects the elongation of the PEA y. The Hertzian contact model is switched according to the prevailing

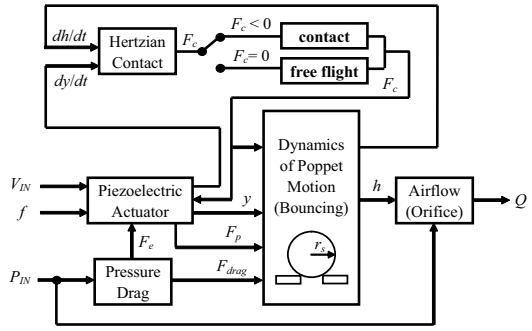

Figure 2.2: Block diagram of an unconstrained valve model

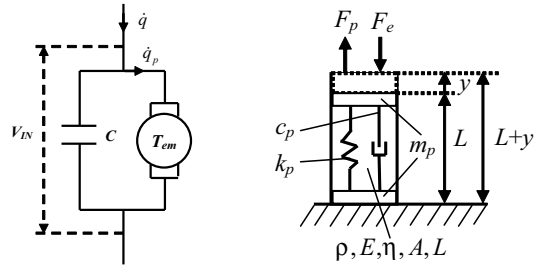

(a) Electrical domain (b) Mechanical interaction

Figure 2.3: Electromechanical model of a piezoelectric actuator

conditions of the contact or free flight state. Penetration between a poppet and a PEA is denoted as δ, such that $h = y + \delta$ represents the position of the poppet according to the dynamics of a bouncing ball.

The input parameters have to be selectively chosen beforehand, considering the flow rate output needed for the valve to perform on-off operations. In particular, this model serves to discern the tendency of the frequency/voltage/flow rate responses.

2.2.2 Model of PEA

In this section, the electrical and mechanical model of a PEA is described. PEAs are basically utilized for their piezo effects, in which electrical and mechanical domains are coupled. In natural piezoelectric materials, a hysteresis phenomenon exists between an electrical voltage and an electrical charge, which lies solely in the electrical domain. In this section, the PEA is modeled as a major mechanical part; for simplicity, the hysteresis model is omitted. Using only the electromechanical term and omitting the hysteresis part, the model of a PEA is illustrated in Fig. 2.3 [43].

The piezo effect or the efficiency of the electromechanical transducer is represented by the transformer ratio T_{em}. The current $\dot{q}_p$ is the current

transduced from the mechanical side as a result of interaction with the externally applied load. Let F_e be the external force counted as a load to the PEA. This external force includes air pressure p applied at the PEA cross sectional area and the contact force, which will be defined in the subsequent section.

Based on the assumptions that the PEA displacement is restricted to one-dimension and that pressure affects only the upper part of the poppet, the electromechanical equations for a simplified model of PEA are [43]:

$$y = G(F_p - F_e), \tag{2.2.1}$$

$$F_p = T_{em} V_{IN}. \tag{2.2.2}$$

Figure 2.3(b) shows that the mechanical domain of a PEA is modeled by mass-damper-spring system. In practice, the PEA is used as an actuator for a vibrational dynamic force generator. At one side, the PEA is clamped to a rigid base; at the other side, it receives external loads from the pressurized air and during contact with the poppet. Then mass m_p, damping coefficient c_p, and stiffness k_p can be calculated from the material and geometrical properties of a PEA as $m_p = \rho AL$, $k_p = EA/L$, and $c_p = \eta A/L$, respectively. The operator for the mechanical behavior of a PEA that relates its elongation and normal force, taking into account only the first peak resonance, is therefore [43]:

$$G(s) = \frac{N_p(s)}{D_p(s)}, \tag{2.2.3}$$

where

$$N_p(s) = \frac{m_p}{\pi^2} s^2 + c_p s + k_p, \tag{2.2.4}$$

$$D_p(s) = \frac{4m_p}{\pi^2} s^2 + c_p s + k_p. \tag{2.2.5}$$

Fig. 2.4 shows the characteristics of the PEA system when the values of mass, damping, and stiffness variables are doubled, which indicates that the displacement of a PEA is amplified for increased mass and stiffness, whereas an increase of damping value results in lowering the displacement amplitude. It can be observed that increasing the valve mass will have the resonant frequency shifted leftward, while it is contrary for the stiffness parameter.

2.2.3 Hertzian Contact Model

This simulation model uses Hertzian contact model [44] to describe the contact between a poppet and an orifice. In this model, we consider the

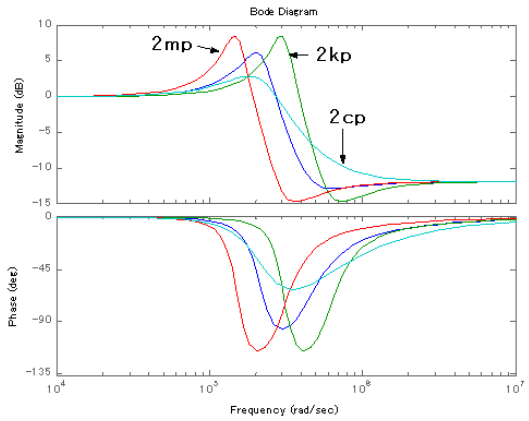

Figure 2.4: Characteristics of PEA system that is dependent on the mass, damping, and stiffness variables

contact between a poppet and a tubular PEA as a sphere acting on a flat plane. This assumption is fulfilled if the diameter of the orifice is not larger than 25% of the diameter of the poppet. The contact model is based on the Hertzian contact theory for a homogeneous, and frictionless elastic contact. It assumes that no external force is at work except for the contact forces. For the contact to be more realistic, a dissipation factor is introduced into the contact model by adding a coefficient of restitution. Since the Hertzian contact model apparently cannot account for the dissipation energy, an internal damping between two colliding objects was added into the model. With reference to [44], the contact force model with hysteresis damping factor is determined from the equation:

$$F_c(\tau) = K\delta^{\frac{3}{2}} + \mu\delta^{\frac{3}{2}}\dot{\delta}. \tag{2.2.6}$$

The coefficient K is a constant that depends on the properties of the material, Young's modulus and Poisson's ratio, and the radius of the spherical poppet r_s [45, 46]. Let E_s and E_p be the Young's moduli associated with the poppet and PEA, respectively, and υ_s and υ_p be their Poisson's ratios, then the coefficient K can be described by

$$K = \frac{4\sqrt{r_s}}{3\left(\frac{1-\upsilon_s^2}{E_s} + \frac{1-\upsilon_p^2}{E_p}\right)}. \tag{2.2.7}$$

The hysteresis damping coefficient μ is expressed in terms of the coefficient of restitution e:

$$\mu = \frac{3K(1-e^2)}{4\left(V_p^{(-)} - V_s^{(-)}\right)}. \tag{2.2.8}$$

The bouncing of a rigid poppet is realized by the normal impulse component resulting from the reaction force of PEA based on the Hertzian contact model. A change in momentum of a rigid poppet body can be calculated as:

$$m_s V_s^{(+)} - m_s V_s^{(-)} = \int_0^{\tau} F_c(\tau) d\tau. \tag{2.2.9}$$

The approach used in this model assumes that impact occurs instantaneously in an infinitesimally short time $\triangle\tau$, while the contact force is regarded as constant. We consider only the maximum contact force that can be derived by setting $\dot{\delta}$ equal to zero. Therefore, (2.2.9) can be simplified to

$$m_s V_s^{(+)} - m_s V_s^{(-)} = F_{c_{max}} \triangle \tau, \tag{2.2.10}$$

$$F_{c_{max}} = K\delta_{max}^{\frac{3}{2}}. \tag{2.2.11}$$

If the acceleration of penetration $\ddot{\delta}$ is constant, the Hertzian motion of deformation can be described by the kinematic equations [46]

$$\dot{\delta}^2 = \dot{\delta}_0^2 + 2\ddot{\delta}\delta, \tag{2.2.12}$$

$$\delta_{max} = \delta_0 + \frac{1}{2}\ddot{\delta}\left(\frac{\triangle\tau}{2}\right)^2, \tag{2.2.13}$$

where $\dot{\delta}_0$ is given by $\dot{\delta}_0 = V_s^{(-)} - V_p^{(-)}$. Using (2.2.12), the maximum deformation is provided by setting $\dot{\delta}$ to zero

$$\delta_{max}^{\frac{5}{2}} = \frac{5m_s}{4K}\dot{\delta}_0^2. \tag{2.2.14}$$

The duration of impact is derived from (2.2.13) where $\ddot{\delta} = K\delta_{max}^{\frac{3}{2}}/m_s$

$$\triangle\tau = 2\sqrt{2}\left(\frac{m_s}{K}\right)^{\frac{1}{2}}\delta_{max}^{-\frac{1}{4}}. \tag{2.2.15}$$

2.2.4 Contact Dynamics of Unconstrained Poppet

The approach in this simulation considers all respective motions of the poppet as bouncing motions. The poppet will bounce periodically if the force of a PEA is large enough to overcome the poppet weight and pressure drag. Thus, the generated force from a PEA determines the jumping height of the poppet. This approach assumes that the force coupling acts in one direction, with the line of force action defined by the connecting point between a poppet and a PEA. The contact dynamics are governed by contact force law for a simple one D.O.F oscillator, as shown in Fig. 2.5.

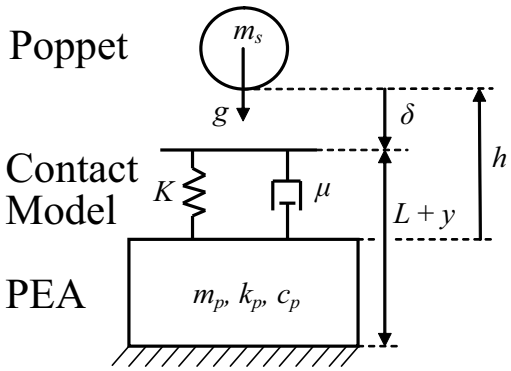

Figure 2.5: Contact force law of a sphere bouncing on a flat plane

A conditional transition where the poppet hits the PEA is called a contact state, whereas any other condition is called a free-flight state. These states can be physically described by the following sets of equations:
a. Contact state ($\delta < 0$)

$$m_s V_s^{(+)} - m_s V_s^{(-)} = (F_{c_{max}} - m_s g - pA) \triangle \tau, \tag{2.2.16}$$

b. Free-flight state ($\delta > 0$)

$$m_s \ddot{h} = m_s \dot{V}_s^{(+)} - m_s g - F_{drag}. \tag{2.2.17}$$

The pressure drag affecting the motion of a particle has been described [47]:

$$F_{drag} = C_D \frac{\pi}{2} r_s^2 \rho_f |\bar{u}_f - \bar{u}_p| \left(\bar{u}_f - \bar{u}_p\right). \tag{2.2.18}$$

The static forces acting on the poppet are indicated in Fig. 2.6, which shows the contact force F_c, pressure drag F_{drag} and drag coefficient C_D versus poppet diameter $2r_s$ in the initial contact state. In the optimum driving condition where the applied input voltage is sufficiently high, the force applied by PEA is comparatively high relative to the pressure drag. Under that condition, the influence of pressure drag on poppets of different sizes is extremely small and negligible, where the poppet motion is thus depending on the contact force involved (Fig. 2.6). Therefore, poppet sizes eventually have no effect on the flow rate output.

2.2.5 Mechanical Model of Unconstrained Valve Mechanism

This section describes the the poppet contact mechanism, PEA interaction with external pressure payload, and valve output flow dependency on the input parameters. So far, the model of a PEA has been considered an

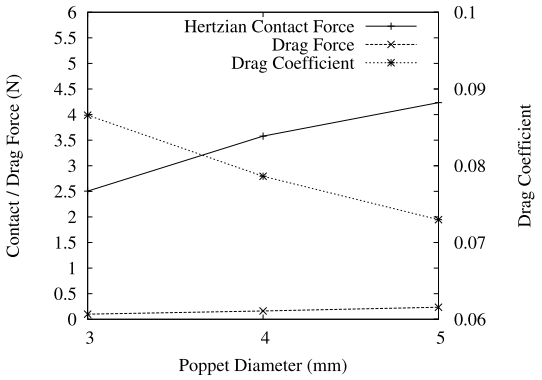

Figure 2.6: Contact force and pressure drag for different poppet sizes

actuator with a free stroke that excludes the external load. The existence of an external load will affect the frequency characteristics of the PEA. For valve application, two cases may be distinguished, namely, a contact state in which the PEA is connected with the external mass and a free-flight state in which there is no interaction force between the external mass and the PEA. Since the average contact time is extremely short compared with the time of free-flight, the free-flight state is dominant for the most part. We therefore compare three conditions: (1) a PEA is continually in contact with an external mass, (2) a free-flight condition and contact force F_c to change PEA behavior, and (3) a free-flight condition with a contact force assumed to be minor and thus omitted.

During the contact state as in condition (1), the externally applied force to the PEA F_e is influenced by the contact force F_c, the poppet weight W_s, and the air pressure pA. The interaction with the external loads is denoted by mass m_e, damping c_e and stiffness k_e, as shown in Fig. 2.7(a) and (b). The expression for the interaction force is therefore $F_e(s) = D_e(s)y(s)$ where $D_e(s) = m_e s^2 + c_e s + k_e$ [43]. A new operator for the mechanical behavior of the total system can be derived:

$$G(s) = \frac{N_p(s)}{N_p(s)D_e(s) + D_p(s)} \tag{2.2.19}$$

During the free-flight state of condition (2), the contact force F_c and air pressure pA are exerted onto the PEA as externally applied forces, whereas, during the free flight state of condition (3), only the air pressure pA is regarded as influencing PEA behavior. For this purpose, the PEA model in (2.2.3) is modified to include the behavior of the PEA and its integrated valve system. The total mechanical system of PEA and its external load used for the analysis of condition (2) and (3) are represented as a mass-damper-spring model, as shown in Fig. 2.7(c) and (d), respectively. The average density of a PEA material is higher if applied with than

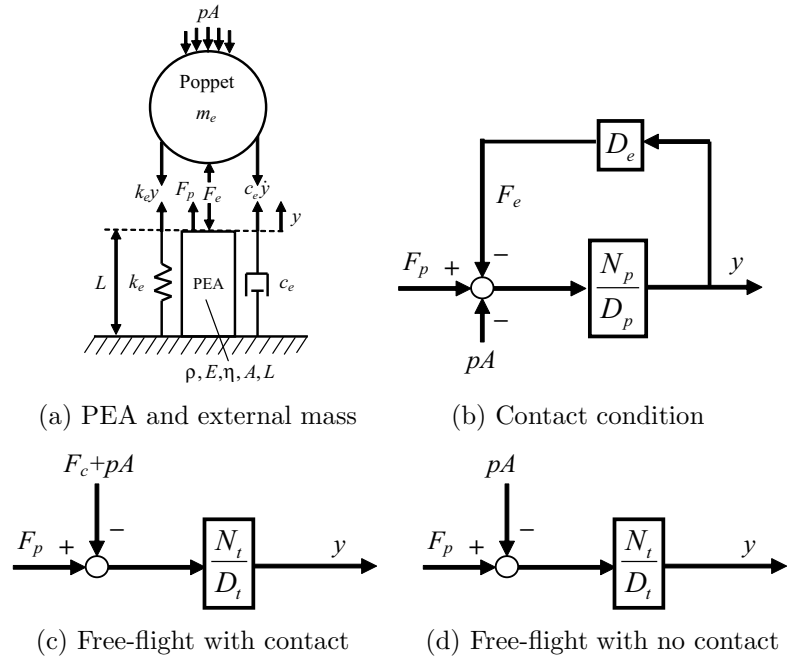

(a) PEA and external mass (b) Contact condition

(c) Free-flight with contact (d) Free-flight with no contact

Figure 2.7: Representation of the total system connecting between a PEA and an external load

without pressure. For example, two actuators of equal cross sectional area with length L_1 and L_2 are regarded as exerting the same pressure load. If the pressure is expressed as $p = \rho A L a_p$, and if the acceleration a_p is equal for both actuators, the ratio of pressurized density can be written as $\rho 1/\rho 2 = L2/L1$. The total mass m_t is dependent on the pressurized density. Thus, the operator for the mechanical behavior of the total system can be rewritten from (2.2.4) and (2.2.5) as:

$$N_t(s) = \frac{m_t}{\pi^2} s^2 + c_t s + k_t, \tag{2.2.20}$$

$$D_t(s) = \frac{4m_t}{\pi^2} s^2 + c_t s + k_t, \tag{2.2.21}$$

where $m_t = m_p + m_v$, $c_t = c_p + c_v$, and $k_t = k_p + k_v$ are the total mass, damping, and stiffness, respectively.

Experimental results revealed that the input pressure and voltage influenced the frequency behavior of the total system. Regardless of the size of a PEA, altering the input pressure or voltage affects the frequency responses. Experiments were conducted to determine the relationships among damping, stiffness, input pressure, and input voltage. As depicted in Fig. 2.8(a), there were linear relationships among damping, stiffness, and input pressure, whereas Fig. 2.8(b) shows that the relationships among damping, stiff-

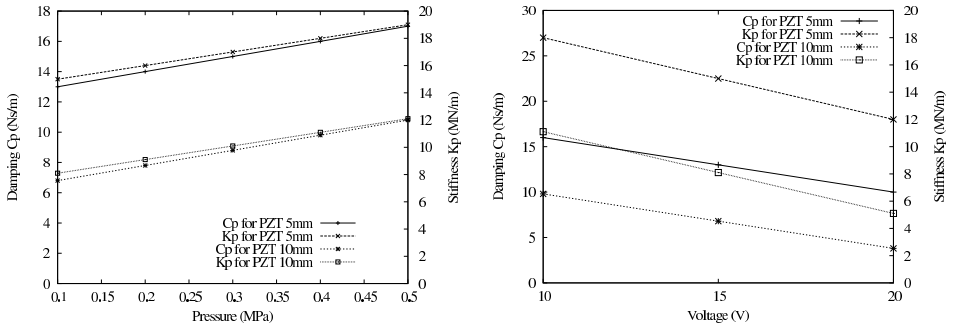

(a) Pressure-damping-stiffness (b) Voltage-damping-stiffness

Figure 2.8: Relationship of input pressure, input voltage, damping, and stiffness

Table 2.1: Model parameters for different sizes of Fuji Ceramics PEAs

Parameters	Symbol	PEA size (mm)		
		5x5x10	5x5x5	3x3x5
Mass	m_p	0.0017 kg	0.00085 kg	0.000425 kg
Damping	c_0	21 Ns/m	41 Ns/m	31 Ns/m
Stiffness	k_0	1.71e7 N/m	2.4e7 N/m	1.75e7 N/m
Mechanical Operator	G	1.5e-8 m/N	7.5e-9 m/N	3e-8 m/N
Transformer ratio	T_{em}	8.5 C/m	8.5 C/m	2 C/m

ness, and input voltage were also linear. These relationships could be estimated using the first order approximations:

$$c_t(V_{IN}, p) = c_t(V_{IN}) + (p - p_0)c_{poff}, \tag{2.2.22}$$

$$k_t(V_{IN}, p) = k_t(V_{IN}) + (p - p_0)k_{poff}, \tag{2.2.23}$$

$$c_t(V_{IN}) = c_{voff}V_{IN} + c_0, \tag{2.2.24}$$

$$k_t(V_{IN}) = k_{voff}V_{IN} + k_0. \tag{2.2.25}$$

From Fig. 2.8, these increments were estimated to be c_{poff}= 10 ms, $k_{poff} = 1{\cdot}10^7$ m, c_{voff}= - 0.6 Ns/mV, and $k_{voff} = -6{\cdot}10^5$ N/mV. The initial pressure value p_0 was 0.1 MPa, c_0 and k_0 were acquired from Fig. 2.8. The parameterizations of PEAs used in this simulation are specified in Table 2.1 (see [48]).

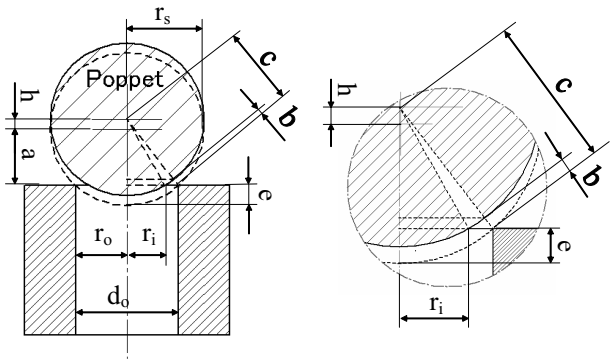

(a) 1-D poppet movement

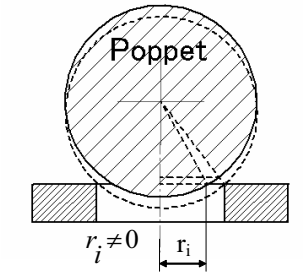

(b) Partial open area

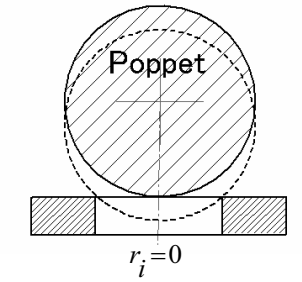

(c) r_i is zero

Figure 2.9: One dimensional poppet movement and its valve area

2.2.6 Airflow Characteristics

This section formulates the valve opening area and flow of fluid in an unconstrained valve. For the sake of simplicity, we assumed that poppet motion was restricted to one dimension (Fig. 2.9). Based on this assumption, we can derive a simple term to determine the area of orifice opening from the poppet bouncing height. We assume an aperture b between the poppet and orifice plate as the poppet bounces along the vertical line, which is calculated from $b = c - r_s$. With reference to Fig. 2.9(a), an experession for the partially opened valve area can be calculated as $A_o = \pi(r_o + r_i)b$. As the poppet moves higher, up to a certain limit, the maximum valve opening area is attained, $A_{max} = \pi r_o^2$. Combining these equations, the valve opening area can be calculated as:

$$A_o = min[\pi(r_o + r_i)b, \pi r_o^2]. \tag{2.2.26}$$

Using the Pythagorean theorem, the following equations can be generated:

$$a^2 = r_s^2 - r_o^2, \tag{2.2.27}$$

$$r_s^2 = r_i^2 + (a + h)^2, \tag{2.2.28}$$

$$c^2 = r_o^2 + (a+h)^2. \tag{2.2.29}$$

The determining variable is h, which changes the values of r_i and b. When the poppet is about to separate from the orifice (Fig. 2.9(b)), beyond which the poppet is no longer intersected with the orifice plate, then $r_i = 0$, as indicated in Fig. 2.9(c). Using equations (2.2.27) to (2.2.29), the following set of equations is obtained:

$$r_i = max[(r_o^2 - 2h\sqrt{r_s^2 - r_o^2} - h^2)^{\frac{1}{2}}, 0], \tag{2.2.30}$$

$$b = (r_s^2 + 2h\sqrt{r_s^2 - r_o^2} + h^2)^{\frac{1}{2}} - r_s. \tag{2.2.31}$$

The flow of an incompressible fluid through an orifice can be divided into sonic and subsonic flow, depending on the pressure drop ratio between p_{in} and p_{out}, which is derived as [49]:

$$Q = \frac{p_{in} A_{eff}}{\rho_{air}} \sqrt{\frac{2}{RT}} f(z), \tag{2.2.32}$$

where

$$f(z) = \begin{cases} \sqrt{\dfrac{\kappa}{\kappa+1}\left(\dfrac{2}{\kappa+1}\right)^{\frac{2}{\kappa-1}}} & (0 \le z < 0.528) \\ \sqrt{\dfrac{\kappa}{\kappa-1}\left(z^{\frac{2}{\kappa}} - z^{\frac{1}{\kappa}+1}\right)} & (0.528 \le z \le 1) \end{cases}$$

The effective valve area A_{eff} is defined as $A_{eff} = C_d A$. The theoretical orifice opening A_o is in practice smaller, so the effective valve area is modified using a discharge coefficient C_d to account for geometrical conditions [49].

2.3 Experimental and Simulation Results

The derived simulation model was verified using an experimental system constructed as shown in Fig. 2.10, in which the input voltage, input frequency and output flow rate were recorded to obtain voltage/flow rate and frequency/flow rate plots. An Agilent 33120A function generator was used to provide the input rectangular waveform frequency. The generated flow rate in the valve corresponding to the input voltage/frequency was measured with a Yamatake CMS0050 gas mass flow meter, which was connected to a D/A converter board for data acquisition using a PC. The valve investigated was composed of multilayer piezoelectric stacked actuators (Fuji Ceramics Corp.), in which a 10 mm height has about 100 stacked layers.

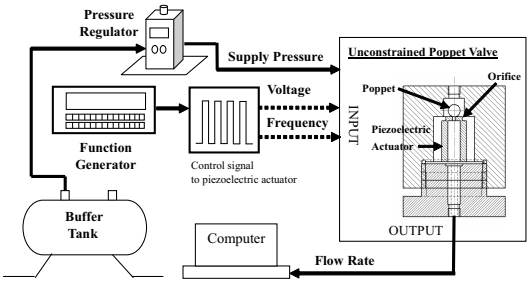

Figure 2.10: Schematic representation of the unconstrained poppet valve

Table 2.2: PEA size, input voltage and pressure for experiment

Type	PEA (mm)	Poppet (mm)	Voltage (V)	Pressure (MPa)
I	5 x 5 x 10	2, 3, 4	15	0.2, 0.5
II	5 x 5 x 5	2, 3, 4	20	0.2, 0.3, 0.5
III	3 x 3 x 5	3	15, 20	0.2

The output flow rate was mainly dependent on the poppet flight height. That is, the parameters of particular concern were the input voltage, input frequency, inlet pressure, and PEA size. For three valves with PEA dimensions of 5 x 5 x 5 mm, 5 x 5 x 10 mm, and 3 x 3 x 5 mm, the flow rate response experiments were conducted under rectangular inputs with frequencies ranging from 0 to 60 kHz. The same orifice size ϕ 0.8 mm was used for PEA 5 x 5 x 5 mm and 5 x 5 x 10 mm, while PEA 3 x 3 x 5 mm was tested with a smaller orifice size ϕ 0.5 mm due to the lack of force. The experimental conditions are listed in Table 2.2.

Extensive experimental testing was performed to assess the frequency/flow rate behavior under the conditions presented in Table 2.2. Based on the specified input voltage and inlet pressure, the frequency/flow rate response of the valve with the three PEAs are plotted in Figs. 2.11 - 2.16. These results indicate that flow rate output increases monotonically with input frequency until the peak flow rate is reached, at which an abrupt change was observed. The flow rate then begins to decrease, returning to zero at higher frequencies. These phenomena regarding peak flow rate can be related to the resonant frequency of the total mechanical system, consisting of the PEA and the valve body. The resonant frequency had a tendency to shift to the left as either the size of the PEA was enlarged or the inlet pressure was reduced (see Figs. 2.11 - 2.15). Moreover, resonance occurred at lower frequency as the voltage was increased (Fig. 2.16). Around the resonant region, where peak flow rate occurred, the flow rate did not change significantly in relation to poppet size (Figs. 2.11 - 2.15). Therefore, poppet

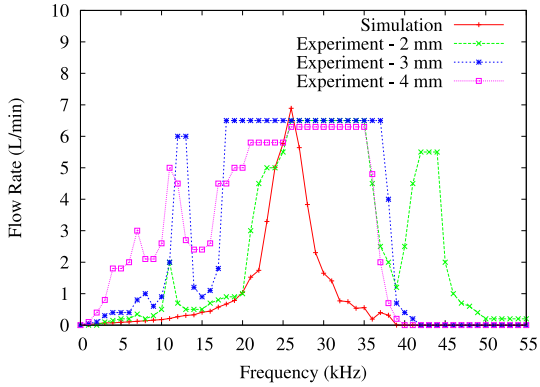

Figure 2.11: Simulated frequency/flow rate response for PEA 5 x 5 x 10 mm at a supply pressure of 0.2 MPa (orifice ϕ 0.8 mm, input voltage 15 V)

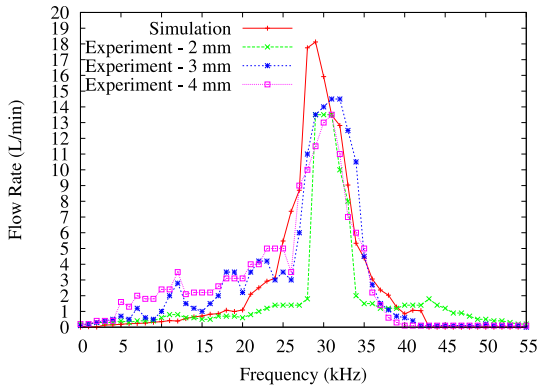

Figure 2.12: Simulated frequency/flow rate response for PEA 5 x 5 x 10 mm at a supply pressure 0.5 MPa (orifice ϕ 0.8 mm, input voltage 15 V)

size had no influence on flow rate output at the resonant frequency and its adjacent region. In contrast, poppet size had a significant effect on flow rate output at other frequencies.

2.4 Discussion and Simulation Verification

To validate the proposed simulation model, a series of experiments was carried out using different poppet and PEA sizes at various supply pressures. Valve behavior was simulated by solving the dynamic model using a continuous numerical method in Matlab/Simulink environment. With reference to the frequency response models presented in Fig. 2.17, the simulation results are compared for the three conditions considered. When we assessed the agreement between our theoretical results and the experimental results, we found that the estimated simulation results for condition

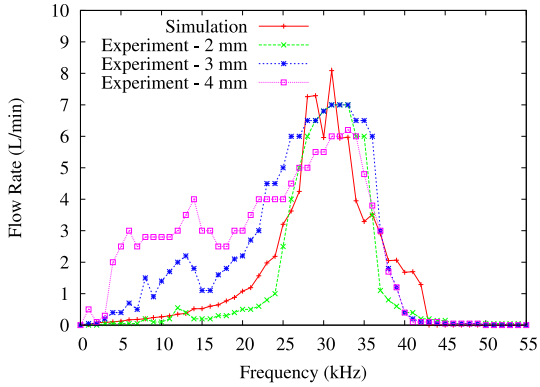

Figure 2.13: Simulated frequency/flow rate response for PEA 5 x 5 x 5 mm at a supply pressure 0.2 MPa (orifice ϕ 0.8 mm, input voltage 20 V)

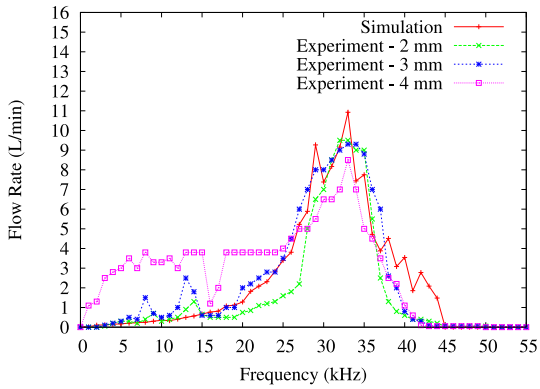

Figure 2.14: Simulated frequency/flow rate response for PEA 5 x 5 x 5 mm at a supply pressure 0.3 MPa (orifice ϕ 0.8 mm, input voltage 20 V)

(1) in Fig. 2.17 were not closely consistent with the experiment findings; moreover, the computations were costly and time-consuming. The results of conditions (2) and (3) were similar and the computation processes were significantly reduced compared with the closed loop model of condition (1). In addition, the simulation time for condition (3) was about half of that for condition (2), so that using the model in condition (3) resulted in a higher efficiency for almost the same results. Validation of this model was supported by the fact that the contact time was infinitesimal, thus the contact force did not change the properties of the internal PEA. The model in condition (3) thus allows us to collect an abundant amount of data while saving a great amount of time. As shown in Fig. 2.18, the simulation results of condition (1) indicated similar results for the three poppet sizes. Thus, one simulation result could be taken as representative for the three poppet sizes. In subsequent simulations, we will use the model in condition (3) to

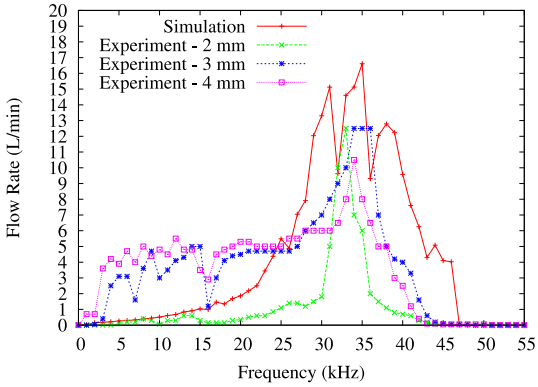

Figure 2.15: Simulated frequency/flow rate response for PEA 5 x 5 x 5 mm at a supply pressure 0.5 MPa (orifice ϕ 0.8 mm, input voltage 20 V)

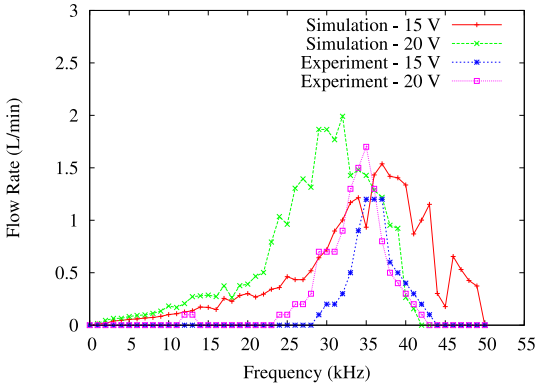

Figure 2.16: Simulated frequency/flow rate response for PEA 3 x 3 x 5 mm at various input voltages (orifice ϕ 0.5 mm, supply pressure 0.2 MPa)

save on simulation time for one poppet size only, *i.e.*, poppet ϕ 3 mm.

Comparisons of the experimental and numerical results with 100-layer stacked PEAs at 15 V are shown in Figs. 2.11 - 2.12 for input pressures 0.2 and 0.5 MPa, respectively. Similarly, Figs. 2.13 - 2.15 show the flow rate results obtained with 50-layer stacked PEAs driven at 20 V for input pressures 0.2, 0.3 and 0.5 MPa, respectively. The experimental results in Figs. 2.11 - 2.15 show that there were no major changes around the peak flow rate for different poppet sizes. Nonetheless, the flow rate response differed at the low frequencies. Simulation results for poppets of ϕ 2 mm, ϕ 3 mm, and ϕ 4 mm show no subtle differences among them. Therefore, the simulation model could not explain the differences between the various poppet sizes at low frequencies. Based on the observation of poppet motion, we could distinguish poppet motion from flow rate generated in accordance with input frequency as 1) no bouncing (spinning), 2) bouncing, and 3) idle

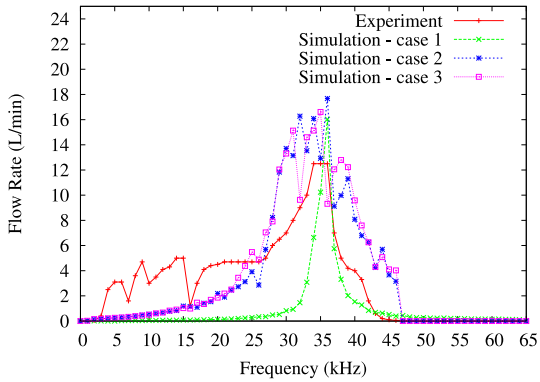

Figure 2.17: Comparative study of simulation models for PEA 5 x 5 x 5 mm, poppet ϕ 3 mm, orifice ϕ 0.8 mm, supply pressure 0.5 MPa and input voltage 20 V

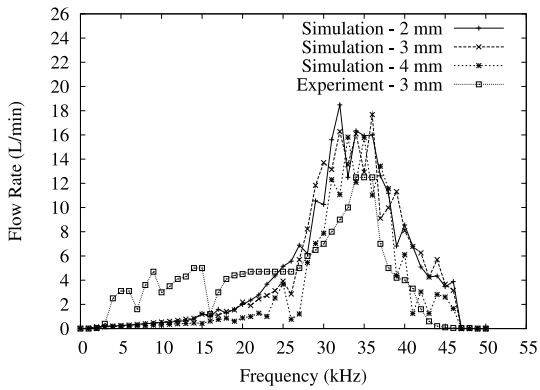

Figure 2.18: Simulation results of different poppet sizes for the model in condition (1), PEA 5 x 5 x 5 mm, orifice ϕ 0.8 mm, supply pressure 0.5 MPa and input voltage 20 V

motions. Spinning motion takes place at low frequencies, whereas a higher input frequency will cause the poppet to have a bouncing motion. At higher frequencies, poppet motion becomes weaker, resulting in idle motion. As a result, the large errors in Figs. 2.11 to 2.15 show that the bouncing model is incorrect and inappropriate for the low frequency range.

The cause of the simulation error is related to the assumption that the poppet is restricted to a one dimensional bouncing model. At mid-high frequency ranges around the resonance frequency, the simulation was in good agreement with experimental results. This simulation also verified that the bouncing ball model is suited to the real physics observed in the experiment. The results observed indicate, however, that the proposed model is not generally applicable to the low frequency range. Figs. 2.11 and 2.15 show disagreement between simulations and experiments at mid-high fre-

quency ranges and the differences were considered a special case caused by uncertainties in the real valve and the lack of knowledge in fluid dynamics. Even so, the proposed simulation model could describe the tendency of valve behavior at low, mid-high, and high frequencies. This paper was not intended to present precise simulation, but to discuss prediction of flow tendencies towards miniaturization. Since the main focus of this study was on on-off control, where the valve is switched between zero and the resonant frequency, the effect of poppet size at low frequency is not crucial and can be simply ignored.

In regard to PEA sizes, the simulation model was able to elaborate the behavior of valves effectively as the experimental findings. A comparison involving the PEA sizes is given in Fig. 2.16 for PEA size 3 x 3 x 5 mm. This figure shows that the simulated results closely match the experimental results, even though the input voltage was varied. Thus, the proposed model was validated and an accurate result can be obtained if the valve is driven in the vicinity of the resonant frequency.

The proposed model was also verified by inspecting the relationship between the input voltage and outlet flow rate to observe the behavior of an unconstrained poppet valve as a flow control valve. Comparison of average flow rate between the experimental and simulation results is shown in Fig. 2.19 for PEA 5 x 5 x 5 mm, ϕ 3 mm poppet, and ϕ 0.8 mm orifice at supply pressure of 0.5 MPa. Although there was a slight discrepancy, the simulated result agreed well with the experimental results; however, the simulation could describe the tendency of voltage-flow rate behavior. The flow rate was not linearly proportional to the input voltage, and there was an oscillation in the flow rate. This nonlinearity makes it difficult to control, therefore, this evidence suggests that an unconstrained valve is inappropriate for use as a proportional flow control valve.

This unconstrained valve utilizes a mechanism driven by vibrational force, which causes the poppet to bounce. When the valve is switched on, the outlet flow appears to be oscillating due to the vibratory poppet motion. While it is deactivated, there is no outflow from the valve. This general principle is applied as the basic method of an on-off control valve. Fig. 2.20 shows the trends of flow response for the valve with different input voltages. The switching time was 800 ms for the valve to turn on, and deactivation took about 1600 ms until it was fully closed. The measurement results are presented as the mean flow rate and standard deviations in Table 2.3. Driving the valve at respectively higher voltage resulted in an increase of flow rate, although this was accompanied by an unpredictable oscillation. Flow oscillation was weakened at low driving voltages because of reduction in the bouncing height. Therefore, the flow response seems to be stable, as shown by the small value of standard deviation. A nearly constant flow

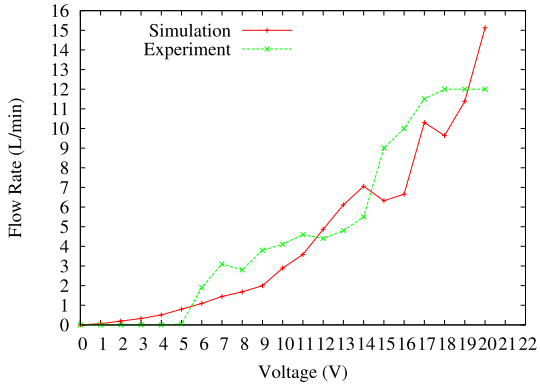

Figure 2.19: Flow rate - voltage relationship of an unconstrained on-off valve (orifice ϕ 0.8 mm, poppet ϕ 3 mm, PEA size 5 x 5 x 5 mm, supply pressure 0.5 MPa, frequency 34 kHz)

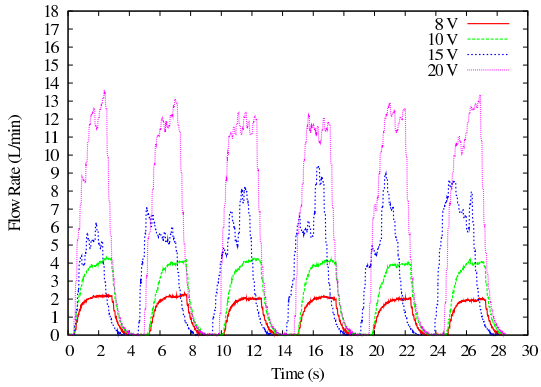

Figure 2.20: On-off switching response at various input voltage (orifice ϕ 0.8 mm, poppet ϕ 3 mm, PEA 5 x 5 x 5 mm, supply pressure 0.5 MPa)

rate was attained at low input voltages. As observed for on/off switching repeatability, valve performance was considerably better at low voltages.

This phenomena can be theoretically explained using the simulation results for poppet bouncing height as shown in Fig. 2.21. As observed from the simulation results, the poppet bouncing trajectory was considerably uniform with higher period at low input voltages, whereas at high voltage ranges the poppet moves randomly (or chaotic) with slower bouncing periods that causes an obvious oscillation in the output flow rate. Chaotic behavior of the poppet bouncing motion was also confirmed by experiment for a valve with PEA 5 x 5 x 10 mm, orifice ϕ0.8 mm, and poppet ϕ4 mm, and the poppet bouncing trajectory is plotted in Fig. 2.22.

The influence of the orifice material to the poppet bouncing height (or output flow rate) was verified in Fig. 2.23, which shows a slight reduc-

Table 2.3: Mean flow rate and standard deviation for on-off switching

Input Voltage (V)	$\bar{Q} \pm \sigma$ (L/min)
8	2 ± 0.0782
10	4 ± 0.0684
15	6 ± 1.1898
20	11.5 ± 0.7466

tion in the resulted flow rate for a soft material stainless steel compared to spring steel. The experimental results thus validated the simulation model in Eq. 2.2.6 - 2.2.8 , indicating the importance of the material of orifice in designing an unconstrained valve. The simulation model and experimental findings suggest that the valve operation is fundamentally similar to a poppet bouncing system, where the generated impact force is dependent on the surface material. In valve design, the material of orifice will eventually contribute to the maximum bouncing height.

2.5 Conclusion

We presented here an analysis and simulation model of an unconstrained ON-OFF poppet valve, which includes the modeling of a PEA, Hertzian contact, dynamics of poppet motion, and airflow through an orifice. The flow rate generated and the input/output relationship between input frequency/flow rate and voltage/flow rate at different levels of inlet pressure were measured experimentally. Simulation models were built and verified experimentally for valves with different piezoelectric dimensions. The modeling of each subsystem was introduced in order to generate an overall valve model based on the dynamics of a bouncing poppet. Numerical simulations were implemented in MATLAB/Simulink environment and the results were compared with experimental findings. The simulated and experimental results showed good agreement around the resonant frequency, despite the mismatched results at low frequency, thus validating the proposed simulation model. Based on the experimental and simulation results, unconstrained valves were characterized as frequency-controlled ON-OFF valves. These findings indicate that this analytical model can be used to estimate the input/output behavior of unconstrained valves with different parameters.

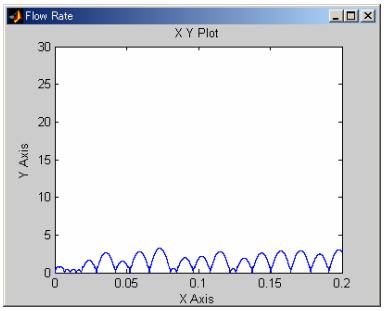

(a) Voltage 8 V (Q_{avg} = 1.544 L/min)

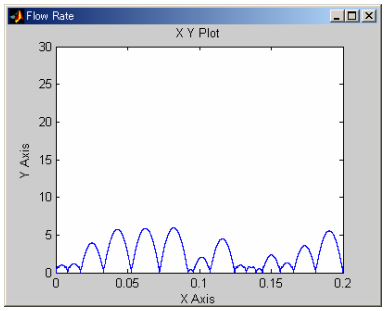

(b) Voltage 10 V (Q_{avg} = 2.518 L/min)

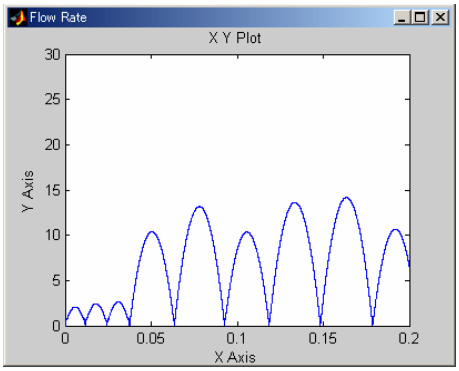

(c) Voltage 15 V (Q_{avg} = 7.01 L/min)

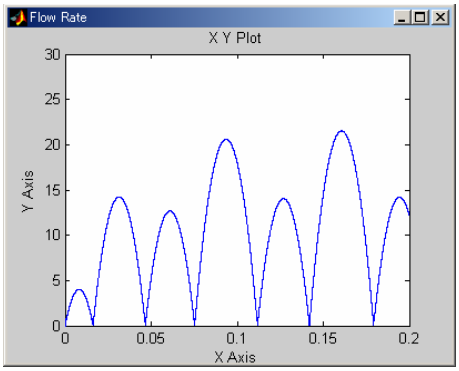

(d) Voltage 20 V (Q_{avg} = 10.548 L/min)

Figure 2.21: Simulation results of valve output flow rate in corresponding to poppet bouncing height for valve with PEA 5 x 5 x 5 mm, orifice ϕ0.8 mm, poppet ϕ3 mm, supply pressure 0.5 MPa (x-axis represents the traveled time in second and y-axis indicates the output flow rate in L/min unit)

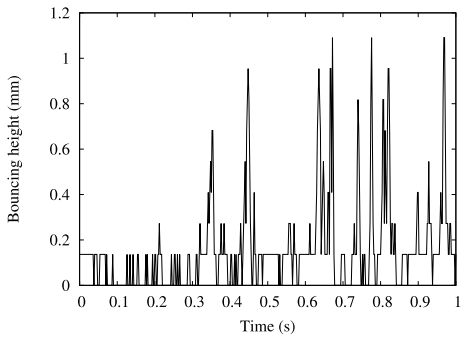

(a)

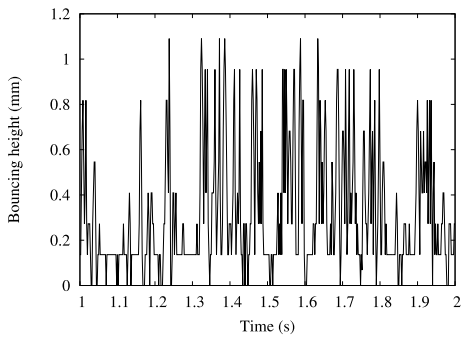

(b)

Figure 2.22: Experimental results of poppet bouncing trajectory recorded using high-speed camera for a 2 second span. (a) Time span: 0 to 1 second, and (b) Time span: 1 to 2 second.

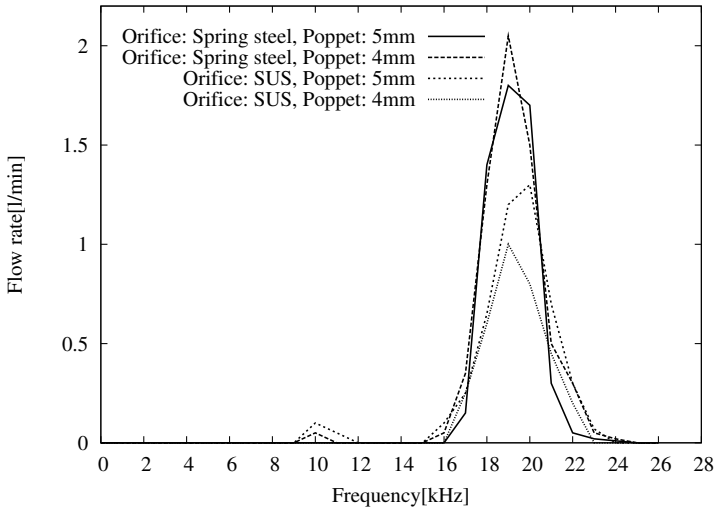

Figure 2.23: Valve flow response for orifices with different materials

Chapter 3

Valve Design

3.1 Input - Output Relationship

This section shows the design concept for the miniaturization of piezoelectrically driven unconstrained valves. Design variables that affect the flow behavior of an unconstrained on-off valve, as schematically given in Fig. 3.1(a), include: 1) the sizes of the PEA, 2) spherical poppet and orifice diameter, 3) the thickness of valve base, 4) the geometry and material properties of the valve body, and 5) the internal empty volume inside the valve.

The unconstrained valve's advantage is its compactness, so we looked at valve miniaturization design issues based on the representative overall unconstrained-valve model in Fig. 3.1. Valve inputs are pressure p, driving frequency f, and voltage V_{IN}, with output flow Q, whose input-output relationship is written as Q =f(f, V_{IN}, p). Dynamic force generated by the PEA is calculated as $F_{dyn} = -y\omega^2 m_{eff} \sin \omega t$ [50]. In preliminary design determining PEA size, force should be sufficient to withstand the pressure load, yielding the following inequality:

$$y\omega^2 m_{eff} \sin \omega t > (P_{IN} - P_{OUT}) A_{eff} + W_s. \tag{3.1.1}$$

3.2 Miniaturization Design

The valve input-output relationship of input pressure, frequency,and voltage also requires an understanding of unconstrained-valve design parameters, shown in Fig. 3.1 to consist of a PEA, poppet, orifice, valve geometry and material, and base thickness. Of these, PEA size, poppet diameter, and orifice diameter are the most crucial factors in determining whether a valve will work appropriately, as calculated in Eq. 3.1.1. Mechanical design

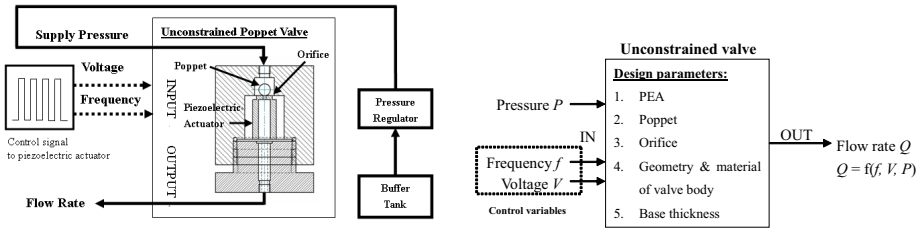

Figure 3.1: Control of a piezoelectrically-driven unconstrained poppet valve. (a) Schematic diagram, and (b) Input-output and control parameters of unconstrained valves

requires a dynamic piezoelectric force a few times higher than the pressure load to compensate for the poppet-orifice ratio influence neglected in Eq. 3.1.1. This ratio helps determine poppet bounce height and flow characteristics. Valve performance deteriorates rapidly if an orifice is too large, so orifice diameter must be designed properly, as must PEA size and orifice diameter to achieve high output flow. Flow output is proportional to poppet diameter, with larger poppets having higher flow and vice versa.

3.2.1 PEA Selection

The accurate overall electromechanical PEA model [48], [43] in Fig. 2.3 is used to assess valve miniaturization feasibility. The following electromechanical equations quantify the piezoelectric effect:

$$q = CU_p + q_p, \tag{3.2.1}$$

$$q_p = T_{em} y, \tag{3.2.2}$$

$$F_p = T_{em} V_{IN}, \tag{3.2.3}$$

$$y = M(F_p - F_e). \tag{3.2.4}$$

Assuming no loss at the PEA, electrical and mechanical energy are equal, *i.e.*, $V_{IN} q_p = F_p y$. Power generated by the PEA is calculated as the time derivative of energy:

$$V_{IN} \dot{q}_p = F_p \dot{y}. \tag{3.2.5}$$

Force F_p and voltage V_{IN} are proportional (Eq. 3.2.3), so we intrepret a linear correlation between current $\dot{q}_p$ and PEA elongation rate $\dot{y}$ from

Eq. 3.2.5. PEA elongation rate influences flow output because it determines poppet bounce height. The faster a PEA elongates, the greater the generated contact force and output flow. We conclude that controlling the outlet flow is equivalent to controlling PEA input current (or velocity). Current control is difficult, but current can be "steered" from input voltage. Average current i [50] required for sinusoidal PEA operation is as follows:

$$i = \dot{q} = fCV_{IN}. \tag{3.2.6}$$

If A is a single electrode surface area, capacitance C is written as [51]:

$$C = \frac{L\epsilon_{33}^{T}A}{d_s^2}. \tag{3.2.7}$$

Eqs. 3.2.6 and 3.2.7 show that current flow to the PEA is determined by PEA length L and cross-section A. The miniaturized valve limits permissible current flow to the PEA, weakening generated velocity (power). One way to acquire sufficient power for a small unconstrained valve is to increase input voltage, which could be hazardous or make PEA driver miniaturization difficult. As a consequence to power deterioration, the orifice must be smaller to compensate for excessive pressure drag, which reduces output flow. Miniaturization thus correlates with the tradeoff between current (flow rate) and valve size.

3.2.2 Poppet and Orifice Sizes

Combinations of poppet - orifice diameters also have its role in determining the poppet bouncing height and flow characteristics, therefore the poppet-orifice combination has to be properly chosen to obtain a high flow efficiency. Fig. 3.2 shows the experimental results for poppet - orifice - output flow test, where the influence of poppet-orifice combinations for sinusoidal input waveform are observed in Figs. 3.2 & 3.3, while Fig. 3.4 indicates the flow response at various input voltages. The experimental results showed unpredictable trends of poppet-orifice combinations, however, flow is maximized at a poppet-orifice ratio of four to five. To avoid complex calculation, we use 5 for our design. Optimal valve performance can be achieved when the poppet flight is maximal, as incurred in Chapter 2. This, in turn, depends on the combination of PEA and the orifice diameter. Valve performance deteriorates rapidly when the orifice size is too large compared to the poppet size, and the flow rate output will also decrease if the orifice diameter is too small. To achieve high output flow, both the size of piezoelectric actuator, orifice and the poppet diameters have to be suitably proportional.

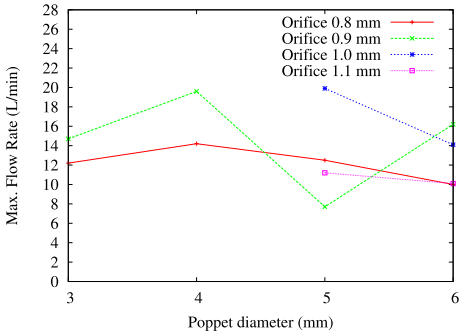

Figure 3.2: Poppet size - flow rate relationship for various orifice diameters

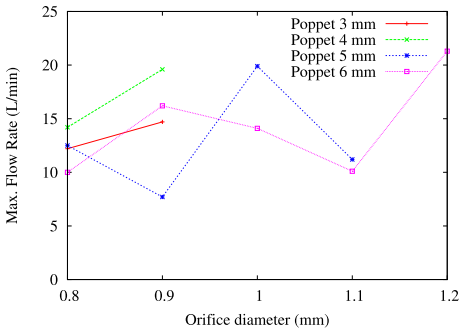

Figure 3.3: Orifice size - flow rate relationship for various poppet sizes

3.2.3 Valve Base Thickness

In addition, the external body of the valve assists in transferring vibrational energy generated by the PEA to the poppet. The mechanical properties of the valve body are effective in augmenting output flow rate (Fig. 3.5(a)). Fig. 3.5(b) shows the relationship between frequency and flow rate, indicating that a valve with a thin base has a higher flow rate. This may be due to the function of the diaphragm, which resembles a mechanism that assists in mechanically amplifying the induced displacement of a PEA, thus increasing its power. The estimated displacement amplification w_0 of the valve base is then given by the equation [52, 53]:

$$w_0 = f(\nu)\left(\frac{P_{IN}R_b^4(1-\nu)}{E_b t_b}\right)^{1/3}, \tag{3.2.8}$$

where $f(\nu)$ is a function of Poisson's ratio [53]. Eq. 3.2.8 shows that displacement w_0 is inversely proportional to the cubic root of t_b. Therefore, if all other parameters are unchanged, the amplified deflection is larger for thin than for thick diaphragms.

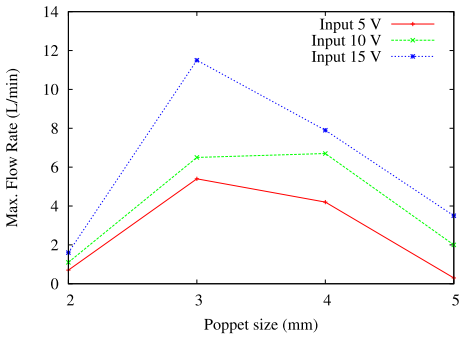

Figure 3.4: Poppet size - flow rate relationship at different input voltages

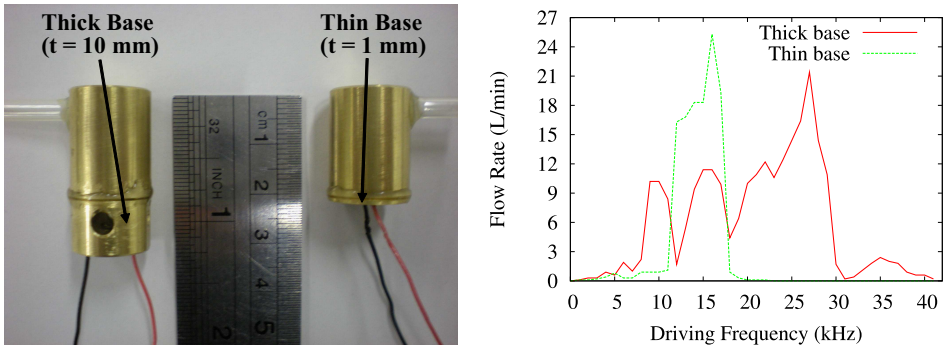

(a) (b)

Figure 3.5: Flow rate characteristics of miniaturized unconstrained valves. (a) Variation of the valve baseplate, and (b) Cumulative effects of changing the geometry of the valve body

3.2.4 Geometry and Properties of Valve Body

The role of valve body is to assist in transferring vibrational energy generated by the piezoelectric actuator to the poppet, whose property determines valve behavior related to overall mass m_t, damping c_t, and stiffness k_t. The influence of valve body to the output flow rate was studied using two different materials for the valve body, *i.e.*, acrylic ($m_{acryl} = 12.04$ g) and aluminum ($m_{al} = 23.63$ g), as shown in Fig. 3.6(a). The comparison is given in Fig. 3.6(b), showing no significant changes, meaning that valve case material does not significantly affect output flow, despite a slight shift in peak flow location related to the difference in m_t, c_t, and k_t. However, the strength of material becomes important when the valve is miniaturized as a thin valve body requires high-strength material to withstand high pressure load. This suggests that the selection of material is necessary for the miniaturization design, but has no remarkable influence to the output flow rate.

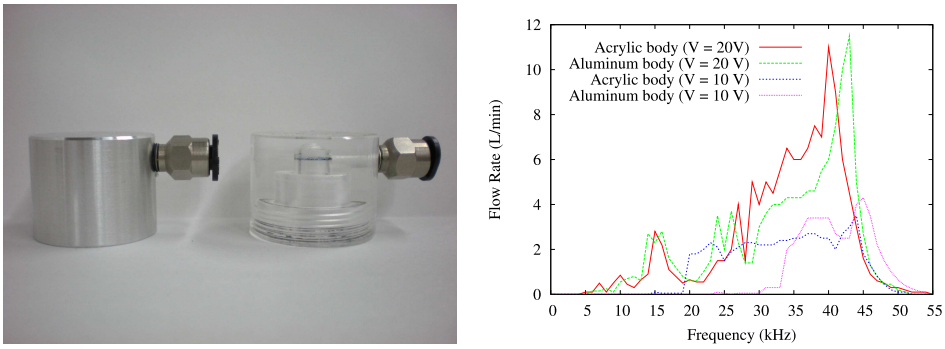

(a) (b)

Figure 3.6: Unconstrained valve with different material for the valve body. (a) Aluminum and acrylic body, (b) Comparison of the generated flow rate for input voltage 10 & 20 V (PEA 5 x 5 x 5 mm, orifice ϕ0.8 mm, poppet ϕ4 mm, and pressure 0.5 MPa)

To see if changes in valve body geometry affect output flow, we looked at two prototypes, one with small and the other with large internal hollow volume, as shown in Fig. 3.7(a) and (b). The comparison in Fig. 3.7(c) shows that a valve with large volume has higher flow, so internal space functions similarly to accumulator gas storage. Assuming that there is no flow resistance, *i.e.*, no change in the inlet and outlet pressure $P_{IN}(t) = P_{OUT}(t) = P_s(t)$, then mass flow at the valve inlet is written as [54]:

$$\dot{m}_1 = \frac{V_h}{n}\left(\frac{1}{k_{pol}}\right)^{\frac{1}{n}} P_s(t)^{\frac{1-n}{n}}\dot{P}_s(t) + \dot{m}_2(t), \tag{3.2.9}$$

where $n = 1$ isothermal and $n = 1.4$ for isentropic states, and $k_{pol} = pV^n$. The flow of an incompressible fluid through an orifice $\dot{m}_2$ can be rewritten from Eq. 2.2.32 into:

$$\dot{m}_2 = \frac{P_{IN}A_{eff}}{\rho}\sqrt{\frac{2}{RT}}f\left(\frac{P_{OUT}}{P_{IN}}\right), \tag{3.2.10}$$

Substituting Eq. 3.2.10 into Eq. 3.2.9, Eq. 3.2.9 can be rewritten into:

$$\dot{m}_1 = \frac{V_h}{n}\left(\frac{1}{k_{pol}}\right)^{\frac{1}{n}} P_s(t)^{\frac{1-n}{n}}\dot{P}_s(t) + \frac{P_{IN}A_{eff}}{\rho}\sqrt{\frac{2}{RT}}f\left(\frac{P_{OUT}}{P_{IN}}\right). \tag{3.2.11}$$

Introducing valve constant k_{valve}, the relationship of airflow through an orifice and accumulator in Eq. 3.2.11 is rewritten simplest as $\dot{m}_1 = k_{valve}\dot{m}_2$, where $k_{valve} = f(V_h, \dot{P}_s(t))$. Mass flow $\dot{m}_1$ is linearly proportional to the hollow accumulator volume so that designing a valve with large accumulator volume yields higher flow, but this contradicts miniaturization objectives, indicating that miniaturization applying the accumulator principle also involves a tradeoff between flow and valve size.

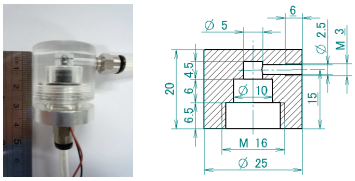

(a) Small hollow volume

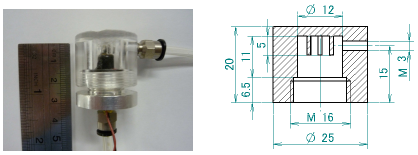

(b) Large hollow volume

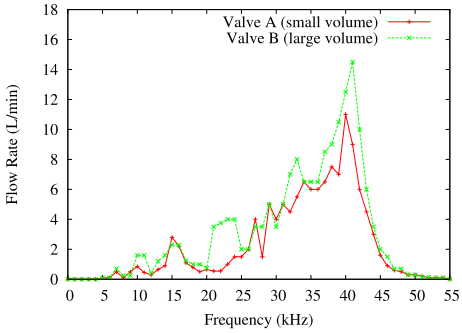

(c) Flow - frequency graph

Figure 3.7: Flow characteristics in correlation with valve hollow volume. (a) Small volume, (b) Large volume, and (c) Frequency - flow graph (PEA 5 x 5 x 5 mm, ϕ4 mm poppet, ϕ0.8 mm orifice, 20 V input voltage, and 0.5 MPa pressure).

3.3 Fabrication of Unconstrained Valves Towards Miniaturization

Fabrication of the first prototype of unconstrained valves, is called "design 1" in this paper. In an attempt to miniaturize the first prototype, a new design having a single screw was introduced to eliminate the unused space inside the valve, making it more compact and it will be called as "design 2" in the following sections. A further miniaturization from the design 2, *i.e.* design 3, has a more compact size, which was successfully achieved by eliminating the O-rings and fasteners as well as reducing the valve internal volume, therefore it becomes slimmer [58]. Prototype of design 3 has the minimal volume and therefore steel or other metalic material was used for the valve body to ensure adequate strength. Different miniaturization designs 1 - 3 for unconstrained valves are shown in Fig. 3.8(a), (b)and (c).

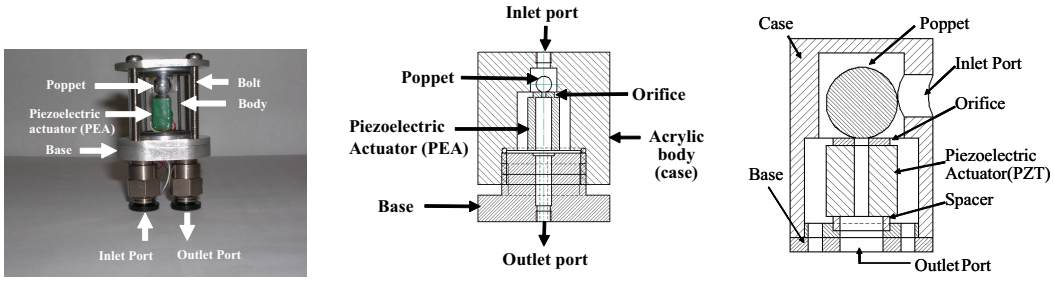

(a) (b) (c)

Figure 3.8: Miniaturization design of unconstrained valves: (a) design 1 (acrylic body fastened by four screws), (b) design 2 (acrylic body fixed to the base), and (c) design 3 (metal body connected using adhesive bond)

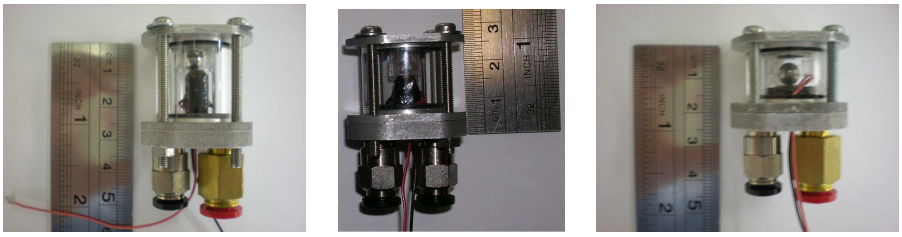

(a) Type 1-5510 (b) Type 1-555 (c) Type 1-10102

Figure 3.9: Fabricated unconstrained valves according to the structure in design 1. (a) PEA 5 x 5 x 10 mm (type 1-5510), (b) PEA 5 x 5 x 5 mm (type 1-555), and (c) PEA 10 x 10 x 2 mm (type 1-10102)

Design 1 consists of a PEA, a poppet, four O-rings, four screws, body and case. For this particular design, PEA occupies most of the space with a lot of vacant space inside the valve. Three prototypes of design 1, as shown in Fig. 3.9, were fabricated with PEA 5 x 5 x 10 mm (valve type 1-5510), PEA 5 x 5 x 5 mm (valve type 1-555), and PEA 10 x 10 x 2 mm (valve type 1-10102), where each prototypes has orifice ϕ1.2 mm and poppet ϕ6 mm. Comparisons of the output flow for driving voltage 25 V are given in Fig. 3.10, where the test results indicate a decrease in flow rate for PEA with short stacks. From experimental results, it can be concluded that the stacked length of PEA is crucial to increase the output flow, while the PEA cross-sectional area has little influence on the output flow.

Design 2 was developed for the intention to miniaturize the valves by eliminating the vacant internal space of design 1. In the similar manner, several prototypes of design 2 were fabricated using PEA 5 x 5 x 10 mm (valve type 2-5510), PEA 5 x 5 x 5 mm (valve type 2-555), PEA 10 x 10 x 2 mm (valve type 2-10102), and PEA 3 x 3 x 5 mm (valve type 2-335) shown in Fig. 3.11, which is comprised of a PEA, a poppet, an O-ring, valve body

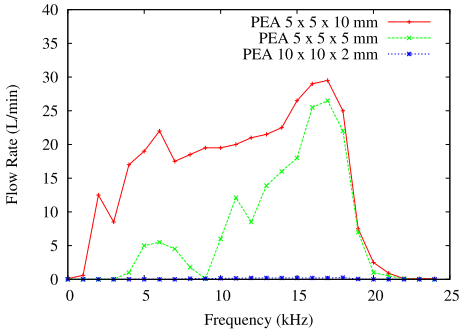

Figure 3.10: Flow rate - frequency relationship of unconstrained valves design 1 (orificeϕ1.2 mm, poppetϕ6 mm, pressure 0.5 MPa, input voltage 25 V)

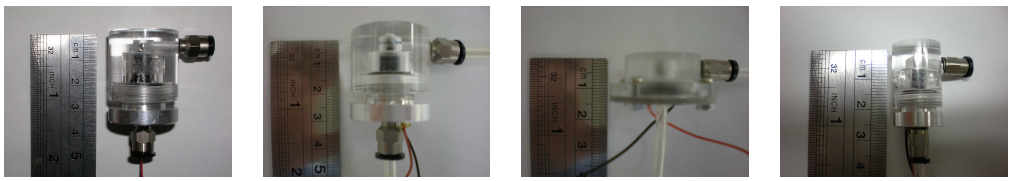

(a) Type 2-5510 (b) Type 2-555 (c) Type 2-10102 (d) Type 2-335

Figure 3.11: Fabricated unconstrained valves according to the structure in design 2. (a) PEA 5 x 5 x 10 mm (type 2-5510), (b) PEA 5 x 5 x 5 mm (type 2-555), (c) PEA 10 x 10 x 2 mm (type 2-10102), and (d) PEA 3 x 3 x 5 mm (type 2-335)

and case. To make it compact, the location of air inlet port is placed at the side of the valve body. The inlet port can be possibly located at the top surface where the air flows from the top downward, making the flow as simple as a straight line. An insight drawn from experiments indicates that the inlet port at the side has a better stability in practice, therefore, the inlet port is designed to be at the side.

The experimental result for design 2 is shown in Fig. 3.12 for orifice ϕ1.2 mm, poppet ϕ4 mm, input voltage 20 V and pressure 0.5 MPa. Comparing the results of design 1 and 2 (Figs. 3.10 & 3.12), it can be said that valves of design 1 have higher flow, which clearly implies that the internal vacant space has a role in determining the flow rate as explained earlier in Chapter 2. However, the internal vacant space consequently makes the overall size larger, suggesting size-flow rate tradeoffs in the valve design. Appropriate selection of poppet-orifice ratio is a way to help optimize the valve efficiency. This was verified by experiment shown in Fig. 3.13, where orifice ϕ0.8 mm has obviously higher output flow compared to ϕ1.2 mm. The experimental result in Fig. 3.13, PEA 10 x 10 x 2 mm has relatively low flow

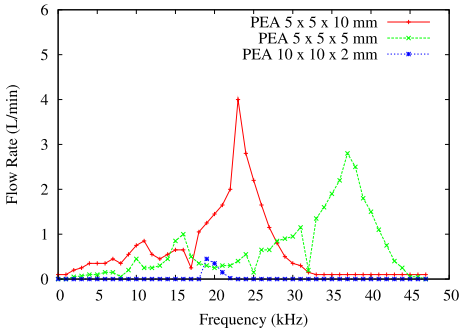

Figure 3.12: Flow rate - frequency relationship of unconstrained valves design 2 with spinning motion for PEAs 5 x 5 x 10 mm, 5 x 5 x 5 mm and 10 x 10 x 2 mm (orifice ϕ1.2 mm, poppet ϕ4 mm, input voltage 20 V, pressure 0.5 MPa)

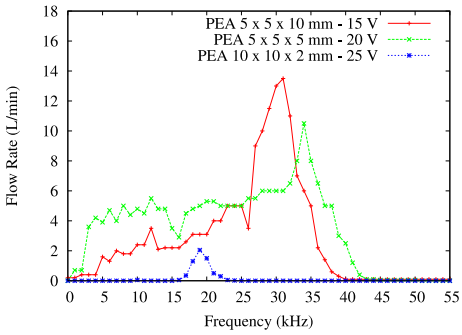

Figure 3.13: Flow rate - frequency relationship of unconstrained valves design 2 with bouncing motion for PEAs 5 x 5 x 10 mm, 5 x 5 x 5 mm and 10 x 10 x 2 mm (orifice ϕ0.8 mm, poppet ϕ4 mm, pressure 0.5 MPa)

rate as a result of inappropriate poppet - orifice ratio. As a consequence, a valve with small PEA size needs to be designed with a low poppet-orifice ratio to attain high efficiency. In Fig. 3.14, we developed a miniaturized valve of design 2 using PEA 3 x 3 x 5 mm with a smaller orifice diameter ϕ0.5 mm. The test result showed zero flow rate at inlet pressure 0.5 MPa, therefore, the experiment were carried out at lower pressure of 0.2 MPa (Fig. 3.14).

Based on the obtained results for design 2, we built new prototypes of design 3 with PEA of larger size has large orifice diameter while small PEA has a approximately small orifice size. As shown in Fig. 3.15, the design of prototypes for design 3 are divided into two: a) PEA 5 x 5 x 10 mm (type 3-5510) and PEA 5 x 5 x 5 mm (type 3-555) with orifice ϕ1.0 mm and poppet ϕ5 mm, and b) PEA 3 x 3 x 5 mm (type 3-335) and PEA 3 x 3 x 2 mm (type 3-332) with orifice ϕ0.5 mm and poppet ϕ3 mm. Design 3 has the

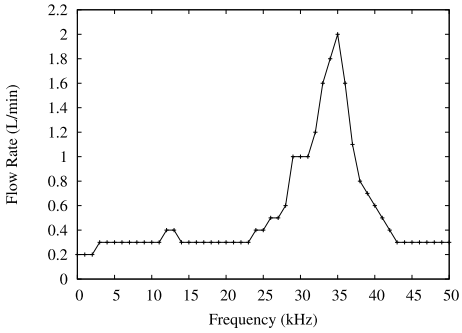

Figure 3.14: Flow rate - frequency relationship of unconstrained valves design 2 with bouncing motion for PEA 3 x 3 x 5 mm (orifice ϕ0.5 mm, poppet ϕ3 mm, input voltage 20 V, pressure 0.2 MPa)

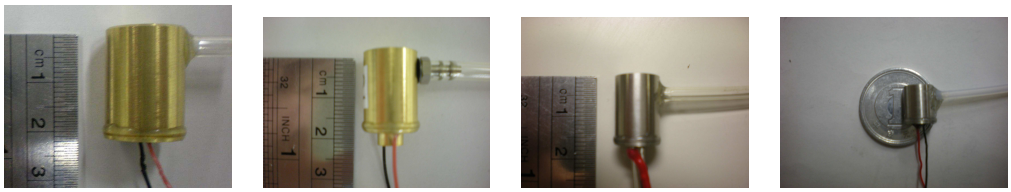

(a) Type 3-5510 (b) Type 3-555 (c) Type 3-335 (d) Type 3-332

Figure 3.15: Fabricated unconstrained valves according to the structure in design 3. (a) PEA 5 x 5 x 10 mm (type 3-5510), (b) PEA 5 x 5 x 5 mm (type 3-555), (c) PEA 3 x 3 x 5 mm (type 3-335), and (d) PEA 3 x 3 x 2 mm (type 3-332)

minimum number of parts where the O-rings are removed and the fasteners are replaced with adhesive bonding thus the total valve size is much more compact. Experimental results for valve type 3-5510 and 3-555 are shown in Fig. 3.16 for input voltage 24 V and pressure 0.5 MPa, while Fig. 3.17 shows the results for valve type 3-335 and 3-332 with input voltage 25 V and pressure 0.2 MPa.

The comparison of size and maximum output flow for prototypes design 1, 2 and 3 are summarized in Table 3.1. If the valves with PEA 5 x 5 x 10 mm are compared among design 1-5510, design 2-5510, and design 3-5510, design 1 has the highest output flow rate while design 3 has the most compact size with flow rate of 26 L/min. Comparing the size and the obtained flow rate, design 3 is preferable to design 1 or 2 although there is always a tradeoff between size and output flow. In applications for human-assist or wearable robots where the control valves have to be mounted on the robot or human, size is the primary concern. With respect to this, design 3 is considered as the most suitable design of unconstrained valves for robotic use. In reference [58], a miniaturized unconstrained valves had

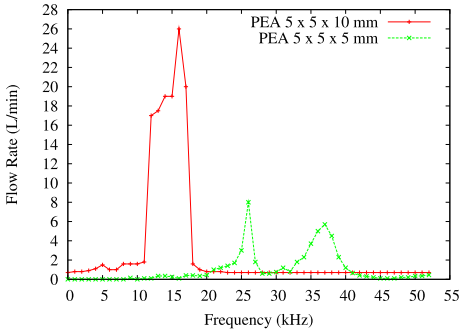

Figure 3.16: Flow rate - frequency relationship of unconstrained valves design 3 for PEAs 5 x 5 x 10 mm and 5 x 5 x 5 mm (orifice ϕ1.0 mm, poppet ϕ5 mm, input voltage 24 V, pressure 0.5 MPa)

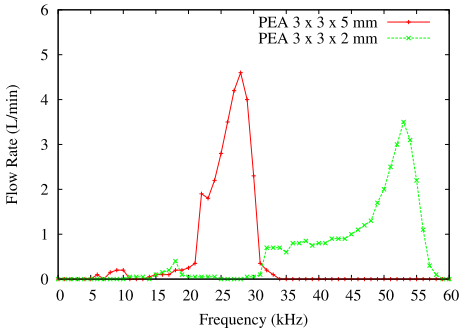

Figure 3.17: Flow rate - frequency relationship of unconstrained valves design 3 for miniaturization purpose using PEAs 3 x 3 x 5 mm and 3 x 3 x 2 mm (orifice ϕ0.5 mm, poppet ϕ3 mm, input voltage 25 V, pressure 0.2 MPa)

been developed using PEA 3 x 3 x 2 mm with total size of ϕ7 x 9 mm and flow rate 3.5 L/min (0.2 MPa). Fig. 3.18 shows the comparison between an unconstrained valve (design 3-332), a solenoid on-off valve and a pilot operated solenoid 3/2 directional control valve (DCV). The dimensions of solenoid on-off valve and pilot operated solenoid 3/2 DCV are 32 x 26 x 10 mm and 32 x 12 x 7 mm are compared, showing the volumetric ratio of solenoid valve : pilot operated 3/2 DCV : unconstrained valve design 3-332 = 18 : 6 : 1.

Table 3.1: Dimensions and flow rate of the fabricated unconstrained valves

Valve design	Prototype	Size (mm)	Max. flow rate (L/min)
Design 1	design 1-5510	30 x 26 x 30	29.5 L/min (0.5 MPa)
	design 1-555	30 x 26 x 25	26.5 L/min (0.5 MPa)
	design 1-10102	30 x 26 x 22	0.25 L/min (0.5 MPa)
Design 2	design 2-5510	ϕ28 x 33	13.5 L/min (0.5 MPa)
	design 2-555	ϕ28 x 28	10.5 L/min (0.5 MPa)
	design 2-335	ϕ15 x 25	2 L/min (0.5 MPa)
	design 2-10102	ϕ28 x 12	2 L/min (0.2 MPa)
Design 3	design 3-5510	ϕ15 x 21	26 L/min (0.5 MPa)
	design 3-555	ϕ15 x 20	8 L/min (0.5 MPa)
	design 3-335	ϕ10 x 15	4.5 L/min (0.2 MPa)
	design 3-332	ϕ7 x 9	3.5 L/min (0.2 MPa)

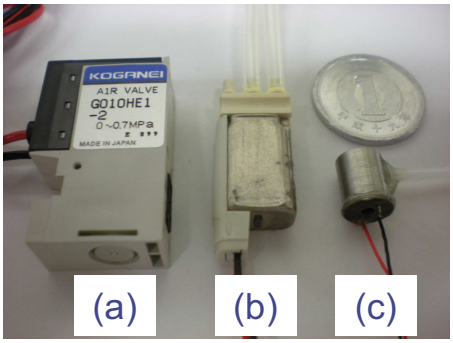

Figure 3.18: Comparison of miniaturized pneumatic valves: (a) solenoid valve (dimensions 32 x 26 x 10 mm), (b) pilot-operated solenoid 3/2 DCV (dimensions 32 x 12 x 7 mm), and (c) miniaturized unconstrained valve prototype of design 3-332 (dimensions ϕ7 x 9 mm)

3.4 Flow Characteristics of Unconstrained Valves

Unconstrained valves have two control variables as indicated in Fig. 3.1, *i.e.*, input frequency and voltage. Unlike the general solenoid on-off valves that is controlled by PWM input and has a constant flow output, unconstrained valves can be switched on and off with adjustable flow control due to the additional variables. The flow regulation can be implemented by varying the input voltage or frequency, where the output flow rate is a function of input frequency, voltage, and pressure ($Q = \mathrm{f}(f, V_{IN}, p)$). As a consequence, unconstrained valves possess more flexibility for the control of pneumatic actuators compared to the conventional solenoid valves.

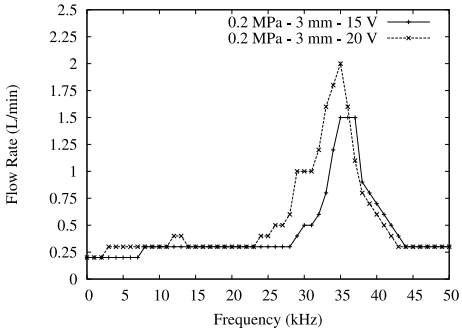

Figure 3.19: Frequency/flow rate response at various input voltages (PEA 3 x 3 x 5 mm, orifice ϕ0.5 mm, supply pressure 0.2 MPa)

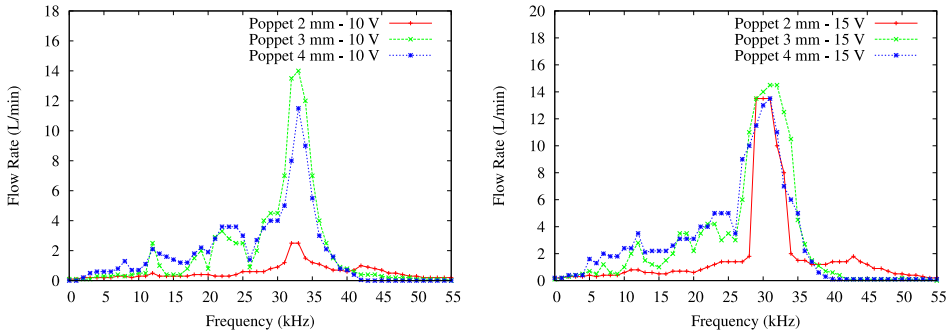

(a) Input voltage 10 V (b) Input voltage 15 V

Figure 3.20: Flow rate/frequency response of unconstrained valves for the observation of the influence of poppet sizes and input voltage (PEA 5 x 5 x 10 mm, orifice ϕ0.8 mm, supply pressure 0.5 MPa)

Unconstrained valves have a peak flow that is correlated to resonant frequency of the total mechanical system, consisting of the PEA and the valve body. The peak flow or resonance is also dependent on the input voltage, where the peak occurs at lower frequency as the voltage is increased (Fig. 3.19). Around the resonant region where the peak flow is found, two types of distinguishing flow characteristics were observed in relation to poppet sizes: a) the flow behavior has a slight difference in corresponding to the poppet size, which often occurs at low input voltage (Fig. 3.20(a)), and b) the flow rate did not change significantly and independent from the poppet size (Fig. 3.20(b)). From experimental results shown in Fig. 3.21 for the relationship between flow rate, input voltage and pressure (orifice ϕ0.7 mm, poppet ϕ4 mm, frequency 15 kHz), it is shown that the input voltage has saturation area where an increase in the input voltage will not change the output flow. Referring to Fig. 3.20 and Fig. 3.21, it can be said that the poppet size has no influence to the output flow rate when it is saturated.

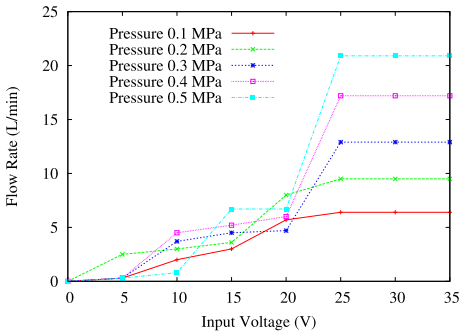

Figure 3.21: Flow rate - voltage relationship for different supply pressure

The generated flow is closely related to the opening area between the orifice and poppet, where the orifice is seated firmly wherefore the aperture is mostly realized through the motion of poppet. Based on the observation of poppet motion, we could distinguish two motions in accordance with input frequency: 1) no bouncing (spinning), 2) bouncing, and 3) idle motions (Fig. 3.22). Spinning motion takes place at low frequencies, whereas a higher input frequency near the resonance mode will cause the poppet to have a bouncing motion. At higher frequencies, poppet motion becomes weaker, resulting in idle motion. As observed, we can draw a direct connection between poppet motion and output flow by controlling the frequency. In addition, the bouncing motion of a poppet is also dependent on the input voltage. Spinning motion occurs at low voltage and above a certain voltage level, the poppet will have enough power for the initiation of bouncing motion otherwise the poppet is in spinning motion. To realize a bouncing motion, the valves should be excited with sufficiently high voltage or it is also possible by taking for granted the resonance mode.

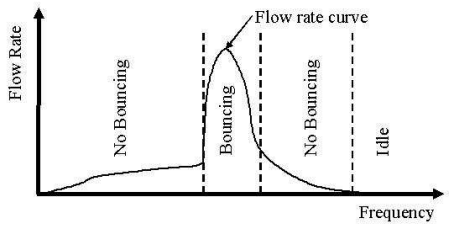

Figure 3.22: Poppet motions correlated to the flow rate output

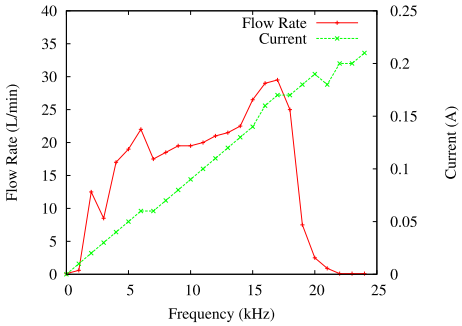

Figure 3.23: Current consumption for driving an unconstrained valve (input voltage 25 V, orifice ϕ1.2 mm, poppet ϕ6 mm, pressure 0.5 MPa)

Besides the input voltage, an observation of the input current, as shown in Fig. 3.23, indicates that the required current increases along with the increase of operating frequency. A theoretical study to match with the experimental result is referred to [55]. The average current required for a PEA in dynamic operation is calculated by:

$$i = fCU_{p-p}, \tag{3.4.1}$$

where the current consumption is linearly proportional to the input frequency from the calculation in Eq. 3.4.1.

The discussion on input - output relationship in this chapter is limited to the mechatronics point of view. In respect to the pneumatic or fluid dynamics viewpoint, valve with different internal geometry or shape may behave differently as the air flow dynamics may change according to the design. For instance, a slight change was observed in the size discrepancy of poppet cage, where a large poppet cage allows more space for the poppet movement thus resulting in higher flow rate and vice versa. It can be said that the difference of internal structure related to the principle of air flow is applicable to the valve design as well. Despite the high flow rate, the on-off switching operation for a valve having large poppet cage was occasionally impaired. In contrary, designing a valve with small poppet cage has high switching stability but lower flow rate as consequences.

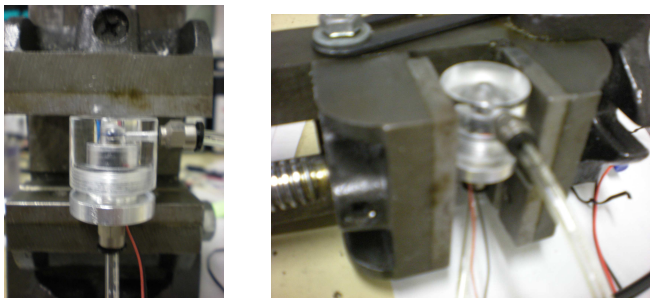

(a) Full/half-clamped (b) Side-clamped

Figure 3.24: Clamping condition for the flow stability test. (a) the valve was clamped vertically at the top and bottom (fully-clamped or half-clamped), (b) the valve was clamped from the side

3.5 Valve Mount and Clamping

The unconstrained mechanism may raise a presumption of performance abnormality due to the position / direction changes especially when the posture of the valve is reversed upside down. A simple experiment was carried out to assess the flow performance against the change of angular inclination, and it can be convincingly proven that unconstrained valves performed well irrespective of the direction changes.

Another aspect that may change the frequency - flow rate characteristics of the valve is the existence of additional objects in the valve vicinity that may give disturbance to the vibration-driven unconstrained valves. A small change in the mass, damping, and spring properties of the valve due to the existence of additional objects, such as a clamp or any supporting devices, will affect the overall valve performance. To assess the flow behavior under the existence of external objects, the unconstrained valves were experimented to check its flow stability, comparing the different clamping conditions (Fig. 3.24), while the experimental results, given in Fig. 3.25, were executed for different situations: unclamped, fully-clamped, half-clamped, and side-clamped. The results are separately shown for two poppet motions, *i.e.*, bouncing and spinning motion (Fig. 3.25(a) and (b)). It revealed that valve driven with bouncing motion (close to the resonant mode) could maintain the flow stability no matter of the clamping conditions, whereas the spinning motion is vulnerable to the external disturbance. For practical use in robotic applications, driving the valve at the resonant frequency will increase both the valve efficiency (higher flow rate) and flow stability as well.

In the production of multiple unconstrained valves, the mass - spring - damper parameters of the total valve system is vital for fabrication or as-

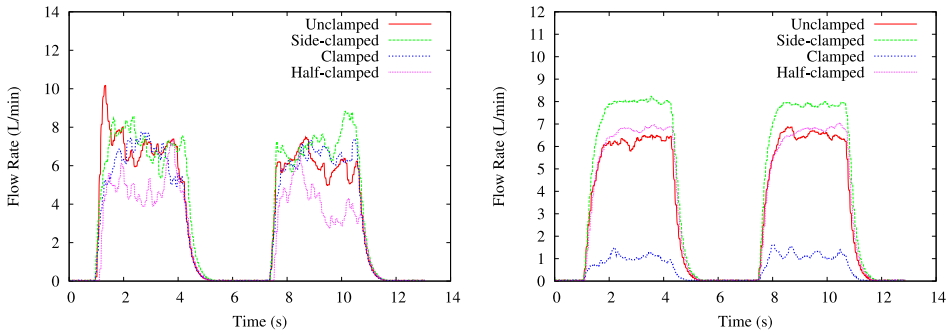

(a) Bouncing motion (b) Spinning motion

Figure 3.25: Flow stability test where the unconstrained valve is clamped. Experiments can be categorized into two conditions for poppet at (a) bouncing motion, and (b) spinning motion

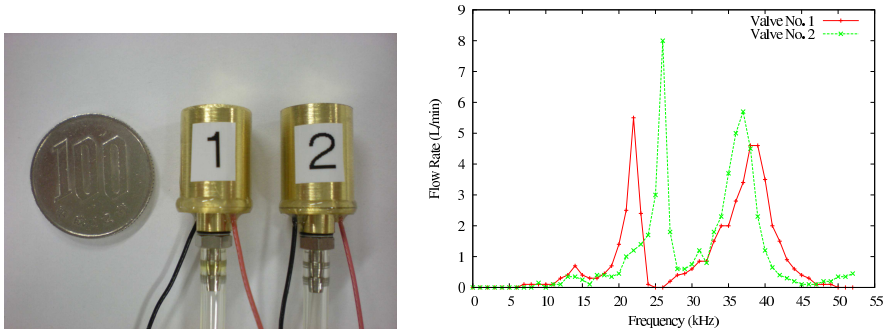

(a) Identical valves (b) Flow characteristics

Figure 3.26: Repeatability test for identical unconstrained valves. (a) Unconstrained valves with PEA 5 x 5 x 5 mm, orifice ϕ1 mm, poppet ϕ5 mm (mass of valve 1 & valve 2 = 10.86 g & 11.83 g). (b) Frequency - flow rate relationship for valve 1 and valve 2

sembly process. Two identical valves could have a totally different behavior if there is a slight difference during the assembly process that changes the value of mass - spring - damper parameters. To state this issue, two valves with the same dimension and specification were compared in Fig. 3.26(a), namely valve 1 (10.86 g) and valve 2 (11.83 g). Fig.3.26(b) shows the measured results for both valves, which indicated that both valves have different frequency - flow rate characteristics even though they are identical. The different flow characteristics may be considered as the result of the underestimated facts that the stacked-PEA has different number of piezoelectric layers, the most vital part of unconstrained valves.

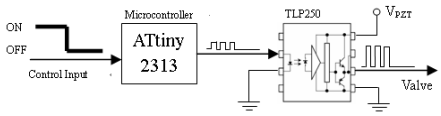

Figure 3.27: Schematic of PWM-control interface for unconstrained valves

3.6 Modulated Digital Unconstrained Valves

3.6.1 Pulse Width Modulated (PWM) Control Valve

This section introduces a direct PWM control capability for a frequency-controlled unconstrained valves. Unlike solenoid valves that are basically on-off switching valves controlled by a PWM input command, an unconstrained valve is responding directly to the input frequency or voltage. Because a direct PWM-commanded feature is somewhat mandatory in the practice of pneumatic control for robotic applications, an additional interface is required to transform PWM input command into a corresponding frequency-base input to unconstrained valves. For an unconstrained valve to perform PWM control by responding directly to input on-off commands via a built-in interface, a microcontroller is embedded to generate frequency waveforms. Introducing microprocessor control capabilities into unconstrained on-off valves involves two functional tasks, a periodic pulse generator for PEA and on-off switching control. Input reading of on-off status can be recognized easily by the microprocessor, and the harmonic output signal from the microcontroller is sent to a piezo driver to drive the PEA.

This PWM controller interface consists of a microprocessor and a piezo-driver unit with a schematic as shown in Fig.3.27. The realization of a digital PWM-controller using a Toshiba TLP-250 photocoupler for the piezo-driver measures 35 x 17.5 x 15 mm. Further miniaturization effort was achieved by changing the components with smaller IC packages, *i.e.* using PIC 12F683 for the microprocessor and the piezo-driver was implemented in HCPL-0314 photocoupler from Avago Technologies. A smaller PWM-control interface with HCPL-0314 photocoupler measures (L) 17 x (W) 17 x (H) 14 mm, and comparison to TLP-250 photocoupler is shown in Fig. 3.28(a). Valve performance for piezo-driver TLP-250 and HCPL-0314, represented by the frequency - flow rate relationship, is given in Fig. 3.28(b). The experimental results showed that the valve performance was deteriorated for the small IC package, which means that the total size and valve performance has tradeoffs related to the selection of IC packages.

PWM control using a microprocessor embedded into an unconstrained on-off poppet valve, *i.e.*, an unconstrained digital PWM-control switch-

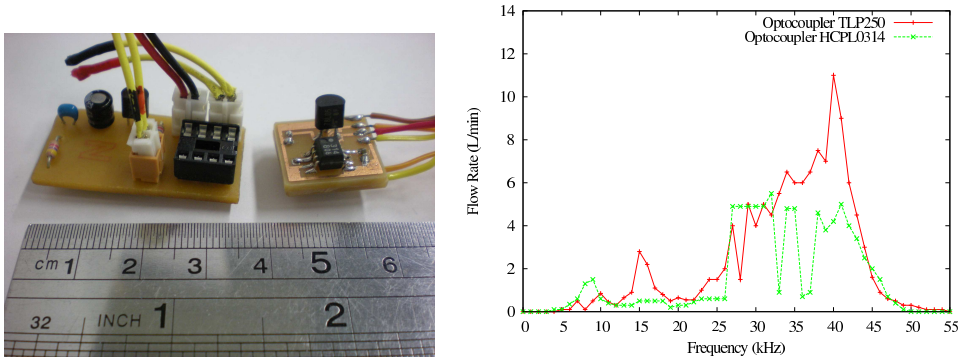

(a) PWM control interface (b) f - Q relationship

Figure 3.28: Miniaturized PWM controller board (a) with photocoupler HCPL-0314 as piezo-driver, (b) Comparison of valve performance for piezo-driver TLP-250 and HCPL-0314

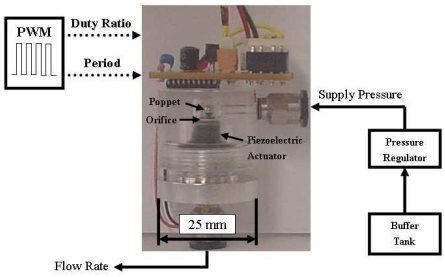

Figure 3.29: Miniaturized digital unconstrained PWM-control valve

ing valve, is illustrated in Fig. 3.29. The major difference between this type of PWM-controlled unconstrained digital switching valve compared to solenoid-driven on-off valves is that the driving voltage and frequency can be customized for unconstrained valves to adjust for flow changes, whereas the conventional solenoid valves has only pulse-modulated control. This unconstrained valve can also serve as a frequency-related flow regulator (Fig. 3.28(b)) in addition to pulse-width-modulated switching capability, which will benefit for the the applications of pneumatic control.

3.6.2 Valve ON-OFF Response

This section describes the ON-OFF response of unconstrained valves, where an unconstrained digital valve was switched over at a voltage of 10 to 20 V while the control pulse width was modulated from 20 - 80% and the results are shown in Fig. 3.30(a). It can be seen clearly in Fig. 3.30(c) that higher voltages were associated with higher flow rates but these were accompanied by harsh flow vibration. On the other hand, application of a lower voltage

Table 3.2: Valve response time for pressure 0.2 to 0.5 MPa

P	Valve Response Time(s)			F(s/L)	
(MPa)	Fill	Exhaust	β	Fill	Exhaust
0.2	0.632	0.8015	1.2682	23.0237	29.1985
0.3	0.733	0.9965	1.36	26.7031	36.3024
0.4	0.8905	1.262	1.4172	32.4408	45.9745
0.5	0.948	1.484	1.5654	34.5355	54.0619

to the valve caused a decrease in flow rate, with damping of the vibration and the flow became steady as shown in Fig. 3.30(b). The unconstrained mechanism means that the vibration cannot be eliminated completely, and in most cases the vibration will remain. A good result is that it could accomplish the pulse width modulated on-off operation satisfactorily; even the flow would unavoidably oscillate when activated.

3.6.3 Valve Response Time

Valve response time is defined as the time required for a control valve to fill a certain volume to 90% of supply pressure or to exhaust the volume to 10% of supply pressure [56]. The formula for valve response time, omitting the factor of valve dead time, is as follows:

$$\tau = F \times V_h, \tag{3.6.1}$$

As it is difficult to measure the valve dead time, it has been omitted here. However, the precise valve response time can be estimated from the variable F obtained by experiment. A valve with ϕ0.8mm orifice and a ϕ3mm poppet was experimentally deployed to fill and exhaust a constant volume, $V_h = 27.45$ mL, at various supply pressures. The valve response times are specified in Table 3.2, and the experimental results are shown in Fig. 3.31.

For comparison, we can see that the valve response time varied for different supply pressures. It takes a shorter time to fill a constant volume with lower pressure, and *vice versa*. Factor F is listed in Table 3.2 for the calculation in (3.6.1). The discrepancy in valve response time for fill and exhaust can be explained theoretically by considering the temperature inside the chamber as a series of adiabatic curves for the charging process and close to the isothermal assumption for discharge [57]. For the charging process (adiabatic, *i.e.*, $\Delta\, Q = 0$) :

$$\dot{p} = \kappa \left\{ \frac{RT}{V_h}(\dot{m}_1 - \dot{m}_2) - \frac{p}{V_h}\dot{V}_h \right\}, \tag{3.6.2}$$

and for the discharging process (isothermal, *i.e.*, T = constant):

$$\dot{p} = \frac{RT}{V_h}(\dot{m}_1 - \dot{m}_2) - \frac{p}{V_h}\dot{V}_h. \tag{3.6.3}$$

The above equations reveals that the charging speed is evidently 1.4 times faster than the discharging process. Several tests, as listed in Table 3.2, provided conclusive evidence that the valve response time to discharge is approximately β times higher than those when it is used to charge a volume. From this, Eq. (3.6.2) and (3.6.3) can be simplified as:

$$\dot{p} = \alpha \left\{ \frac{RT}{V_h}(\dot{m}_1 - \dot{m}_2) - \frac{P}{V_h}\dot{V}_h \right\}. \tag{3.6.4}$$

3.7 Conclusion

Miniaturization of valves is accompanied by a tradeoff between valve size and output flow, placing hindrance on valve miniaturization. Simply using high voltage input to increase flow is a trivial solution but high-voltage drivers are usually bulky and difficult to miniaturized, making it desirable to limit the operating voltage. Maximizing flow requires the following unconstrained-valve design parameters be considered:

- A compact valve with a high flow is designed by appropriately combining the poppet - orifice diameter based on PEA size and a poppet - orifice ratio exceeding 4.
- Base thickness is functionally similar to a diaphragm. A thin base inevitably has a higher flow.
- Experiments confirm that the valve material does not affect the output flow.
- Large accumulator volume (hollow valve space) leads to higher flow but contradicts the purpose of miniaturization.

Comparing different miniaturization designs 1-3 for unconstrained valves shows that design 1 has the highest flow, followed by designs 2 & 3. Design 3 has the most minimum size and part number, which uses a slim base similar to a diaphragm to amplify the output flow. A miniaturized prototype of design 3 with PEA 3 x 3 x 2 mm has been realized, having a total size ϕ7 x 9 mm and flow rate 3.5 L/min (0.2 MPa) [58]. The valve flow dependency on input voltage, poppet size, supply pressure, and mounting/clamping conditions was described. Finally, a digital PWM-controller was embedded into a piezoelectrically-driven unconstrained valve and the valve ON-OFF response time for charging and discharge process were measured.

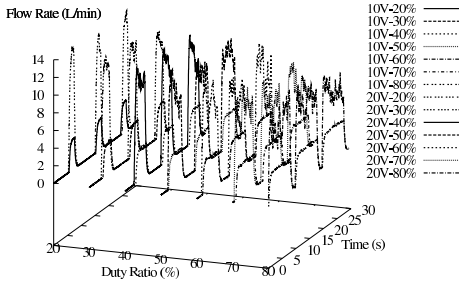

(a) Duty ratio 0.2 to 0.8 with input voltage 10 V and 20 V

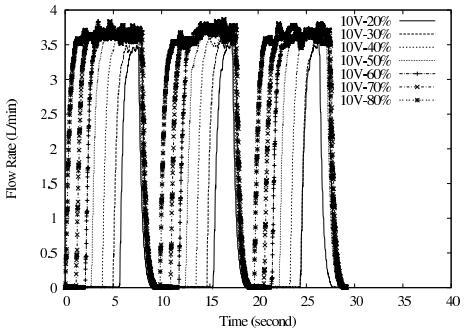

(b) Input voltage 10 V

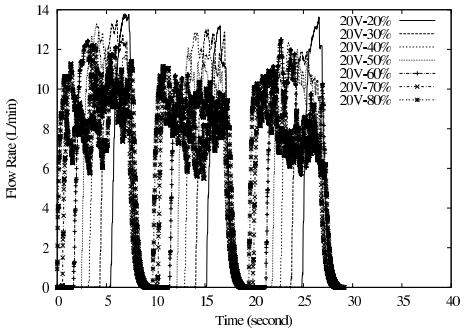

(c) Input voltage 20 V

Figure 3.30: PWM control of valve tested at various voltage and duty ratio

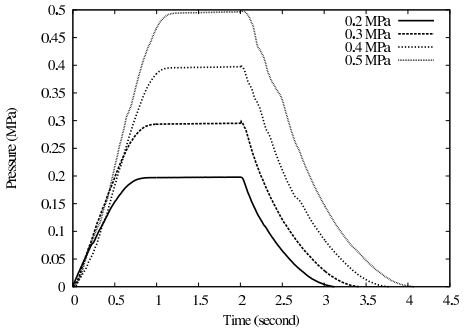

Figure 3.31: Valve response time of various supply pressure

Chapter 4

Advantages and Features of Unconstrained Valves

4.1 Requirement of On-Off Valves

This section focuses on the performance requirement of an on-off valve and discusses design parameters in achieving the optimum valve specifications. In [59], several criterions that are important for the design of a fast-acting valve are categorized into: sealability, method of closure, shape of the closing element, actuation method, actuation dynamic characteristics, flow characteristics, flow path inside the valve body, and material of parts comprising the valve. Depending on the applications, several criterions are crucial and have to be considered to the maximal design while others are insignificant. Each criterion should be carefully considered depending on the application in where the valve is used. The main objective for the development of unconstrained valves is to be used as a control device for wearable (human-assist) robots, therefore, flow-to-weight(size) ratio may be the first priority. In general, several aspects that are considered important for the applications in robotics include valve switching time and flow-to-weight(size) ratio.

Literature study on the approaches to improve the valve dynamic response can be found in [60, 61], which discuss the investigation on the influence of the armature mass to the valve response. Kushida and Kajima-Kawamura reported that high speed valve operation can be possibly obtained by:

- Reducing the weight of moving parts or decreasing the moving mass as much as possible
- Increasing the generated force from solenoid to actuate the armature

- Eliminating the resistance force due to frictions or opposing reaction

The contradiction in valve design is that a need of large solenoid force will generally require larger armature, resulting in an increased size and weight of the moving parts. Additionally, a larger inductance required for the solenoid causes a slower current response, which in total lead to a slower operation response. Optimal design does not solely mean to necessarily reduce the weight of the moving parts but the improvement is achieved by redesigning the parameters of the solenoid, *i.e.*, dimension of the solenoid and the number of coil turns. This suggested that design parameters have to be optimized to achieve high-speed operation under given conditions.

In regard to the valve switching time is the delay (or offset) normally occurs at the instantaneous opening and closing times. During the operation of a valve, the electromechanical interactions possess a delay as the time difference between the exciting pulse is triggered and the moment the valve begins to deliver the flow. The delays promote a dead-time, commonly known as offset, which will eventually affect the control accuracy of the total system because most accurate control requires the minimal pulsing time [62]. For pneumatic control, accurate control in turn requires minimizing the valve opening and closing times.

Another important aspect except the valve weight and switching response is the flow-to-weight ratio, which is a measure for the amount of flow rate in proportion to valve weight. The conclusions drawn from the miniaturization of valves is that miniaturized valves tend to have a decreasing flow rate because the miniaturized actuators are usually weaker. The difficulty in solenoid miniaturization has initiated the search for a new high-force actuator that is small and lightweight. Smart actuators are suitable candidates for their high power density, high-efficiency, low weight, and small volume. In [30], stacked-PEA was considered as the most appropriate actuator among the smart actuators for the development of a compact valve. The desired requirement for autonomous robots are high output flow and small size, which is crucial for the operation of a pneumatic actuator to increase high frequency bandwidth range. However, the valve miniaturization using PEA also has a tradeoff between size and obtainable flow rate as outlined in the previous chapter. The common practice to increase the efficiency of PEAs by adding an inductor in series with the piezoelectric actuator is known to be effective to increase the power density. The series connection between an external inductor and a PEA, which is primarily a capacitive load, is called a second-order LC tuner. This LC tuner is effective to improve the output flow of an unconstrained valve while keeping the size small.

This chapter is organized as follows. Section 2 of this chapter investigates the switching time (offset) of an unconstrained valve. Section 3

presents the method to improve the valve output flow rate using a second-order LC tuner, where the simulation and experimental results are presented. Section 4 draws a comparison between unconstrained valves and the currently available pneumatic valves. Section 5 introduces briefly the pro and cons of unconstrained valves for use in robotics, which covers an application note for controlling a pneumatic cylinder and artificial muscle.

4.2 Switching Time

As mentioned earlier, the poppet of an unconstrained valve has two types of motion, *i.e.*, bouncing and spinning motion. Experiments were conducted to find the time required to open the unconstrained valves for both the bouncing and spinning motion, and the result of three time trials for the bouncing motion is shown in Fig. 4.1. The results in Fig. 4.1 show that the opening time is comparatively similar each other, while the measured deadtime or offset for three time trials are 50, 50 and 80 ms, respectively. The experimental result revealed that the excitation of bouncing motion happens randomly, which also causes the random offset at the switching phase. Fig. 4.2 shows the comparison of switching time for the bouncing and spinning motion. From experiments, it revealed that the valve opening time of the spinning motion is quite slow until it reaches the steady setpoint. The offset of spinning motion is about 80 ms, which is more or less similar to the previous result of the bouncing motion. The randomized offset time may be suppressed by the control of the poppet motion, which suggests a feedback control for the valve.

Even though the unconstrained valves have the same dead-time for the bouncing and spinning motion, the bouncing motion has shorter opening time, which made it suitable for the improvement of control accuracy. Most solenoid on-off valves have a switching time between 3 to 5 ms [63, 64], and a special design of solenoid to achieve a high-speed solenoid valve with switching time less than 1 ms has been reported in [61]. Yokota and Akutu proposed a high-speed displacement control method for the poppet valve and a high-speed digital valve with switching time of 100 μs has been presented in [65], which is extremely fast in comparison to the unconstrained valves. In regard to valve switching time, it is clear that unconstrained valves are inferior from the solenoid on-off valves in regard to the control accuracy.

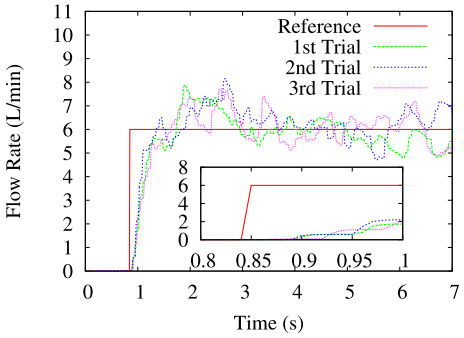

Figure 4.1: Time offset of unconstrained valve with bouncing motion tested for three time trials

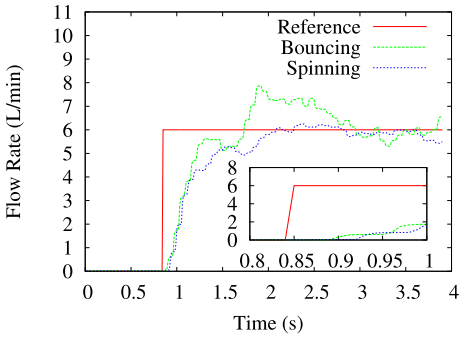

Figure 4.2: Comparison of time offset for bouncing and spinning motion

4.3 LC Tuner to Enhance Flow

The miniaturization effort always has to face with the tradeoffs between output flow and size, which limits the attainable flow-to-weight ratio. The reason is that the sizes of PEA and orifice has to be selected as small as possible for a miniaturized unconstrained valve, therefore, the attainable flow is consequently low. A way to increase the output flow by increasing the input supply voltage is impractical, which at the same time arouses the difficulties in miniaturizing high-voltage power driver. Therefore, the miniaturization problem is a selection between the valve size, operating voltage, desired flow rate, and size of the control driver. Design for the miniaturized unconstrained valve is to find the optimum condition that minimizes the sizes of valve and control driver, and maximizes the output flow, which has no matched solution. As an alternative solution, a second-order LC tuner is widely known for its simplicity and compactness, where a high efficiency is maintained by connecting an inductor in series with the PEA. The amplification is solely affected by an inductor, so a tuning process to determine the suitable inductor value is relatively easy. In this

Table 4.1: Voltage and current generated by LC tuner at resonance.

Inductance L_{coil} (μH)	Voltage (V)	Current (A)	Peak flow (L/min)
150	25	0.27	0.8
100	30.3	0.32	1.3
56	31.3	0.36	1.6
40	26.3	0.31	1.1
2.7	20.8	0.24	0.7
0	20.3	0.2	0.4

section, an experimental result is provided to show the effectiveness of an LC tuner to improve the valve performance, followed by the description of the theoretical background to further understand the characteristics of a LC-tuning valve.

4.3.1 Experimental Results

The effectiveness of a LC tuner to increase the output flow is investigated through experiments to compare the generated flow rate between using a LC tuner and PEA alone. As shown in Fig. 4.3(a), higher flow rate was obtained from a LC tuner compared to a capacitive PEA alone, which shows an improvement in the valve efficiency using a LC tuner. The experimental results in Fig. 4.3(a) showed a peak value at $L_{coil} = 56$ μH, while a tendency of decreasing output flow was observed for the other inductances. The relationship between inductance - output flow can be described as a hyperbolic function with the peak illustrates the resonant frequency. Therefore, it is necessary in the implementation of an LC tuner to find the peak value by selectively tuning the appropriate inductance. An theoretical description is given in the section 4.3.2 for the estimation of inductance during the tuning process.

The plot of current consumed during the valve operation helps to further understand the behavior of an LC tuner as shown in Fig. 4.3(b). By mapping the maximal obtained flow and current for each inductor, it is clear that the output flow is proportional to the supplied current. Fig. 4.4 shows the current waveforms when the valve has the peak flow at the resonance for input voltage 20 V. The descriptions of the supply voltage and current for each inductance are compared in Table 4.1. From the experimental results, it can be concluded that LC tuner amplifies both the input voltage and current, and multiplies the output flow depending on the inductance. An increase of approximately 3 to 4 times are obtained for the output flow for $L_{coil} = 56$ μH.

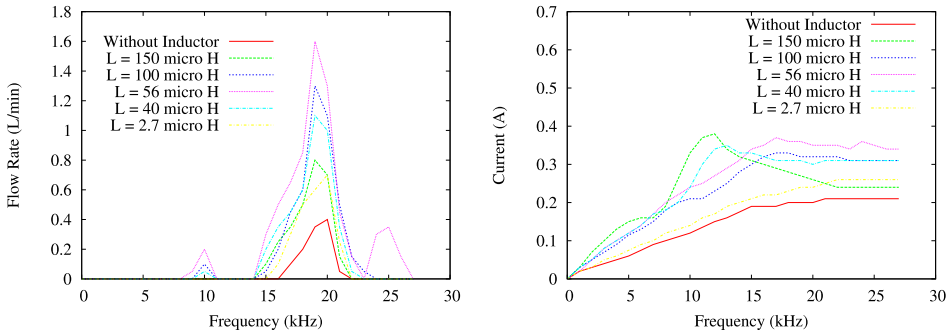

(a) (b)

Figure 4.3: Experimental results for LC tuners with inductor L_{coil} = 150, 100, 56, 40 and 2.7 μH (PEA 10 x 10 x 2 mm, capacitance $C = 500$ nF, input voltage 20 V, pressure 0.2 MPa). (a) flow rate - frequency relationship, and (b) Current consumption - frequency relationship

4.3.2 Theoretical Background

The theory behind the PEA and LC tuner is basically a driver circuit to amplify the current flowing into a PEA taking the advantages of resonance behavior between an inductor in series to a PEA. In the following, the relationship between the current output from an LC tuner and the valve output flow is studied by using an electromechanical model of a PEA to relate the generated current with the mechanical output of a PEA, which is required to select the inductance of a LC tuner. Finally, the simulated result of the LC model are given as an illustration to compare the resonance behavior for different inductances.

4.3.2.1 Electrical model of an Piezoelectric Actuator

Refer to Chapter 2 for the multi-stacked PEA model where the piezoelectric wafers are in series mechanically and in parallel electrically, the complete electromechanical model of a PEA reported in [43, 48] are reproduced in Fig. 4.5 to differentiate the hysteresis and piezo effect. H represents the hysteresis effect and U_h is the voltage due to the hysteresis effect. The piezo effect is represented by T_{em}, which is an electromechanical transducer with transformer ratio T_{em}. The capacitance C represents the sum of the capacitances of the individual piezo wafers. The total current flowing through the PEA is $\dot{q}$. The charge q_p is the transduced charge from the mechanical side. The voltage U_p is due to the piezo effect. The total voltage over the PEA is V_{IN}. The force F_p is the transduced force from the electrical side. The force F_e is externally applied. The resultant force $F_p - F_e$ mechanically drives the piezo material. The resulting elongation of the PEA is denoted by y. The

mechanical relation between F_p and y is denoted by M. Assuming there is no loss at the PEA, the correlation between current $\dot{q}_p$ and PEA elongation rate $\dot{y}$ according to Eq. 3.2.5 is $V_{IN}\dot{q}_p = F_p\dot{y}$. If higher current is supplied to the PEA, the PEA will move at higher speed that will alternatively increase the force F_c transmitted to the poppet as specified in Eq. 2.2.16 - 2.2.17. Based on this hypothesis, we can conclude that the valve output flow is related to the control of PEA current / velocity.

Since the electrical characteristic of a PEA is essential in the analysis and design of an LC tuner, the equivalent circuit model of a PEA are given in Fig. 4.6. Without considering the energy dissipation and PEA hysteresis, PEAs are often simply considered as capacitances in their equivalent circuit models. PEA behaves like a capacitor if there is no resonance, therefore, PEA elements modeled as capacitors are often satisfactory. For the application of unconstrained valves, the consideration of energy dissipation can not be omitted because the valve includes the transfer of power from a PEA to the poppet. For this purpose, an accurate equivalent circuit model proposed in [66] is used to describe the physical meanings of a PEA. As shown in Fig. 4.6(a), the equivalent circuit is divided into two parts: the non-resonant and resonant parts. The impedance of the non-resonant and resonant parts, denoted by Z_c and Z_r are as follows:

$$Z_c(s) = \frac{R_p(R_s + \frac{1}{sC_0})}{R_p + R_s + \frac{1}{sC_0}} \tag{4.3.1}$$

$$Z_r(s) = R_m + sL_m + \frac{1}{sC_m} \tag{4.3.2}$$

The total impedance Z for the whole PEA model is calculated as:

$$Z(s) = \frac{Z_c(s)xZ_r(s)}{Z_c(s) + Z_r(s)} \tag{4.3.3}$$

The physical meaning for each component of the equivalent model in Fig. 4.6(a) is explained in [66]. The component C_0 represents the dominant capacitance of the PEA, while the components L_m, R_m and C_m are relevant to the equivalent mass m, damping coefficient c, and spring constant k, respectively. In the circuit model, the components L_m, R_m and C_m in the resonant part stand for the mechanical resonant mode. Component R_p is responsible for the internal charge leakage, which is related to the energy dissipation.

4.3.2.2 Second-order LC Tuner

The description of LC tuner used in this context is external inductor L_{coil} in series with a capacitive PEA as load C. The PEA also includes internal

resistance as shown in Fig. 4.6(a), so an LRC circuit analogy is used to calculate the LC tuner used in the PEA at a resonance. As illustrated in [67], a PEA itself can be represented as a capacitor C and mechanical impedance Z, *i.e.*, an LRC electrical equivalent circuit. Assuming that the PEA is primarily a capacitive load, an LC tuner can be expressed with the following second-order series LRC circuit:

$$L_t \frac{d^2q}{dt^2} + R_t \frac{dq}{dt} + \frac{1}{C_t} q(t) = V(t), \tag{4.3.4}$$

where

$$L_t = \frac{L_{coil} L_m}{L_{ext} + L_m}, \tag{4.3.5}$$

$$R_t = \frac{R_p R_s R_m}{R_s R_m + R_p R_m + R_p R_s}, \tag{4.3.6}$$

$$C_t = C_0 + C_m. \tag{4.3.7}$$

The complex admittance $Y(s)$ can be solved by arranging Eq. 4.3.4 with the current $i(t) = dq/dt$:

$$Y(s) = \frac{I(s)}{V(s)} = \frac{s}{L_t(s^2 + \frac{R_t}{L_t}s + \frac{1}{L_t C_t})}, \tag{4.3.8}$$

taking the magnitude:

$$|Y(s = i\omega)| = \frac{1}{\sqrt{R_t^2 + (\omega L_t - \frac{1}{\omega C_t})^2}} \tag{4.3.9}$$

Adding an external inductor L_{coil}, the inductor resonates with the precharged PEA assumed as a capacitor at the following frequency:

$$\omega_0 = \sqrt{\frac{L_m + L_{coil}}{L_m L_{coil}(C_0 + C_m)}} \tag{4.3.10}$$

4.3.3 Simulation Results

The LC tuner described in Eq. 4.3.9 is simulated for PEA 10 x 10 x 2 mm with capacitance 500 nF and multiple set of inductances, with the calculated results shown in Fig. 4.7. The simulation assumes the internal PEA resistance $R_t = 10\Omega$. From the simulation results, the current response of an LC tuner shows one peak recognized as the resonance and admittance decreases for higher frequency. Additionally, the resonance for high admittance occurs at lower frequency while resonance at higher frequency is found for the PEA alone. The serially connected external inductor shifts

the resonance at lower frequency to minimize losses in the PEA. Similar results were obtained from experiments shown in Fig. 4.8, which is given here for the validation of the simulation results. Both the experimental and simulation results show that LC tuner generates higher current compared to PEA alone, thus the addition of an external inductor improves the power delivered to the poppet.

4.3.4 Open-loop Valve Control with LC Tuner

With significant power lost due to PEA capacitance and only a small fraction of input electrical energy converted into mechanical work [68], the PEA must be made more efficient to avoid high voltage operation. A method to improve capacitive PEA efficiency is to use an external inductor, recovering unused energy for reuse in the next cycle. Resonance between the inductor and capacitor efficiently and simply recovers charge to achieve a theoretically lossless PEA [68]. As described earlier in Eq. 3.2.6 and 3.2.7, the permissible current flow to the PEA is limited for a miniaturized valve as the length L and cross-sectional area A of a PEA becomes smaller. However, LC tuner could amplify the output flow especially for the miniaturized valve using an external inductor to recover the power loss at PEA.

Similar technique to the LC tuner, known as "charge recovery method" or "lossless LC network", has been widely applied in the design of power electronics for PEAs [68, 69]. When a PEA is supplied with electrical input, only a small fraction of the input electrical energy stored in the volume of the piezoelectric material can be transformed into mechanical work done on the load. The remainder is unused energy that is in fact recoverable. By using the LC tuner which is high-efficiency and theoretically lossless, the stored charge in the PEA can be extracted by immediately returning it in the next cycle. The natural resonance principle occurring in an LC circuit can be exploited to recover charge. For the application in unconstrained valves, the external inductor have to be chosen depending on the size and capacitance of a PEA to have minimum losses at the resonating frequency.

4.4 Size and Weight Comparison

The compact and lightweight valves are indispensable for the applications of wearable robots, however, the miniaturization is hindered by the decreasing output flow as the valve is miniaturized and it is almost practically hard to keep the flow high without increasing the input voltage while making the size smaller. The only alternative to improve the output flow is through using LC tuner to recover the power losses at the internal PEA to retain the energy efficiency as high as possible. Fig. 4.9 draws a comparison for SMC

Table 4.2: Comparison of miniaturized pneumatic valves

Valves	Size (mm)	Volume (mm^3)	Weight (g)	Operating pressure (kPa)	Cv	Power consumption	Leakage	Number of ports
Commercial								
Lee (HDI)	7.5x12.9x34.2	3308.85	4.5	0 - 310	0.013	850 mW	25μLPM@34kPa	3-way
Pneutronics (SRS)	10x15.5x38	5890	6.57	0 - 586	0.0075	2 W	0.016 SCCM	3-way
Numatics (TM series)	10x22x26.92	5922.4	Unknown	0 - 690	0.010	1.2 W	0.3 SCCM	3-way
Clippard EE3-TL	10x18.3x34.2	6258.6	Unknown	0 - 869.5	0.0086	1.1 W	Unknown	3-way
SMC (S070 series)	7x12x32	2688	5	0 - 500	0.011	0.5 W	Unknown	3-way
Microvalves								
Bimetalic [33]	6x6x0.02	7.2	Unknown	0 - 1000	0.0006	1 W	10 mL/min	3-way
Thermopneumatic [70]	8x8x2	128	Unknown	0 - 345	0.001	40 mW	Unknown	3-way
SMA [13]	15x15x15	3375	Unknown	0 - 245	0.0005	370 mW	5 mL/min	3-way
Electromagnetic [23]	10x10x4.3	430	Unknown	50 - 200	0.0022	300 mA	6 SCCM	2-way
Unconstrained valves								
PEA 3x3x5 mm	10x20x21	4200	21.63	0 - 500	C_{vs}=0.0038 C_{ve}=0.008	900 mW (20 V, 45 mA)	(<0.09 L/min)	3-position 3-way
PEA 3x3x2 mm	7x16x16	1792	6	0 - 500	C_{vs}=0.00216 C_{ve}=0.00077	60 V	0.1 L/min	3-position 3-way

S070 series miniaturized pilot-operated solenoid valves measuring 7 x 12 x 32 mm, and unconstrained valves measuring 10 x 20 x 21 mm (PEA size 3 x 3 x 5 mm) and 7 x 16 x 16 mm (PEA 3 x 3 x 2 mm). Without LC tuner, the unconstrained valve has a flow capacity of 2 - 3 L/min at operating pressure 500 kPa. Table 4.2 shows the comparison for miniaturized pneumatic valves, *i.e.*, commercial valves, microvalves, and unconstrained valves. The smallest commercial valve developed to date is the SMC S070 series 3/2 Directional Control Valve (DCV), however, it has a drawback of being a pilot-operated solenoid valve with the high rate of malfunction at low pressure. The microvalves have extremely small size excluding the package size, however, their actual size after packaging may be much larger compared to the size of the valve. Also, the maximum operating pressure and output flow of microvalves are generally too low for use in wearable robots. The overall comparison in Table 4.2 shows that the proposed unconstrained valves are relatively compact among all the valves with operating pressure around 500 kPa. Moreover, the output flow of unconstrained valves could be amplified using LC tuner for application requiring faster actuation.

4.5 Conclusion

Compared to the conventional solenoid valves that are basically controlled by PWM, unconstrained valves have more attractive features, *i.e.*, compactness and frequency / voltage-related flow control (f-Q, V-Q, and PWM-Q control mode). The advantage of using unconstrained valves is because it has three control mode, where the frequency - flow rate (f-Q) mode allows the emulation of PCM control with only one unconstrained valve, making the total valve size compact. In contrary, unconstrained valves lack of mechanical linkage between the poppet and valve seat, therefore a high air pressure from the inlet should exist to directly push the poppet into the

valve seat. The need of high pressure air to close the valve may sometimes causes error during the control operation, which is considered as a disadvantage of unconstrained valves. Concluding the overall advantages and disadvantages, an unconstrained valve is compact and superior in the flow-to-weight ratio compared to other valves, making it suitable for wearable or human-assist robots. The flow-to-weight ratio of unconstrained valves can be further increased using an additional inductor to form a LC circuit. However, a careful attention is needed in using unconstrained valves prior to an unexpected error of the switching operation caused by directional or positional changes.

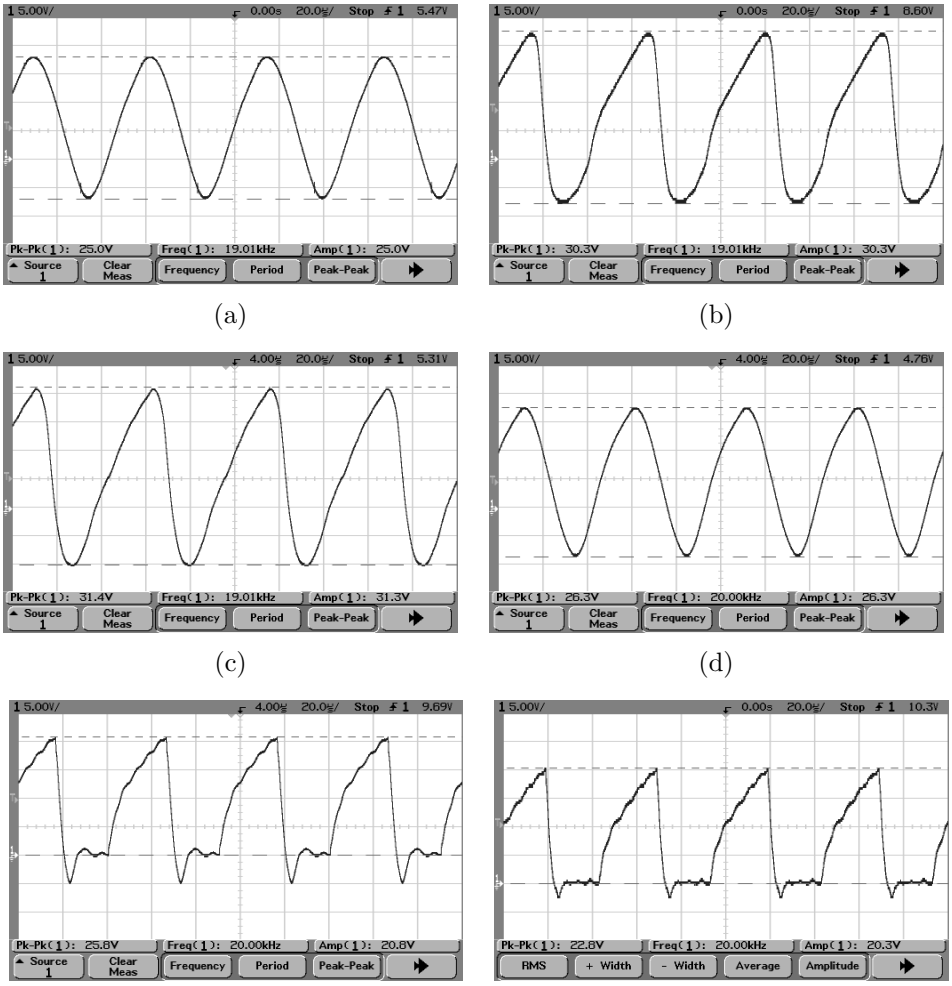

Figure 4.4: Snapshots of the PEA internal voltage(current) snapshots when the valve is driven at resonance with supply voltage of 20 V. (a) $L_{coil} = 150$ μH, (b) $L_{coil} = 100$ μH, (c) $L_{coil} = 56$ μH, (d) $L_{coil} = 40$ μH, (e) $L_{coil} = 2.7$ μH, and (f) with no inductor.

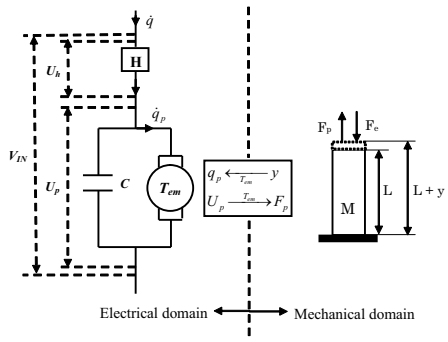

Figure 4.5: Electromechanical model of a piezoelectric actuator refer to [43]

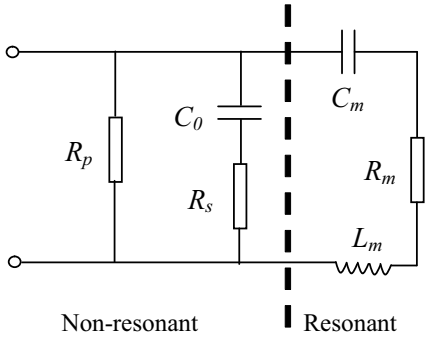

Figure 4.6: Equivalent circuit model of a PEA

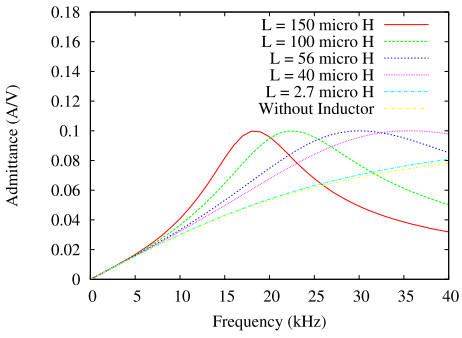

Figure 4.7: Simulated results for the admittance $Y(i\omega)$ of LC tuners with capacitance $C = 500$ nF and inductors $L_{coil} = 150$, 100, 56, 40 & 2.7 μH

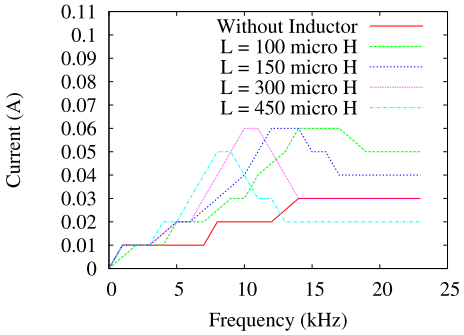

Figure 4.8: Experimental results for the current consumption of a PEA (size 10 x 10 x 2 mm, capacitance 500 nF) when inductors L_{coil} = 100, 150, 300 & 450 μH are connected in series with a PEA.

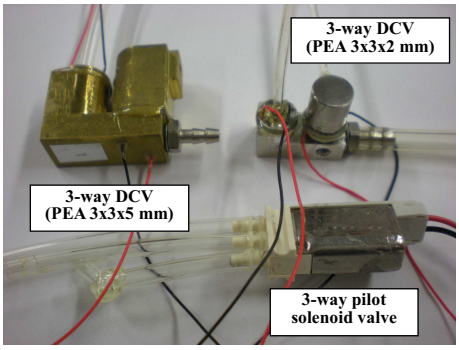

Figure 4.9: Miniaturized unconstrained valves with PEA 3 x 3 x 5 mm and PEA 3 x 3 x 2 mm compared to SMC S070 series miniaturized pilot-operated solenoid valve.

Chapter 5

Miniaturized Pressure Control Valve With Unconstrained Valves

5.1 Introduction

Pneumatic Artificial Muscle (PAM) is a type of pneumatic actuator with an extensive history of applications in biomechanics since 1950s. Due to their relatively short fatigue life and control difficulties when compared with counterpart electric motors, PAMs have not been extensively explored in robotics, motion control, and other industrial applications. Recently, however, PAMs have become more popular in robotics, especially in wearable robots, power-suits, human assistance and rehabilitation robots, because of their high power to weight ratios, low cost, light weight, and inherent compliance. Compliance is an important feature for rehabilitation robots, which must interact safely with humans [71]. Moreover, PAMs generate higher force output than other pneumatic cylinders.

Applications using PAMs for robotic systems also require that the entire pneumatic system be portable. These include humanoid robots [72, 73], wearable robotics for rehabilitation [74], peristaltic locomotion within curving tubes [75], robotic hands [76], and autonomous hybrid microrobots [13]. The principle disadvantage of using pneumatic actuators is the hindrances caused by the weight and size of the bulky compressors, accumulators, and control valves. To ensure the mobility of a pneumatic robot, high-pressure CO_2 tanks [77] and DC-motor driven micro compressors are now utilized as air sources. Micro Electro Mechanical System (MEMS) microvalves have been used to control micro-pneumatic artificial muscle [13, 14], although they are currently limited by their low output flow (< 1 L/min). Further miniaturization from the presently used solenoid-actuated valves has been

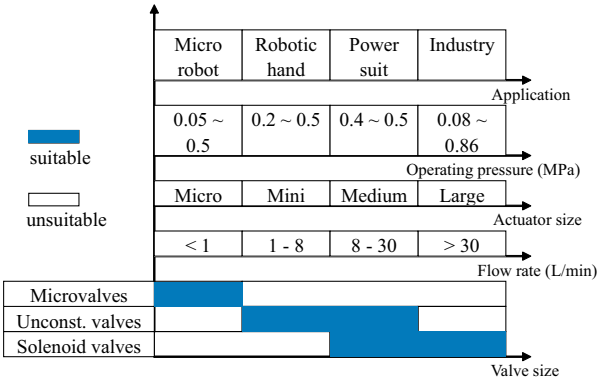

Figure 5.1: General description of valve categories for pneumatic control.

difficult because the generated force depends on the applied current and on the number of turns of wire in the solenoid, which implies that the induced force is too weak on the microscale. The difficulty of using solenoid for miniaturization is in designing a sufficient number of turns; thus, most solenoid driven microvalves do not provide sufficient force for most valve applications [78, 79]. To generate sufficient force, the solenoid itself requires more space than the main valve area. Therefore, research on miniaturization of valves has been shifted to PEAs. The advantages of using PEAs are low power consumption, high response, high potential for downsizing, commercial availability, and MR compatibility; nonetheless, the need for high voltage drives makes the design of wearable robots problematic. The development of new types of miniature valves is required to augment the practicability of pneumatic actuators.

Our approach using a PEA combined with an unconstrained mechanism has been designed for miniaturization and especially for low-voltage operation. Although oscillations was observed in the outflow of miniaturized unconstrained valves, the unsteady flow is not a problem for pressure/position control since its effect is small for PWM switching at kHz frequency. As the attainable flow is in the range of tenths of L/min, the unconstrained valves are intended to control mini to medium size actuators (Fig. 5.1). Standard solenoid valves can be used for the large pneumatic actuators, while microvalves can be used for micro actuators.

The regulating devices for pneumatic cylinders or actuators are basically pressure control valves, servovalves, and on-off valves. Pneumatic systems can be categorized by force or position control, with force control realized by using pressure control valves [80, 81]and position control realized by using servovalves [17], on-off valves [18, 82, 83], or pressure control valves [76, 84]. Recently, a pneumatic revolute actuator was designed using a pair of antagonistic McKibben muscles, which were coupled in parallel and

imitated a biceps-triceps system. Angular position control can be realized by using two pressure control valves or a 5-way servovalve, with the former showing improved control [85]. These applications indicate that pressure control valves are indispensable for both force control and position control. Because of their commonality in controlling pneumatic systems, pressure control valves have become attractive for both industry and robot control.

Pressure control can be accomplished in two ways by using a pressure control valve (pressure regulator) or by using on-off valves. The relatively high weight and cost and the slow responses of pressure control valve makes them problematic for robotic applications [86, 87, 88]. On-off control valves have therefore been designed to be lighter in weight and have faster responses than pressure control valves. The conventional control methods for pressure tracking do not perform satisfactorily, because pneumatic systems are nonlinear. Although there have been many studies on nonlinear control for pressure control valves, few have assessed pressure control using on-off valves. Hybrid fuzzy control (bang-bang + fuzzy control) has been proposed for high-speed on-off valves, which can be designed in microcontrollers [118]. In addition, two pressure control algorithms using solenoid on-off valves, bang-bang and PWM controllers have been compared [86], with bang-bang controllers with dead zones found to be superior to PWM controllers, in that the former used less power and were easier to program. Similarly, a small-sized multi-port pressure control valve has been developed, based on hysteresis control using solenoid on-off valves, for use in wearable robots [89].

Throughout this chapter, we will show the compact unconstrained valves, when compared with solenoid on-off valves, and their simple structure, making the assembly of miniature valves easier. This chapter presents the design and potential of unconstrained valves for miniaturized pressure control valves by demonstrating its trackability in controlling a McKibben actuator. The experimental results of an evaluation of pressure control using unconstrained valves are given, showing the difference between unconstrained and solenoid valves for pressure tracking control.

5.2 Control Algorithms

Nonlinear controller, *i.e.* sliding mode control, pressure observer, and fuzzy control, is commonly adopted in pneumatic actuation to achieve excellent performance of full-state position control. These controllers work well with servovalves or proportional control valves, however, they are usually expensive and bulky for use in multi-joint robots. A low-cost solution uses on-off valves to substitute for servovalves, where the on-off pulse width is modulated to regulate the flow. The other reason of using on-off valves is

shorter dead-time, simplicity, compact size, and other good properties that is attractive for robotics.

The most common pressure control technique for pneumatic systems with on-off valves is to modulate the PWM signal to control the flow. This type of control can also be attained by using a pulse code modulation (PCM) digital control valve driven by a series of on-off valves connected in parallel [90]. PCM and PWM control are commonly used for pneumatic control, where the PCM control is more preferable for its faster tracking control [97]. For verification, two control algorithms are compared to show the difference of PWM and PCM control, *i.e.* PI control that has its base on PWM and Multi-Level Hysteresis (MLH) control that uses PCM. PID is a classic method of control, but its simpler cousin, PI normally will suffice and is simpler to tune [91]. With integral control, the system is more robust than it is without integral control. Integral control automatically adjusts itself, so steady-state error is driven to zero. The digital PI controller has the following form:

$$\Delta U_{PI} = K_p(e_n - e_{n-1} + \frac{\Delta t}{T_i}e_n). \tag{5.2.1}$$

The experimental results shown in Fig. 5.2 indicate that MLH control algorithm has better accuracy and higher frequency bandwidth than PI controller. Similar result has been reported by R. van Ham, *et. al*, which shows the superiority of hysteresis control over the ordinary PWM control [86]. As concerning the total valve size, MLH control algorithm requires 4 valves (two valves each for the supply and exhaust side), whereas PI control requires only 2 valves in total. The selection of using PWM or PCM control is then selected according to the requirement of control accuracy or compactness.

To complement the obtained results for pressure control with solenoid on-off valves, we assessed four control algorithms (Fig. 5.3) to determine the most accurate pressure tracking control for unconstrained valves. The four control algorithms were experimentally compared, where the performance was assessed by comparative evaluation of tracking accuracy and stability. For evaluation purposes, both rectangular and sinusoidal waveforms were utilized to assess the characteristics of unconstrained valves. Control stability was obvious for rectangular waveforms, while tracking accuracy was more obvious for sinusoidal waveforms. The pressure tracking performance of each algorithm is described and discussed separately, and the algorithms are compared at the end.

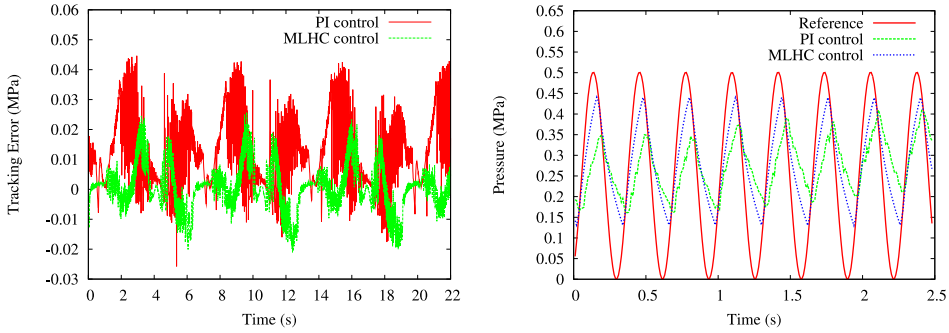

(a) Tracking error @ 0.1 Hz (b) Sinusoidal reference 2 Hz

Figure 5.2: Experimental results of pressure control with PI and MLH algorithm using solenoid on-off valves. (a) Tracking error for sinusoidal reference 100 mHz, and (b) Dynamic tracking response for sinusoidal reference 2 Hz.

5.2.1 Hysteresis Control

This algorithm has only one control variable, *i.e.*, the dead zone threshold. Based solely on intuition, choosing too wide a dead zone threshold will worsen tracking accuracy while providing better stability. Similarly, a narrow dead zone threshold achieves better accuracy, but with tracking oscillations as a direct consequence. This control algorithm has a tradeoff between accuracy and stability associated with its simplicity. Fig. 5.4 compares three dead zone thresholds to show the limitation of this algorithm for tracking accuracy. Increasing the threshold to 0.036 MPa was accompanied by oscillations, showing that accurate and steady tracking is on the borderline between thresholds of 0.036 MPa and 0.073 MPa.

5.2.2 Multi Level Hysteresis (MLH) Control

Multi-level hysteresis control was designed to compensate for the tracking error observed in hysteresis control. Three variables must be determined in this control algorithm: minor flow rate and inner and outer dead zone thresholds. Changes in outer and inner threshold are shown for 0.109 & 0.018 MPa, respectively; 0.109 & 0.036 MPa, respectively; and 0.218 & 0.036 MPa, respectively (Fig. 5.5). The major and minor flow rates were switched at 27 kHz(Q= 21.5 L/min) & 6 kHz(Q= 2 L/min), respectively, for the supply valve, 16 kHz(Q= 26 L/min) & 10 kHz(Q= 1.6 L/min), respectively, for exhaust valve 1, and 14 kHz(Q= 12.5 L/min) & 8 kHz(Q= 1.9 L/min), respectively, for exhaust valve 2. Our experimental results showed that multi-level hysteresis control improved tracking accuracy compared with hysteresis control. Similar to hysteresis control, if the threshold in multi-level hysteresis control is set relatively small, accuracy will increase

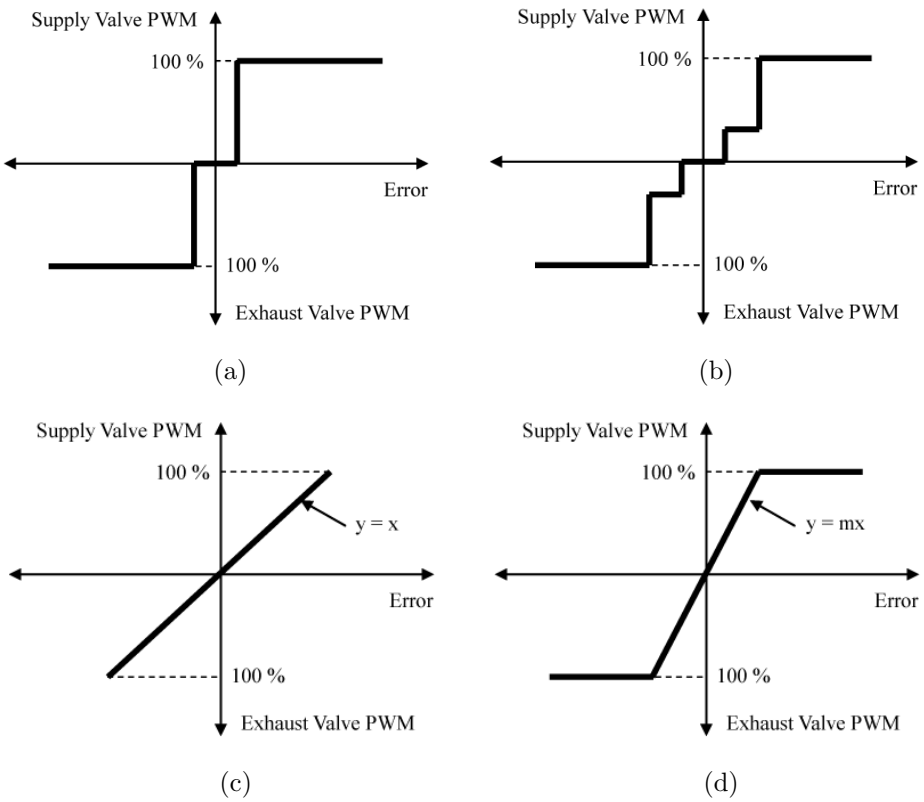

Figure 5.3: Proposed pressure control algorithms for unconstrained on-off valves. (a) Hysteresis control, (b) Multi-level hysteresis control, (c) Proportional PWM control, and (d) Multimode switching: hybrid proportional PWM + bang-bang control

but the system will suffer from oscillations.

The influence of minor flow rate was assessed by comparing two different minor flow rates, low and half flow rate, using the algorithm for threshold 0.109 & 0.036 MPa. Low flow rate refers to the above mentioned setting for minor flow rate, 6 kHz (Q= 2 L/min) for the supply valve, 10 kHz (Q= 1.6 L/min) for exhaust valve 1, and 8 kHz (Q= 1.9 L/min) for exhaust valve 2. Half flow rate refers to 22 kHz (Q= 12.3 kHz) for the supply valve, 12 kHz (Q= 17 L/min) for exhaust valve 1, and 13 kHz (Q= 6.5 L/min) for exhaust valve 2. At half flow rate, tracking accuracy was slightly increased for sinusoidal waveforms, whereas unstable performance was observed in tracking rectangular waveforms (Fig. 5.6). Thus, multi-level hysteresis control with thresholds of 0.109 & 0.036 MPa and low minor flow rate shows better performance.

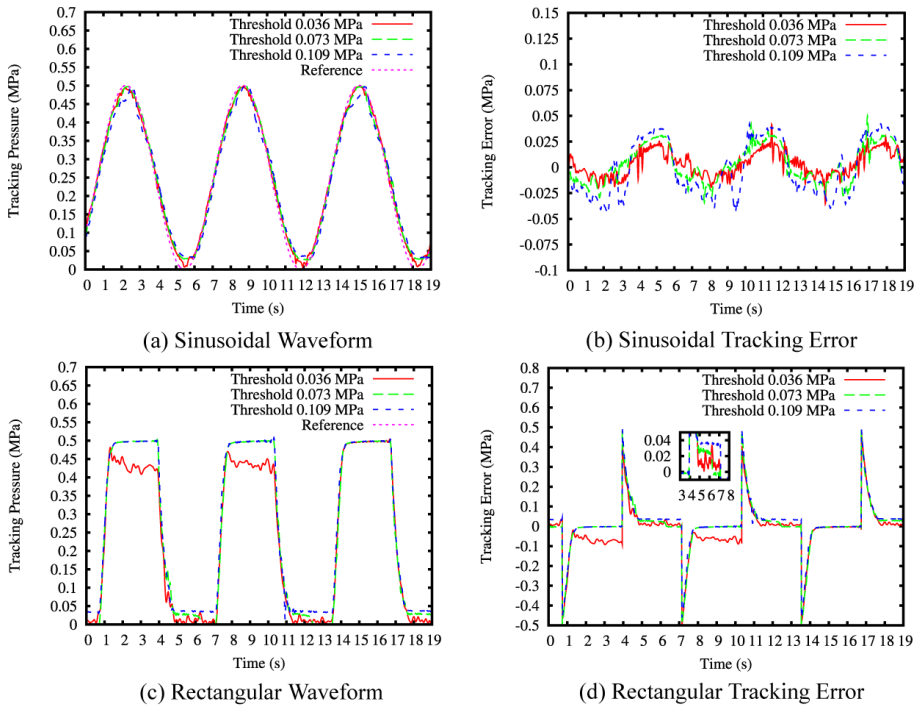

Figure 5.4: Hysteresis control for tracking sinusoidal and rectangular input waveform at 0.1 Hz, input voltage 20 V, pressure 0.5 MPa.

5.2.3 Proportional PWM Control

Because this control algorithm has a proportionally linear relationship between pressure difference and PWM duty ratio, there is no transient tracking error caused by a dead zone, as observed in hysteresis control. The major drawback of this method is sluggish response time, which may deteriorate into tracking inaccuracy (Fig. 5.7).

5.2.4 Multi-mode Switching Control

Bang-bang control is frequently described as time-optimal control but may be limited by the presence of transient errors. In contrast, although proportional control is time-sluggish, it may compensate for transient errors. Multi-mode switching control combines the advantages of both bang-bang and proportional control to derive a faster tracking response with better precision. This algorithm has only one variable, *i.e.*, the gradient m of a linear function $y = mx$. The experimental effects of gradient m are shown in Fig. 5.8. Compared with proportional control, a proper determination of the gradient value may correct for tracking errors. The gradient value, however, has to be correctly chosen, otherwise it will lead to poor tracking

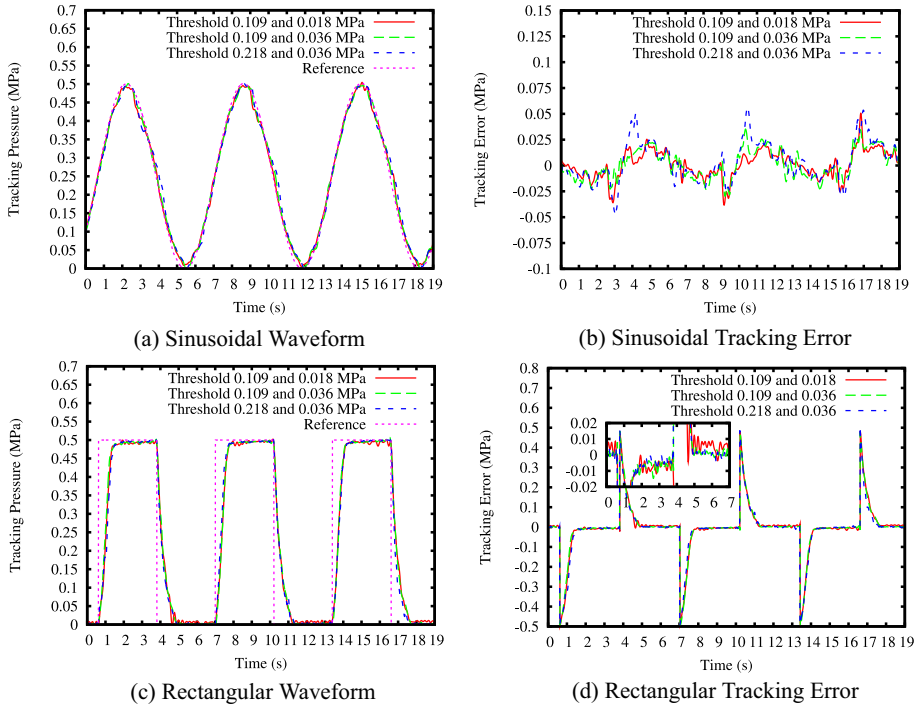

Figure 5.5: Multi-level hysteresis control for tracking sinusoidal and rectangular input waveforms of 0.1 Hz, input voltage 20 V, pressure 0.5 MPa

performance.

5.2.5 Comparative Study

A representative of each control algorithm was selected based on assessments of best performance. The four control algorithms to be compared were determined from direct observations as hysteresis control, with a threshold of 0.073 MPa; MLH control, with thresholds of 0.109 & 0.036 MPa, with low minor flow rate, proportional PWM control, and multi-mode switching control with gradient $m = 4$ (Fig. 5.9). Comparisons indicated that MLH control provided the best tracking control algorithm for both sinusoidal and rectangular waveforms, with a tracking error of 0.04 MPa for sinusoidal input and 0.0164 MPa for rectangular input (Table 5.1). These results were similar to those of pressure control using solenoid on-off valves. The result in optimal control theory shows that every minimum-time control problem has a bang-bang solution, therefore, if the minimum-time control problem has a unique solution then that solution is a bang-bang solution [92].

PWM has been used successfully in electronic control circuits. The extremely short switching times of electronic devices allow the efficient use of PWM at frequencies in the kHz range. On the other hand, using PWM

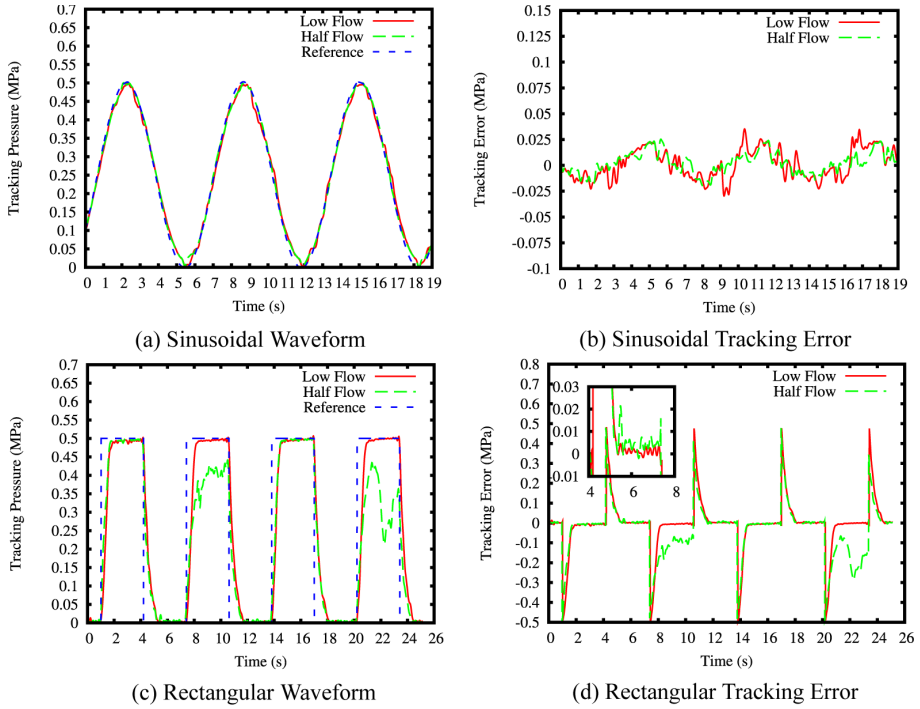

(a) Sinusoidal Waveform

(b) Sinusoidal Tracking Error

(c) Rectangular Waveform

(d) Rectangular Tracking Error

Figure 5.6: Multi-level hysteresis control (threshold 0.109 & 0.036 MPa) for different levels of minor flow rate

Table 5.1: Comparison of maximum tracking error (unit in MPa)

Reference Input Waveform	Pressure Control Algorithms			
	Hysteresis	Proportional	Multi-mode switching	MLH
Sinusoidal	0.0497	0.1407	0.043	0.04
Rectangular	0.0306	0.0541	0.0669	0.0164

to perform hydraulic/pneumatic switching requires valves, whose switching times must be measured in tens or even hundreds of milliseconds - not microseconds or nanoseconds as in the case of electronic circuits. The result is that improperly implemented PWM hydraulic circuits produce unwanted vibrations and pulsations at frequencies that can be transmitted to output actuators [93]. Besides the control accuracy and stability, the know-how of pressure control from the expertise in the field of pneumatic and hydraulics are cited in [94], which clarifies the influence of pressure and temperature in pressure control. Most transducers are designed to produce output that is linear with the applied pressure and independent of other system variables - the most important of these being temperature. Because of this, they respond not only to changes in pressure, but to changes in tempera-

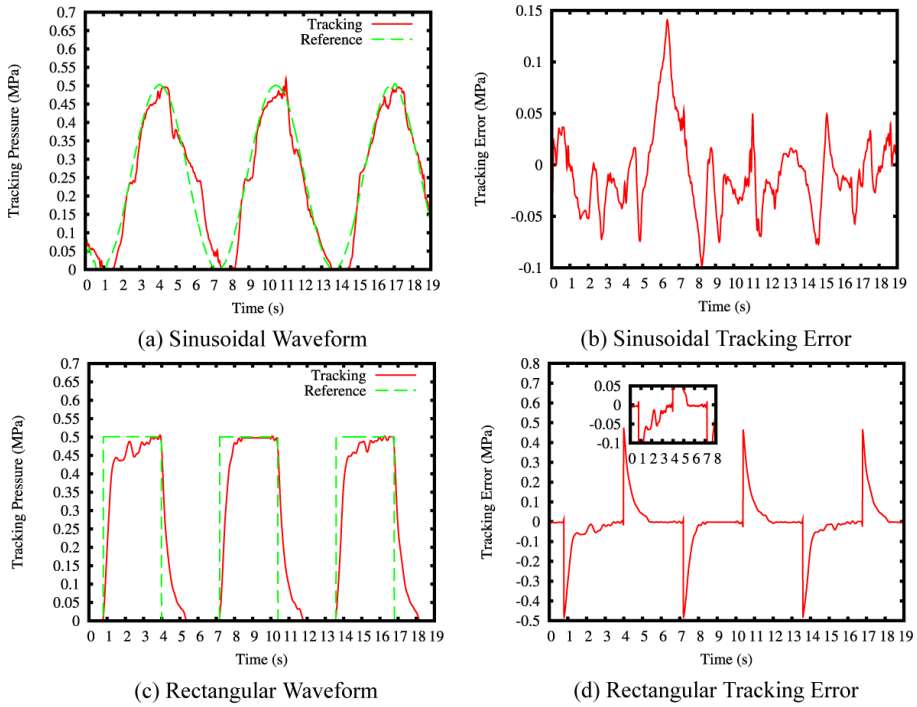

Figure 5.7: Proportional PWM control for tracking sinusoidal and rectangular input waveforms of 0.1 Hz, input voltage 20 V, pressure 0.5 MPa

tures as well. Extreme temperature fluctuations may change a transducer's output signal even though pressure remains constant. Kawashima and Kagawa have proposed an isothermal chamber for unsteady flow generator [95], where the charge or discharge process are made almost isothermal conditions so that the mass flow rate can be generated by controlling the pressure change directly from a servovalve, neglecting the temperature effect. Even though the proposed method could achieve ultra high-precision accuracy, the pressure regulator incorporates servovalve, flow sensor (QFS), isothermal chamber, PD meter, and pressure in a single unit, making them bulky. Our approach based on the bang-bang solution and unconstrained valves for miniaturization uses MLH control because of its simplicity and its ability to be incorporated into microcontrollers for the development of miniaturized pressure control valves for use in strictly limited spaces such as power-suits and pneumatic robotic hands.

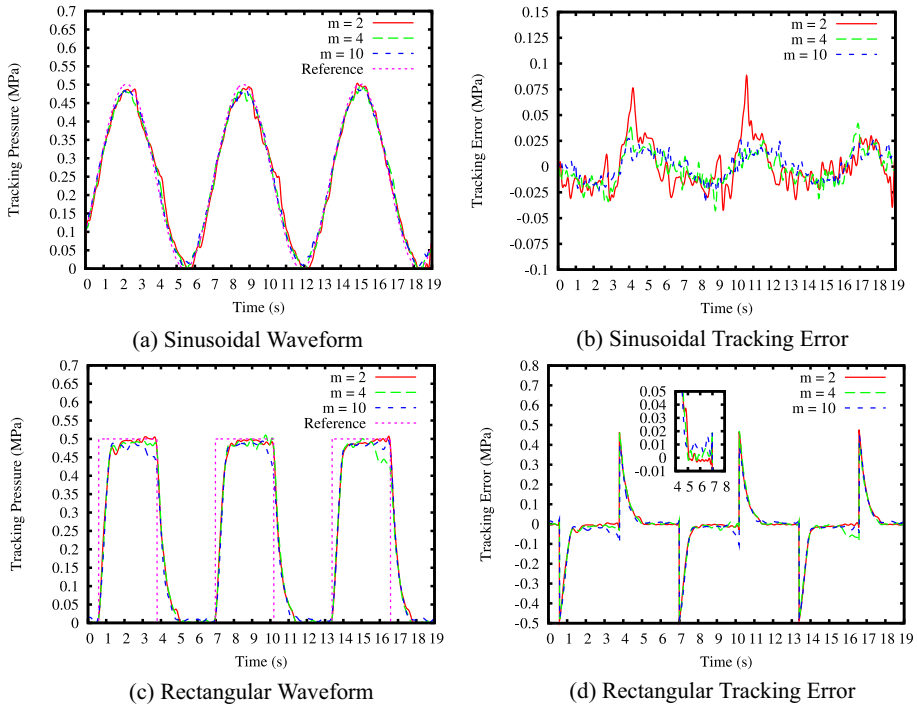

(a) Sinusoidal Waveform

(b) Sinusoidal Tracking Error

(c) Rectangular Waveform

(d) Rectangular Tracking Error

Figure 5.8: Multimode switching control for tracking sinusoidal and rectangular input waveforms of 0.1 Hz, input voltage 20 V, pressure 0.5 MPa

5.3 Unconstrained Valves for Pressure Control

5.3.1 Discrete Frequency Control

Conventional solenoid valves for constant flow output use Pulse Width Modulation (PWM) to regulate flow rate. However, unconstrained valves possess more flexibility for the control of pneumatic actuators compared to solenoid valves because the input frequency and voltage are variables that can be used for flow control [96]. For pneumatic control, the fast tracking control of Pulse Code Modulation (PCM) control is preferred [97, 98]. A PCM configuration requires multiple solenoid valves arranged in parallel, whereas PWM control requires only one valve, making it more compact. PWM or PCM control selection thus becomes a tradeoff between performance and size.

PCM-emulation control is made possible with one unconstrained valve, where input frequency is regulated to control flow. Such space-saving PCM control emulation using an unconstrained valve is called Discrete Frequency Control (DFC), making it suitable for robotic use. Fig. 5.10 shows the configuration of PCM control scheme with multiple solenoid valves and their

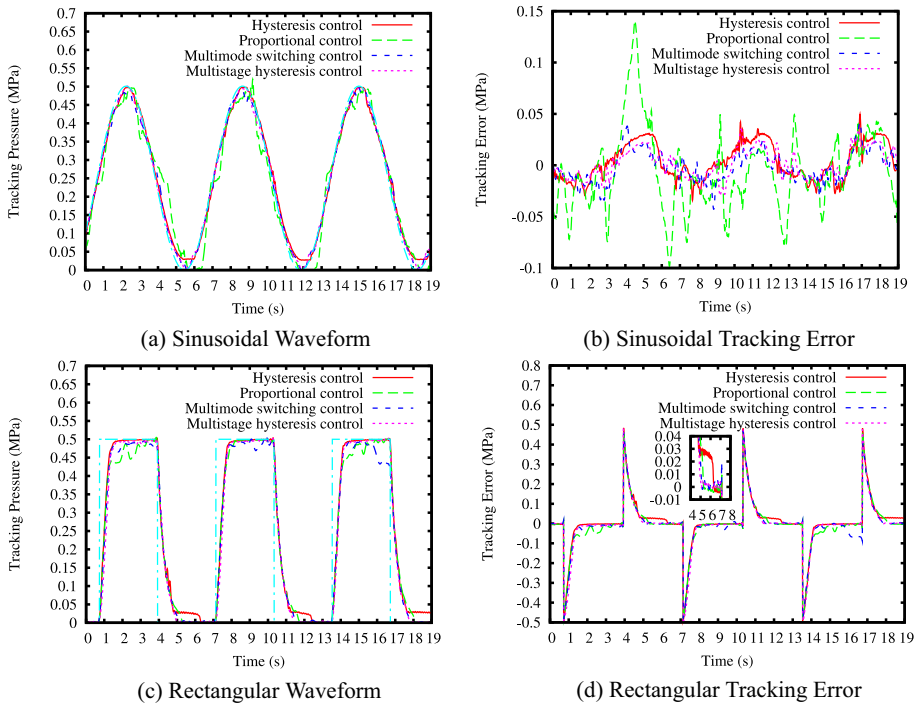

Figure 5.9: Evaluation of pressure tracking control algorithms

substitution with one unconstrained valves utilizing DFC feature. PWM and DFC control differ as shown in Fig. 5.11, where output 4 L/min is required from both. Fig. 5.11(b) shows that DFC control is faster than PWM control. The limitations of mechanical switching in solenoid on-off valves causes the slow response of PWM control, making them unsuitable for high-frequency switching. The obtained results have proved that PCM control tracks faster than PWM control and it also shows the effectiveness of DFC-controlled unconstrained valves to emulate PCM control.

5.3.2 Miniaturized 3/3 Directional Control Valves

Pressure control using solenoid valves requires at least 1 supply and 2 exhaust valves, mainly because the discharging process takes longer to deliver the air outside the actuator. To control pressure with on-off valves, it has been suggested that the exhaust valves flow rate has to be at least 1.4 times greater than that of the supply valve [57]. A minimum of one supply and two exhaust valves are necessary to obtain the same response time to pressurize and depressurize a constant volume. For example, 2 supply and 4 exhaust valves have been used to meet the requirements of a dynamically controlled biped robot [86]. In particular, to improve the tracking accuracy by adopting a two-level hysteresis control method would require as many

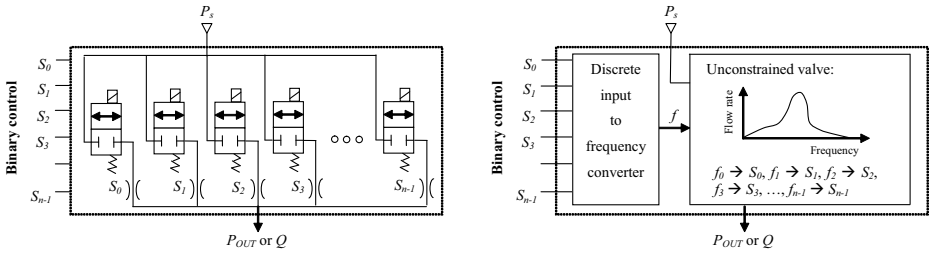

(a) Solenoid valve (b) Unconstrained valve

Figure 5.10: Emulating flow control based on PCM control using (a) solenoid on-off valves, and (b) unconstrained valve with DFC

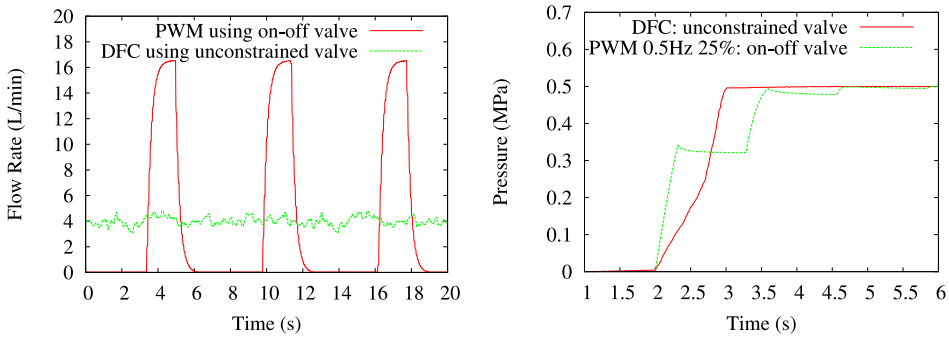

(a) Flow output (b) Pressure response

Figure 5.11: PWM vs. DFC (or PCM) control. (a) Flow output for control using solenoid on-off valve and DFC control using unconstrained valve, and (b) pressure or flow response

as 6 valves (2 supply and 4 exhaust valves). A mount base is necessary to connect all the valves and the integrated valve-mount comprised of 2 on-off valves can be called as 3-position/3-way Directional Control Valve (3/3 DCV). The available commercial valve is mostly a 3/2 DCV that has a disadvantage for robot control because of the inherent inefficiency in allowing pressurized air to switch forth and back when the goal is to keep the position constant [99]. The valve arrangement such that in 3/3 DCV is suitable for a pneumatic actuator to block the pressurized air, ensuring no waste during control.

Similarly for unconstrained valves, a prototype of 3/3 DCV (Fig. 5.12), consisting of one supply and two exhaust valves, was designed for a braided McKibben actuator. The advantage of using unconstrained valves is that two-level hysteresis control can be executed with a total of merely three valves because the major and minor flow can be alternately changed by switching the input frequency, resulting in a compact pressure control valve. The supply valve is ϕ 15 x 30 mm in size, and each exhaust valve is ϕ 15

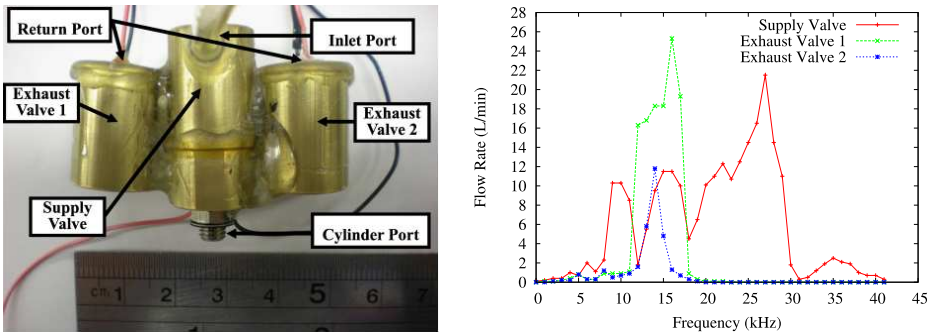

(a) (b)

Figure 5.12: Unconstrained 3/3 directional control valve. (a) 3/3 DCV with 1 supply & 2 exhaust valves (PEA 5 x 5 x 10 mm), and (b) Frequency - flow rate relationship at pressure 0.5 MPa and input voltage 20 V

x 20 mm, while the assembled 3/3 DCV unit measures 30 x 50 x 15 mm. Fig. 5.12(b) shows the frequency - flow rate characteristics for supply and exhaust valves driving at input voltage of 20 V. The low supply voltage is relatively low to ensure application in an autonomously operated wearable robot, where the valve could be driven by batteries. If the supply valve switches on at a frequency 27 kHz and the exhaust valves switch on at frequencies of 16 and 14 kHz with all the valves switch off at frequency 0 kHz, the charging and discharging outflow would be 17 L/min and 43 L/min, respectively (see Fig. 5.13). Due to their unconstrained structure, the flow was rather unsteady when compared with a soleniod valve, which is commonly constrained. the unstable flow, however, had less influence on the pressure response (Fig. 5.13(b)). The amount of time required to pressurize and depressurize a 20 mL volume McKibben actuator is 770 ms, and is equal for the charging and discharging processes.

As mentioned earlier, the flow characteristics of an unconstrained valve can be adjusted by altering the mechanical properties of the valve body, where it is possible to obtain a higher output flow by using a thin diaphragm for the valve base. This approach could be viewed as a practical strategy to miniaturize the 3/3 DCV by rearranging the exhaust valve to have higher flow during discharging process. In this way, pressure control is possible with merely one supply and one exhaust valve (Fig. 5.14). One advantage of using unconstrained valves is their ability to accomplish two-level hysteresis control with only two valves because they can alternate major and minor flow by switching the input frequency. Compared to the conventional method that requires totally six valves for MLH control, unconstrained valves are promising for the realization of a compact pressure control valve with the schematic shown in Fig. 5.15.

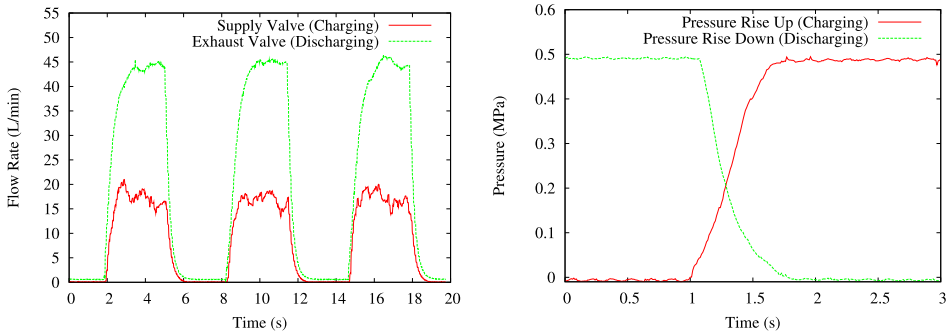

(a) Flow response (b) Pressure response

Figure 5.13: (a) Supply and exhaust valves are switched on & off at a frequency of 0.1 Hz, a supply pressure of 0.5 MPa & an input voltage of 20 V, (b) Pressure response time to fill a 20 mL volume McKibben actuator

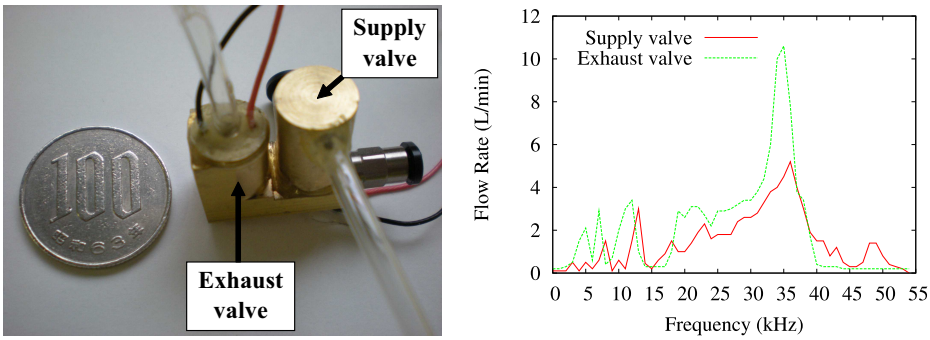

(a) (b)

Figure 5.14: Miniaturized 3/3 DCV comprised of two unconstrained valves with PEA 3 x 3 x 5 mm, orifice ϕ 0.5 mm, and poppet ϕ 4 mm. (a) DCV design with one supply and one exhaust valve measuring 20 x 21 x 10 mm, (b) Frequency - flow rate characteristics.

5.3.3 Pressure Control Using Unconstrained Valves

Air flow dynamics, in both the sonic and subsonic regions, may cause instability during pressure control because of the elimination of mechanical constraints. For unconstrained valves, valve direction and position are considered essential; a slight change or improper arrangement of direction or position may cause an abnormality in pressure control. We have therefore experimentally evaluated DCVs with unconstrained valves to assess their potential for pressure control. The unconstrained 3/3 DCVs are commanded with a reference input and equipped with a pressure feedback that runs continuously to correct deviations from the reference value. The corrective action relies on MLH control, the most accurate control method for

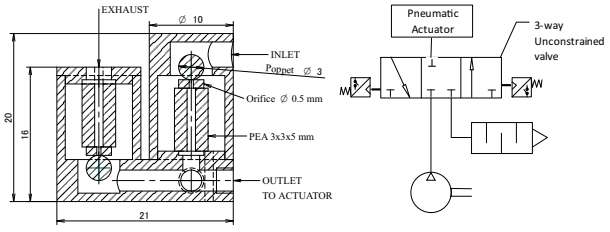

Figure 5.15: Mechanical drawing and the standard pneumatic symbol for unconstrained 3/3 DCV

Table 5.2: Switching frequency of supply & exhaust valves for multi-level hysteresis control

Valves	Switching States				
	FS	SS	I	SE	FE
Major Supply	ON	OFF	OFF	OFF	OFF
Minor Supply	OFF	ON	OFF	OFF	OFF
Minor Exhaust	OFF	OFF	OFF	ON	OFF
Major Exhaust	OFF	OFF	OFF	OFF	ON

unconstrained valves. The objective of MLH pressure-control, which is a time-optimal, is to switch the on-off valves across the different states so that the controlled pressure tracks a reference setpoint within a specified tolerance or hysteresis threshold. A set of five states, namely Fast Supply (FS), Slow Supply (SS), Idle (I), Slow Exhaust (SE), and Fast Exhaust (FE), have been utilized in our two-level hysteresis control algorithm (Table 5.2). The major supply and exhaust valves have higher flow rates, making them optimal for time-optimal tracking; the minor supply and exhaust valves have lower flow rates, making them optimal for precision tracking. The switching principle is determined by the tracking error e defined as $e = P_{ref} - P_{act}$, where P_{ref} is the pressure setpoint and P_{act} is the actual pressure. The general switching state diagram of two-level hysteresis control is shown in Fig. 5.16. If t_{in} and t_{out} are the inner and outer thresholds, then, when the tracking error is positive, the controller will open either the major or minor flow of the supply valve by switching the input frequency. Likewise, when the tracking error is negative, the controller will open the major or minor flow of the exhaust valve to expel the excessive flow.

For both the supply and exhaust valves, the peak flow rate at the resonant was selected as major flow rate, while the minor flow rate had to be as low as possible to realize accurate control performance. Setting the flow rate for the minor valves too high will lead to oscillations in the control value [100]. Based on our previous results, we set the switching conditions

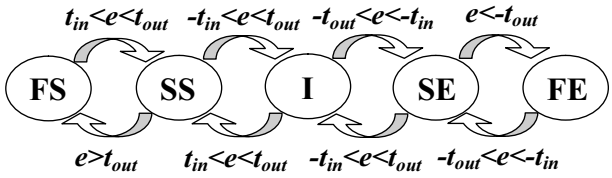

Figure 5.16: Switching state diagram for two-level hysteresis pressure control

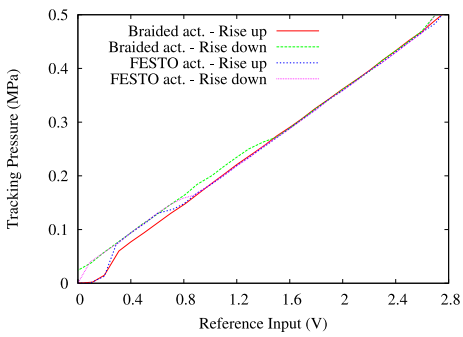

(a)

(b)

Figure 5.17: Pressure tracking using 3/3 DCV for braided McKibben and FESTO fluidic muscle actuator. (a) Tracking results (b) Top: braided McKibben actuator; bottom, FESTO fluidic muscle.

between the major and minor flows for the supply and exhaust valves in MLH control arbitrarily as 25, 12, 16, and 12 kHz. A major problem in bang-bang (hysteresis) control is "chattering", where the supply and exhaust valves continually oscillate near the reference setpoint. To prevent this problem, the tolerance window was determined to be t_{out}=0.034 MPa for the outer threshold and t_{in}=0.0127 MPa for the inner threshold margin, resulting in less accurate control performance.

To verify the effects of disturbances that may come from the actuator, we tested the pressure control of two different flexible actuators, braided McKibben type artificial muscle and FESTO fluidic muscle DMSP-10-40N, with the 3/3 unconstrained DCV. Fig. 5.17 shows how the relationship between the properties of the actuators, *i.e.*, the elasticity and damping properties of the rubber material, results in changes in the hysteresis loop, having no influence on control stability. This finding supports our hypothesis that control instability is mainly caused by flow disturbances because of improper valve arrangements.

Pressure control with an unconstrained mechanism may stall, due to improper orientation or position of the valve, leading to failure in tracking

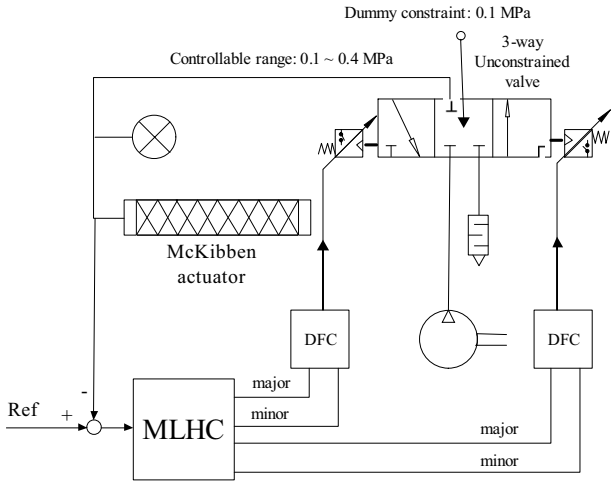

Figure 5.18: Diagram of pressure tracking control using unconstrained valves.

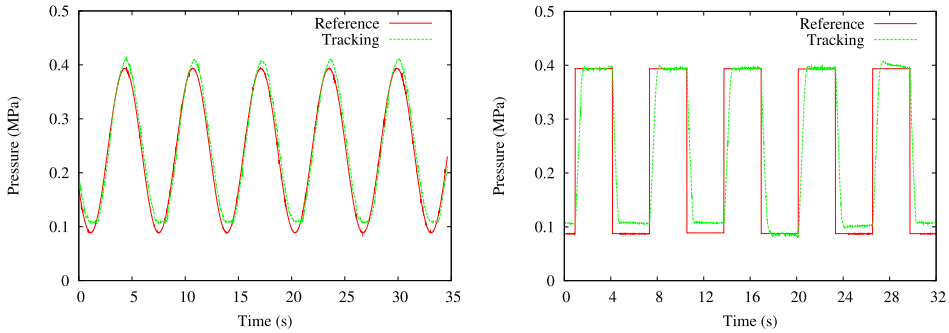

(a) (b)

Figure 5.19: Pressure tracking control using unconstrained valves robust for orientation.

control. Tracking failures may be caused by malfunctions of the on-off operation, either on the supply or on the exhaust side. To counteract the absence of constraints, a pneumatic force of 0.1 MPa was applied to provide constraints in the case of unconstrained on-off valves. Fig. 5.18 shows the pressure control schematic for unconstrained valves, with air pressure of 0.1 MPa used for constraint, limiting the actuator controllable range to 0.1 - 0.4 MPa. With this arrangement, the tracking control was robust for different positions and directions of the valve (Fig. 5.19), indicating that the proposed control method is highly effective for solving the problems.

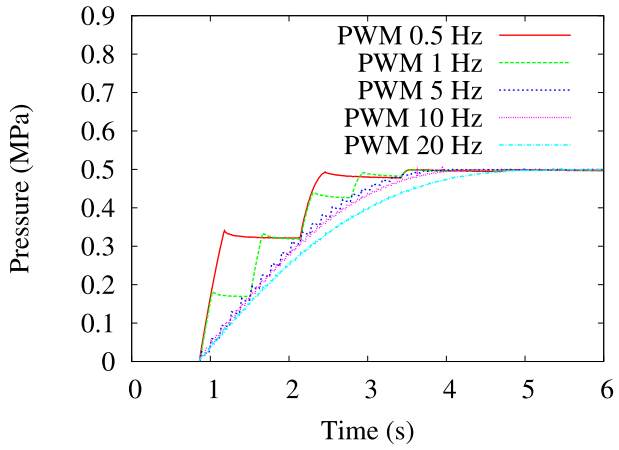

Figure 5.20: Flow response of PWM control using solenoid valves tested for frequency 0.5, 1, 5, 10, and 20 Hz with duty ratio 25%

5.3.4 Difference between Unconstrained and Solenoid Valves

Low level bang-bang or hysteresis control is reportedly superior to standard PWM control. The reason is that PWM control needs to be switched at high frequency to maintain good tracking accuracy, thus requiring a high-speed on-off switching valve. Therefore, the implementation of PWM control depends on the valve switching response. As shown in Fig. 5.20, the response of PWM control becomes sluggish at high-frequency switching, which indicates that the valve switching limit is responsible to increase the valve response. This, in turn, causes the valve failure to work at high frequency bandwidth. For this reason, PCM control performs better than PWM because it has no need for fast-switching response. The advantages of PWM is compactness but it has worse tracking performance, whereas PCM control is bulky but tracks faster. For the conventional solenoid valves, selection is made for PWM or PCM control according to the requirement of tracking response or compactness. Using an unconstrained valve, the control valve tracks faster as well as being compact.

Pressure control using solenoid valves can be found in [86, 89], which shows that MLHC Control algorithm provides the best tracking performance. Three pressure control valve comparison configurations are shown in Fig. 5.21(b), *i.e.*, hybrid unconstrained-solenoid valves, all solenoid valves, and all unconstrained valves. MLH control using solenoid valves requires at least four valves , compared to two unconstrained valves thanks to DFC. The hybrid requires two solenoid valves to expel air and one unconstrained valve to supply it. Using unconstrained valves for pressure control thus provides the most compact system. In experiments, tracking 50 mHz si-

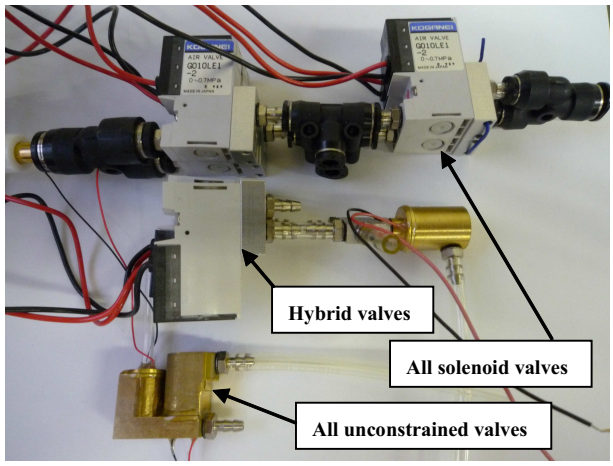

Figure 5.21: Application test using unconstrained valves for pressure control

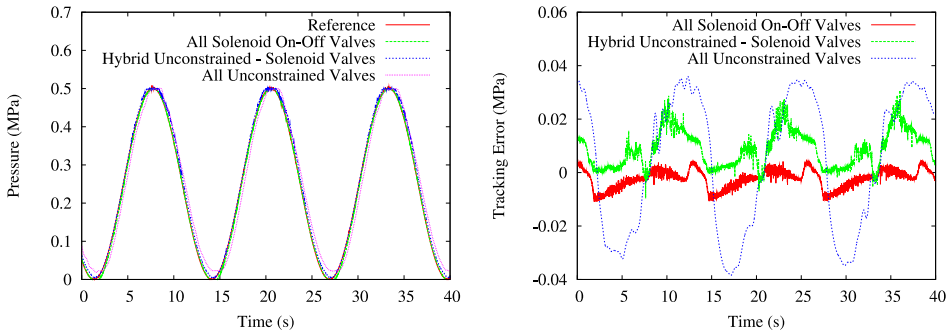

(a) Tracking result (b) Tracking error

Figure 5.22: Pressure tracking result using Multi-Stage Hysteresis control for three valve configurations: solenoids, hybrid unconstrained-solenoid, and unconstrained valves. (a) Tracking result for 50 mHz sinusoidal reference, and (b) Tracking error.

nusoidal reference shown in Fig. 5.22 and compared in Table 5.3, configuration with both solenoid valves gave the best tracking result. Inaccurate unconstrained-valve control was due to non constraint or sluggish valve switching dead time. Even so, the unconstrained valves gave the most compact configuration - the primary requirement for wearable robots. Compared to solenoid valves, unconstrained valves have two extra control variables in addition to PWM control, *i.e.*, input frequency and voltage, which is usable in flow control for PCM-emulation and unconstrained-valve DFC with high miniaturization potential is therefore a breakthrough in using pneumatic power for robotics.

Table 5.3: Combination of unconstrained valves for pressure control

Comparison	Both solenoid valves	Hybrid valve	Both unconstrained valves
No. of valves (supply side) (exhaust side)	4 2 sol. 2 sol.	3 1 uncst. 2 sol.	2 1 uncst. 1 uncst.
Volume (mm^3)	35,720	19,207	4,410
Control range (MPa)	0 - 0.5	0 - 0.5	0.1 - 0.4
Error (MPa)	0.011	0.026	0.038
Repeatability	Excellent	Good	Fair
Switching control	PCM	PCM-DFC	DFC

5.4 Miniaturized Control Board

The main disadvantage of using stack PEA is the requirement for high drive voltages. This especially limits the use of these valves in wearable robots, due to the increased weight and bulky size of high voltage power supplies. Unlike the other piezoelectric valves, the proposed piezoelectrically driven valve does not need high voltage supply due to the poppet-orifice unconstrained mechanism that allows higher bounce height of the poppet compared to valves with constraints. For piezoelectric valves with constraint, high voltage operation is indispensable and the only way to amplify the valve output flow is by increasing the input voltage, where the PEA induced stroke of a PEA increases linearly with the increased voltage.

This section describes the selection of power electronics and the realization of a small-sized pressure control board. The main controller, with a MLH control algorithm and frequency selectors of major and minor flow, were implemented on small-size 8-pin microcontrollers PIC12F683, while the driver for the PEA consisted of a photocoupler TLP250. The driver was mounted with an embedded NAIS ADP1181 pressure sensor, and the sensor output was amplified using ADC623. For miniaturization purposes, the control circuitry was placed on two side of the PCB, which was mounted on the 3/3 DCV (Fig. 5.23(a)). The driver board, which was 26 x 35 x 20 mm in size, weighed approximately 10 g. The valve output flow of miniaturized unconstrained valve is approximately 3-4 L/min (0.5 MPa), which is suitable for driving a mini pneumatic actuator. The tube connection between the valve and actuator was made as short as possible to improve the dynamic response, which leads to the realization of servo drive. The integrated miniaturized pressure control valve and mini pneumatic actuators

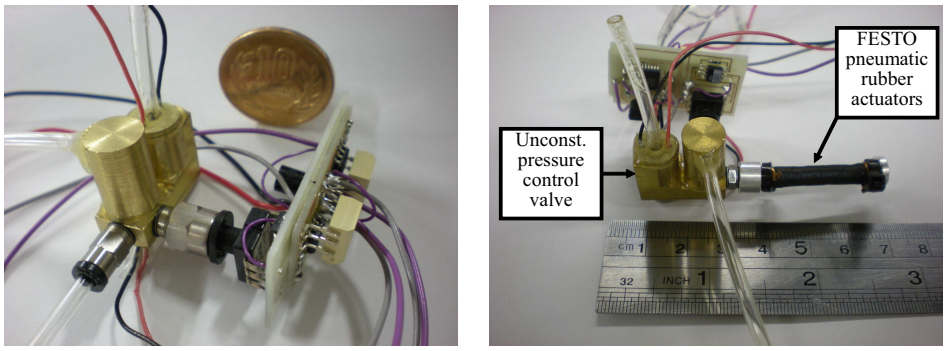

(a) (b)

Figure 5.23: Piezoelectrically driven pressure control valve with unconstrained valves. (a) Piezoelectric driver and pressure control board connected to 3/3 DCV, (b) Integrated miniaturized servo drive (pressure control valve + mini pneumatic actuator).

(FESTO rubber tube ϕ3 x 30 mm) are shown in Fig. 5.23(b).

As the valve size is made smaller by simply miniaturizing the PEA, the output flow tends to drop in relation to the decrease in force generated by the PEA. Miniaturization may also be related to the limitations on the fabrication process of the PEA. Therefore, the final goal is not to overlap with the MEMS microvalves. Unlike most MEMS microvalves that requires high voltages, unconstrained valves are adequate with 24 VDC batteries. These miniaturized pressure control valves with piezoelectric unconstrained valves, have two features, compactness and low voltage drive, that are expected to be useful for a wide range of pneumatic applications, especially for the control of mini pneumatic actuators. Fig 5.24 shows a comparison between an unconstrained pressure control valve (size 37 x 30 x 27 mm) and the standard pressure control valve SMC ITV0030-2CS (size 15 x 50 x 82 mm), making the volumetric ratio 1:2.

5.5 Performance Evaluation

To assess its trackability, transient stability, and accuracy, pressure tracking control was evaluated at various pressure levels and irregular trajectories. Experimental results are shown in Fig. 5.25(a) and (b) for sinusoidal and rectangular waveforms respectively, showing that trackability was fairly good at high pressure, but quite poor at low pressure ranges. Large tracking errors for sinusoidal and rectangular waveforms at pressure 0.4 MPa may have been caused by nonlinearities of the pressure sensor reading or unknown air flow characteristics that easily affected the uncon-

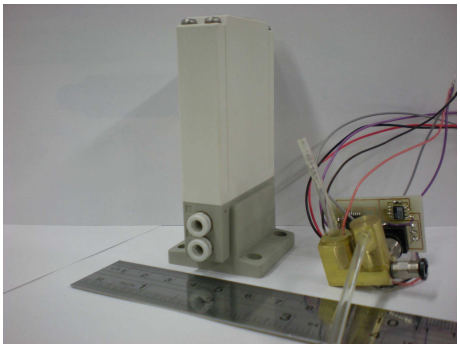

Figure 5.24: Size comparison of pressure control devices using a commercial pressure control valve and unconstrained valves.

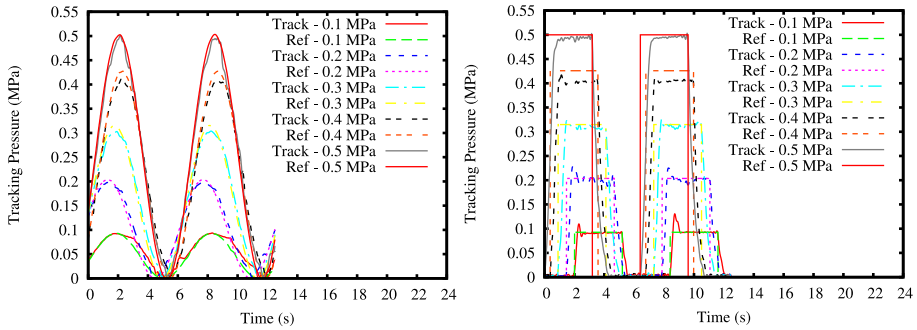

(a) Sine 0.1 to 0.5 MPa (b) Square 0.1 to 0.5 MPa

Figure 5.25: Multi-level hysteresis control (threshold 0.109 & 0.036 MPa) for tracking sinusoidal and rectangular input waveforms at 0.1 to 0.5 MPa, 0.1 Hz, input voltage 20 V.

strained mechanism. A study of pressure control using multi-port solenoid valves indicated that tracking errors can be canceled out by redesigning the control logic [118]. In addition, industrial-use proportional pressure control valves also overshoot when tracking a rectangular waveform [80], a finding frequently observed in pneumatic control systems. Compared with solenoid on-off valves, unconstrained valves performed relatively well, indicating that they were adequate for pressure tracking control.

The dynamic response of pressure tracking for PAM was tested at zero load condition and with mass load. The first control test consisted of an irregular setpoint tracking exercise (Fig. 5.26), and the tracking tests under loaded condition (Fig. 5.27) showed that MLH control are robust against external disturbances, which can be explained using the analogy of pressure observer [101]. The MLH control was found to be reliable against valve orientation and position changes and the valves performed well through a series of dynamic irregular changes. With respect to size, this valve is

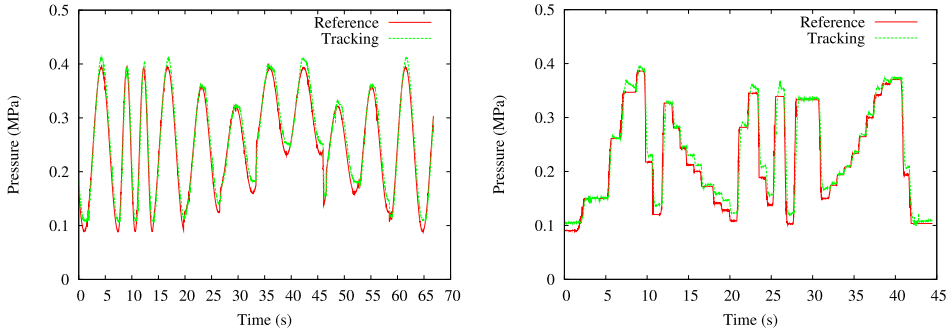

(a) Sinusoidal waveform (b) Rectangular waveform

Figure 5.26: Pressure tracking results for FESTO fluidic muscle ϕ3 x 30 mm for (a) an irregular sinusoidal reference, and (b) an irregular rectangular reference.

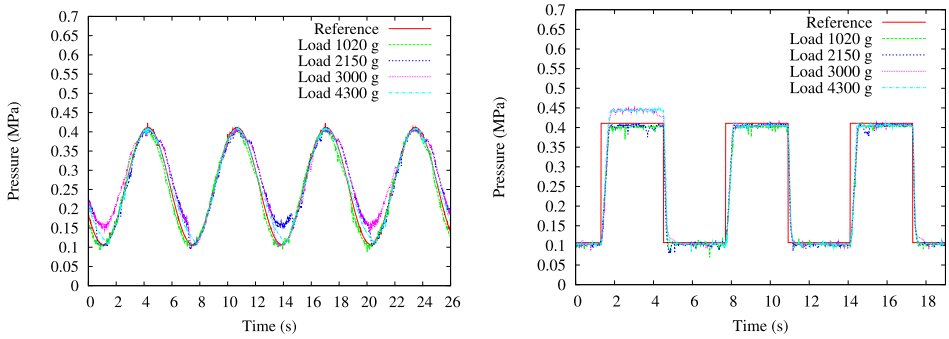

(a) Sinusoidal 0.1 Hz (b) Rectangular 0.1 Hz

Figure 5.27: Pressure tracking results for FESTO fluidic muscle ϕ3 x 30 mm under loaded condition for (a) sinusoidal reference @ 0.1 Hz, and (b) rectangular reference @ 0.1 Hz.

practically useful for wearable robots. The second task was to track a sinusoidal waveform at different frequencies to check the control bandwidth frequency. Fig. 5.28 shows that the limit of pressure control bandwidth for FESTO mini pneumatic actuator (ϕ3 x 30 mm) was approximately 1 Hz, which is sufficient for driving wearable robots although it might be too slow for a fast-acting pneumatic applications. A relevant approach in practical applications to improve the low control bandwidth is possible by increasing the supplying pressure or limiting the use at the low pressure setpoint [41].

5.6 Conclusion

Applications in robotics, such as in wearable robots, power suits, robotic hands, and rehabilitation, are limited by the weight and size of the con-

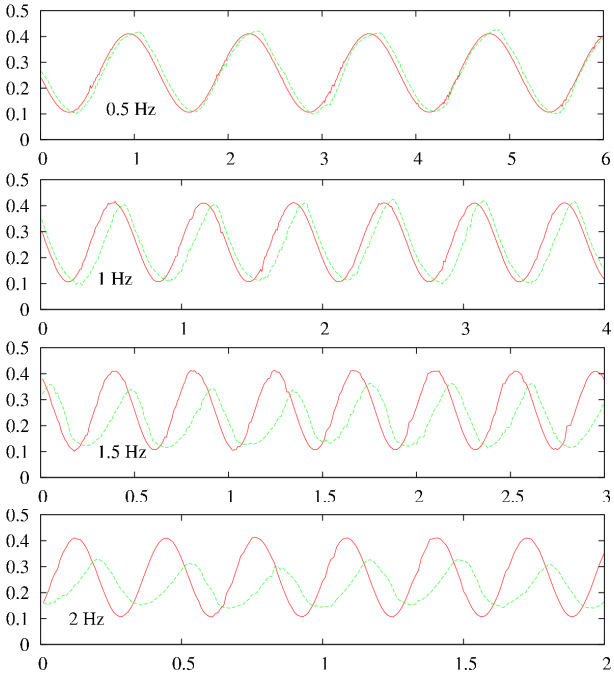

Figure 5.28: Sinusoidal pressure tracking at 0.5, 1, 1.5, and 2 Hz using 3/3 DCV for FESTO mini pneumatic actuator ϕ3 x 30 mm.

trol valves, which hinder their use for pneumatic robots. A miniaturized pressure control valve with unconstrained valves was shown to be much more compact than the existing standard pressure control valves. These unconstrained valves used a multi-level hysteresis control algorithm to regulate pressure with only two valves, instead of four valves for the standard device using solenoid on-off valves. Experimental evaluation showed that these unconstrained valves are practical for pressure control especially its inherent DFC feature that is benefit for miniaturization and faster tracking response. Although the tracking results showed a hysteresis loop and less accuracy, unconstrained valves are practical for pressure control regardless of their inclination, position, and direction. Experimental exercises to track irregular reference setpoints in loaded condition indicate a good dynamic response and robustness against external load. The concept of using unconstrained valves for pressure control is nearing a breakthrough on self-sufficient power-suits or wearable robots.

Chapter 6

Unconstrained Valves for Control of Pneumatic Cylinders

6.1 Introduction

Although pneumatic actuation in automated equipments or industrial equipments is clean and reliable similar to its counterpart electric motors, the use of pneumatic cylinders is inexpensive and relatively safe compared to hydraulic system. The drawback of using pneumatic actuators is the nonlinearity of pneumatic cylinders that causes a difficulty in deciding a suitable controller for accurate and stable positioning. At the early stage of pneumatic cylinder control, their usage was limited to on-off positioning for a trivial application where the cylinder end-effector was controlled to a hard-stop only at the both fixed end. Many research works has been done on nonlinear controller and the derivation of pneumatic dynamic model for a full-state position control, aiming at the achievement of excellent performance. Various nonlinear control algorithms had been proposed, *i.e.*, sliding mode [102, 103], pressure observer [104], and fuzzy controller [105], which used proportional control valves (servovalves). Servovalves are usually expensive because of the need for high-precision manufacturing and a built-in orifice area control circuit. A lower cost solution that has been quite popular for pneumatic robots is by the substitution with solenoid on-off valves, where the pulse width input commands are modulated to emulate flow control similarly to servovalves. The development of PWM-based sliding mode controller has been reported in [106, 107]. PWM control design with compensator for driving a double-acting pneumatic cylinder is presented in [83]. Similar to nonlinear PWM controller, PID controller with velocity and acceleration feedforward gains has been reported by Wang,*et. al.* [108].

A research work based on PWM control that incorporates PID control + friction compensation + bounded integral action + position feedforward is referred to [82]. Ahn and Yokota proposed a fast, accurate, and inexpensive position-control pneumatic actuator with PWM-switching algorithm using a learning vector quantization neural network (LVQNN) [18].

Fast switching response, adequately high flow, and compact size are the desired characteristics of control valves for pneumatic servo actuators. A servovalve or proportional control valve has dead-zone in the vicinity of zero operating point [109], in addition to expensiveness and bulky size. Thanks to the advancement of electronics and computer technology that makes a discovery of new control methods for direct implementation of on-off valves for digital flow / pressure control, which is an imitation for miniaturized proportional control valves. The advantages of using a digitally controlled on-off valves are low-cost, high-reliability, shorter dead time, simplicity, and compactness. The control bandwidth of a pneumatic servo system using digital on-off valves was also increased, however, tradeoff between output flow and valve size may cause unsatisfactory performance of the pneumatic servo actuators. An alternative way to improve the control bandwidth is to connect the valve directly to pneumatic cylinder through the shortest tubing path, which has been reported to increase the frequency bandwidth of up to 10 - 20 Hz [110, 111, 112].

This technique of digital flow control is controlled by a train of pulse inputs that has various modulation methods, *i.e.*, Pulse Width Modulation (PWM) [113], Pulse Frequency Modulation (PFM) [99], and Pulse Code Modulation (PCM) [97, 98]. PWM control is generally used at high frequency modulation inputs thus requires a high-speed switching valve, therefore, its implementation is restricted by the limitation of valve switching time. In regard to pneumatic control, PCM control has been proven to be superior than PWM control. Moreover, PCM control is a binary control and there is no requirement for high-speed switching valves. PFM control was reported in [99] to emulate a biological actuator close to the behavior of muscle fibers at which the muscular activation with trains of identical nerve impulses rely on frequency, not their pulse width. In general, PFM control is not so popular in pneumatic world and is only used for controlling an actuator that emulates the performance of muscle.

This chapter aims at using unconstrained valves for control of pneumatic cylinders. In the following sections, velocity control of a pneumatic cylinder with PCM-control is examined for a single unconstrained valve, thus making the total servo pneumatic system more compact. In summary, the performance dan dynamic response of unconstrained valves is assessed for its reliability and for control of pneumatic cylinders.

6.2 Pulse Code Modulation Control

PCM control is developed to emulate the function of a proportional control valve with only on-off valves, where it is driven by n digital on-off control valves equivalent to a n-bit discrete binary number. The effective cross-sectional area of each valve is equipped with a flow limiter and is designed to be $S_0{:}S_1{:}S_2{:}S_3{:}...{:}S_{n-1} = 2^0{:}2^1{:}2^2{:}2^3{:}...{:}2^{n-1}$. The total combination of PCM control composed of n-number of valves makes the total combination of 2^n steps, which is commonly used for control at low flow rate.

The reliability of flow control valves using PCM control is critical to the control accuracy because the failure of one on-off valve causes a severe disturbance to the control quality and safety of the control plant. If the linear proportion of flow control characteristic is broken due to failure at one of the switching valves, a harsh problem may take place in the closed-loop control system. These unpredicted problems are counted as the disadvantages of PCM control. For use in critical applications, there is often a valve position feedback provision to detect any inconsistency between the control signals and valve position feedbacks. Under most situations the feedback only serves as an alarm that prompts an automatic or manual emergency handling to prevent any fault or damage to the system. In [114], Zhang and Gao introduced a self-compensating PCM compound flow control valve to maintain a good control during valve failures, which increased the valve durability of about 20 to 50%.

However, PCM control is preferable than PWM control for the emulation of flow control because of the faster response in tracking an irregular setpoint. PCM control can be treated as a digital control valve directly controlled from a parallel input/output (I/O) board. Therefore, the valve operation control can be implemented in a microcontroller with no requirement of a digital/analog (D/A) converter, making the total system more compact. Although PCM control has high dynamic performance, its bulky size is a problem for an autonomous robot that has a restricted space. PWM control technique is desirable for autonomous robots because it requires less number of valves. The selection of using PWM or PCM control is decided for the accuracy or compactness according to the control requirement most vital for the system.

A hybrid PCM-PWM control was used as a complement to the PCM control for a flow control valve with finer resolution of controllable range, which is patented in [115]. According to Kojima, a PWM valve with output flow lower than the lowest-bit PCM valves was transplanted to the PCM control valves to realize a time-mean flow rate that is lower than the minimum controllable flow of PCM valve alone. This method of fine-tuning the controllable flow increases the control accuracy.

Unlike the PWM and PCM control using on-off valves, the proposed unconstrained valves are frequency or voltage-controlled, thus is useful for emulation of PCM control with an advantage of being much more compact because the flow control can be possible with a single unconstrained valve. As explained in the previous chapter, the PCM-emulation using unconstrained valves is as simple as merely changing the driving frequency. Consequently, DFC-controlled unconstrained valves can save a lot of space even though the frequency - flow rate relationship is not exactly linearly proportional. Voltage-regulated flow control feature of an unconstrained valve has a linear input-output characteristics, however, the control driver requires an additional D/A converter making it bulky. In this paper, we selected frequency-controlled unconstrained valves for PCM-emulation, despite the irregularity in input-output relationship, because it is easy to implement. Essentially, PCM-emulated unconstrained valves have no harmful influences from any failure in one or more on-off switching valves that often occurs in PCM-control using solenoid on-off valves.

6.3 Using Unconstrained Valves for Pneumatic Cylinders

Unconstrained valves have no mechanical links between poppet and valve seat(orifice) and take for granted the high pressure from the supply inlet to close the valve. In particular, the high air pressure acts as a dummy constraint that replace the function of mechanically-linked constraints. If unconstrained valve is used as supply valve, the pressure difference between the supply tank and actuator sides is zero once the valve is opened thus makes the poppet-orifice not constrained. At this time, the valve lost its ability to shut off, therefore, the dummy constraint is impractical for use as supply valve to deliver air to pneumatic cylinder. Therefore, unconstrained valves can only be used as an exhaust valve, where the pressure difference at the exhaust line between cylinder load and the exhaust port will still provide air pressure for shutting off the valve. In this thesis, unconstrained valves was tested for a single-acting pneumatic cylinder using a hybrid valve system of solenoid and unconstrained valves. The solenoid on-off valves is used to supply air to the cylinder while unconstrained valve has the task to exhaust the air out from cylinder. Fig. 6.1 shows the schematic of hybrid solenoid - unconstrained valves used for speed control of a mini pneumatic cylinder.

PWM and PCM control have their own advantages and disadvantages, which is always a tradeoff between control performance and total size. PWM control is possible with only one valve, however, it will end up with

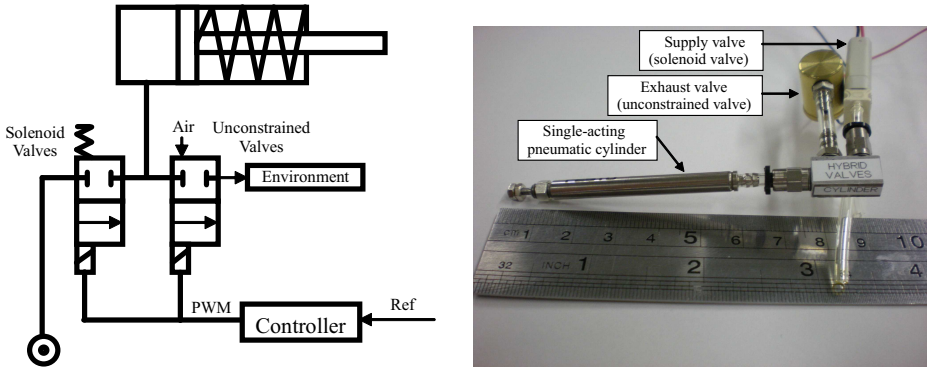

(a) (b)

Figure 6.1: Design of pneumatic cylinder that has semi-speed control metering out valve. (a) Schematic diagram of control configuration for a single-acting pneumatic cylinder using solenoid on-off valves to supply air to the cylinder and unconstrained valve to expel the air out, and (b) Photograph of the hybrid valves realization.

slower tracking response and worse accuracy compared to PCM control. In this context, unconstrained valve is a breakthrough for semi-flow control through the PCM-emulation control. The basic notion on the PCM-emulated flow control relies on the DFC feature of an unconstrained valve, making the PCM control possible using only one unconstrained valve. Although the frequency - flow rate relationship is not fully linear (Fig. 6.2(a), it can still be used to emulate the digital PCM control by picking several frequencies as a discrete input for the speed control. As an example, four discrete frequency 18, 21, 28, and 33 kHz were selected for PCM-emulation at the exhaust valve with four speed levels. Fig. 6.2(b) shows the on-off switching response of the DFC-controlled exhaust valve.

Comparing the speed-control accomplished by PCM control using solenoid on-off valves and hybrid valve system, we can see that the hybrid system has more compact size with total of two valves: one supply and one exhaust valves. Because it is impossible to use unconstrained valves for supply valves, the flow control at the supply side is regulated by a solenoid on-off valve through PWM control while an unconstrained valve at the exhaust valve is designed to emulate PCM control. The flow/speed control of DFC-based unconstrained valves is executed by transformation of discrete input signal into frequency domain to obtain to change the output flow shown in Fig. 6.3.

Application using solenoid on-off valves for driving a single-acting pneumatic cylinder can be found in [116], which proposed a robust control method for a constant velocity against load variation. In this reference,

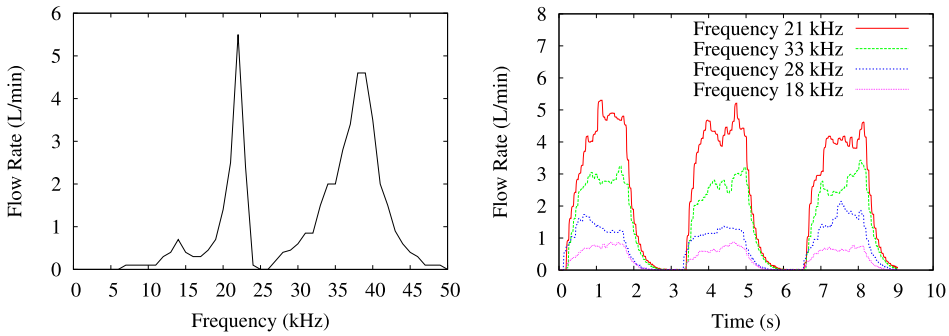

(a) (b)

Figure 6.2: Frequency-related unconstrained valves for PCM-emulation flow control. (a) Frequency characteristics of unconstrained valves (PEA 5 x 5 x 10 mm, input voltage 24 V, pressure 0.5 MPa), and (b) On-off switching response of unconstrained valve at frequency 21, 33, 28 and 18 kHz.

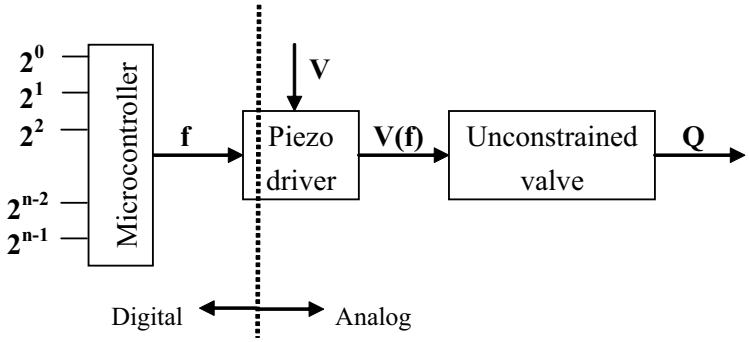

Figure 6.3: Flow control emulating PCM control scheme through varying the input frequency for unconstrained valves.

the authors adopted two on-off poppet valves driven by PWM input. Another application of flow control valve closely similar to unconstrained valve has been proposed in [117] for driving a double-acting pneumatic cylinder. Here, the valve was actuated by a piezoelectric vibrator to close or open the valve and flow control was carried out by changing the input voltage using a function generator and voltage amplifier. In this thesis, we proposed a hybrid solenoid - unconstrained valves controlled by changing the input frequency, not the input voltage, thus eliminating the necessity of voltage amplifier. Finally, the total size of servo system becomes more compact. The disadvantage of using the hybrid solenoid-unconstrained valve for pneumatic cylinder is that the flow control is restricted to the exhaust valve.

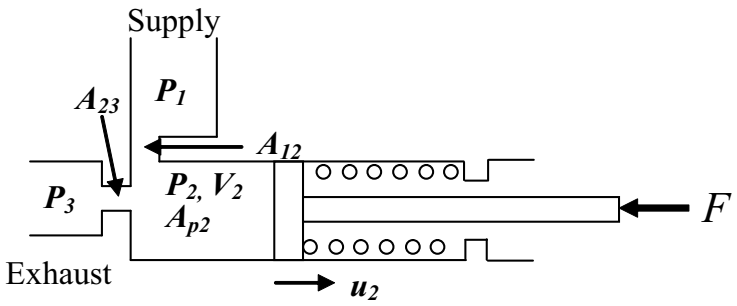

Figure 6.4: Simplified model of a single-acting pneumatic cylinder.

6.4 Control of Pneumatic Cylinder

This section briefly introduces the basic notion of pneumatic cylinder characteristics that is needed for control. If a pneumatic cylinder is controlled to stop at intermediate positions, the complete dynamic equations must be considered. In this section, the relationship of velocity and input flow rate is described to correctly understand the PCM-emulated speed control of a pneumatic cylinder. Using a single-acting pneumatic cylinder drawn schematically in Fig. 6.4, the relationship of velocity to inlet and outlet orifice flows is calculated from [49]:

$$\frac{P_2 A_{p2} u_2}{R T_2} = W_{12} - W_{23}, \tag{6.4.1}$$

where the weight flow at area A_{12} and A_{23} can be written as:

$$W_{12} = \frac{K P_1 A_{12} N_{12}}{\sqrt{T_1}}, \tag{6.4.2}$$

$$W_{23} = \frac{K P_2 A_{23} N_{23}}{\sqrt{T_2}}, \tag{6.4.3}$$

Combining Eq. 6.4.1-6.4.3, Eq. 6.4.1 can be rewritten into dimensionless form as the nonlinear relationship of steady-state cylinder velocity to air flows into and out of pneumatic cylinder:

$$\frac{A_{p2} u_2}{K R \sqrt{T_2}} = \left(\frac{T_2}{T_1}\right)^{\frac{1}{2}} A_{12} C_{12} - A_{23} N_{23}, \tag{6.4.4}$$

where the factor C_{12}, K, and N_{23} is given by:

$$C_{12} = \frac{P_1}{P_2} N_{12} = \left[\frac{\left(\frac{P_1}{P_2}\right)^{\frac{\kappa-1}{\kappa}} \left[\left(\frac{P_1}{P_2}\right)^{\frac{\kappa-1}{\kappa}} - 1 \right]}{\frac{\kappa-1}{2} \left(\frac{2}{\kappa+1}\right)^{\frac{\kappa+1}{\kappa-1}}} \right]^{\frac{1}{2}}, \tag{6.4.5}$$

$$\kappa = \left[\frac{\kappa g}{R} \left(\frac{2}{\kappa + 1} \right)^{\frac{\kappa+1}{\kappa-1}} \right]^{\frac{1}{2}}, \tag{6.4.6}$$

$$N_{23} = \left[\frac{\left(\frac{P_3}{P_2}\right)^{\frac{2}{\kappa}} - \left(\frac{P_3}{P_2}\right)^{\frac{\kappa+1}{\kappa}}}{\frac{\kappa-1}{2}\left(\frac{2}{\kappa+1}\right)^{\frac{\kappa+1}{\kappa-1}}} \right]^{\frac{1}{2}}. \tag{6.4.7}$$

The force acting on the cylinder is calculated from:

$$F_p = (P_2 - P_3)\, A_{p2}, \tag{6.4.8}$$

The selection of pneumatic cylinder requires a combination of force and speed requirement, in which it is desirable to modify Eq. 6.4.4 as a function of area and pressure ratios. Two equations can be derived from the original Eq. 6.4.4 as a plot of stroking velocity versus area A_{12} and A_{23}. The equations to be plotted are:

$$\frac{A_{p2} u_2}{KR\sqrt{T_2}\bar{A}_{12}} = C_{12} - \frac{A_{23}}{\bar{A}_{12}} N_{23}, \tag{6.4.9}$$

$$\frac{A_{p2} u_2}{KR\sqrt{T_2}A_{23}} = \frac{\bar{A}_{12}}{A_{23}} C_{12} - N_{23}, \tag{6.4.10}$$

with:

$$\bar{A}_{12} = \left(\frac{T_2}{T_1} \right)^{\frac{1}{2}} A_{12}, \tag{6.4.11}$$

Ordinarily, it is assumed that temperature is constant T_1=T_2 so that $\bar{A}_{12}$=A_{12}. Assume that the back pressure is zero (P_3=0), the plot for dimensionless velocity calculated from Eq. 6.4.9 is duplicated in Fig. 6.5 for pressure ratio $\frac{P_2}{P_1}$ and area ratio $\frac{A_{23}}{A_{12}}$, as had been reported in [49]. In Fig. 6.5, the dimensionless velocity is given by Eq. 6.4.10 for plot against P_2/P_1 from 0.2 to 1.0 and A_{12}/A_{23} from 0 to 1. The curves in Figs. 6.5 and 6.6 are plots in which the vertical axis is dimensionless velocity, and the horizontal axis represents a linear combination of pressure and area ratios. The lines of constant-area ratio are plots describing the velocity versus pressure ratio, and the lines of constant-pressure ratio are plots of velocity versus area ratio. Both the area and pressure ratio are interpolated linearly on the horizontal axis, not along the curves. From Figs. 6.5 and 6.6, we can observe that the dimensionless velocity and area (or flow) ratios has a proportionally linear relationship, which means that the speed control is identical to regulating the valve flow.

In practice, the forces working at a single-acting pneumatic cylinder are load F_{pc}, friction force f_f, a velocity-dependent damping force cu, and

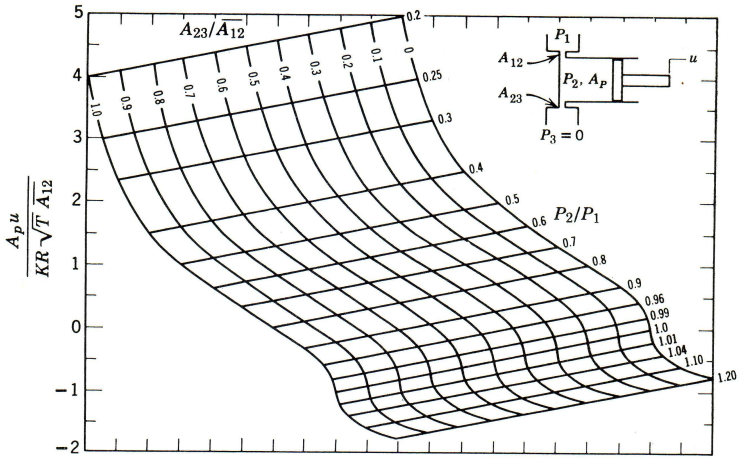

Figure 6.5: Velocity - pressure graph derived from Eq. 6.4.9 for controlling a single-acting pneumatic cylinder. [49]

spring force kX. The sum of all these forces balances the pressure force $A_{p2}\,(P_2 - P_3)$. The equation for load F_{pc} to the cylinder is:

$$F_{pc} = (P_2 - P_3)\,A_{p2} \pm f_f - cu - F_{so} - kX, \tag{6.4.12}$$

where F_{so} is the spring preload force at $X = 0$.

According to [49], pneumatic cylinders are easier to stabilize when loaded because valve is open and air flows in and out to dissipate energy when the system is loaded. Introducing static friction will damp out oscillations, but it also causes positional errors in return, indicating the undesirable existence of friction. Instead, it is usually preferable to add linear damping if this is possible. The use of valve leakage increases pneumatic damping, however, the excessive gas consumption is inefficient. In applications where gas is plentiful, this is often a simple and acceptable solution. In systems where gas is costly, it is essential to have low leakage. A well-known method to increase damping with a closed valve is to attach auxiliary volume to the actuation chamber by means of capillaries. Since unconstrained valves has a relatively small leakage, the damping constant is increased for pneumatic system with unconstrained valves.

6.5 Dynamic Response of Hybrid Solenoid - Unconstrained Valve System

The flow response of hybrid solenoid-unconstrained valves needs to be identified to obtain its open-loop characteristics that may be required for the

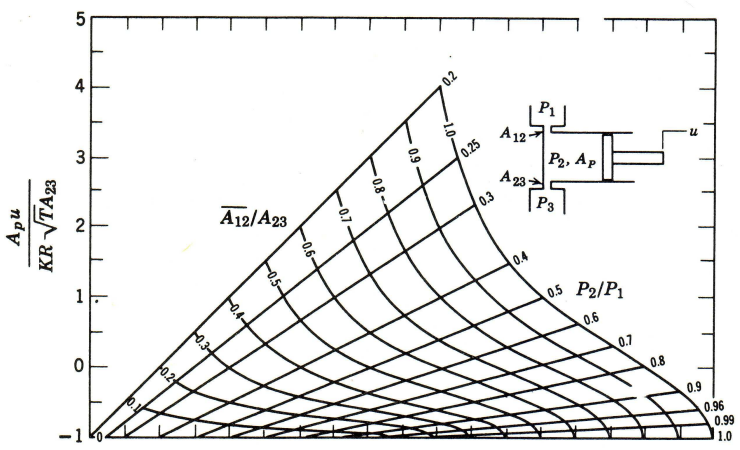

Figure 6.6: Velocity - pressure graph derived from Eq. 6.4.10 for controlling a single-acting pneumatic cylinder. [49]

Table 6.1: Switching time response of hybrid valve (unit in second)

	Supply valve	Exhaust valve			
		f=21 kHz	f=33 kHz	f=28 kHz	f=18 kHz
1^{st} trial	0.12	0.34	0.37	0.36	0.56
2^{nd} trial	0.11	0.26	0.36	0.43	0.67
3^{rd} trial	0.1	0.31	0.37	0.42	0.6
Average	0.11	0.303	0.367	0.403	0.61

control design of pneumatic cylinders. This section provides the experimental results for speed-control performance using unconstrained valves. Firstly, the reliability and practicability of using unconstrained valves for pneumatic cylinders are tested for solenoid valves. The identification results of hybrid solenoid-unconstrained valve are shown in Fig. 6.7, where the supply and exhaust valves were tested for three time trials. Fig. 6.7(a) shows the open-loop response of supply valve with a solenoid on-off valve, indicating a good repeatability of the supply valve response. Fig. 6.7(b) shows the results of exhaust valve with unconstrained valves to emulate PCM control, which verified the practicability of using unconstrained valves for controlling pneumatic cylinders. The repeatability of unconstrained valves for successive times of tests was random, as observed in Fig. 6.8. The main cause of random repeatability is mainly influenced by the non-uniform output flow of unconstrained valves. Table 6.1 assesses the speed-control repeatability using unconstrained valves by evaluating the pressure gradient, which is measured by calculating the pressure rise-up or rise-down time.

Experimental results in Fig. 6.8 show dead-time when the pneumatic

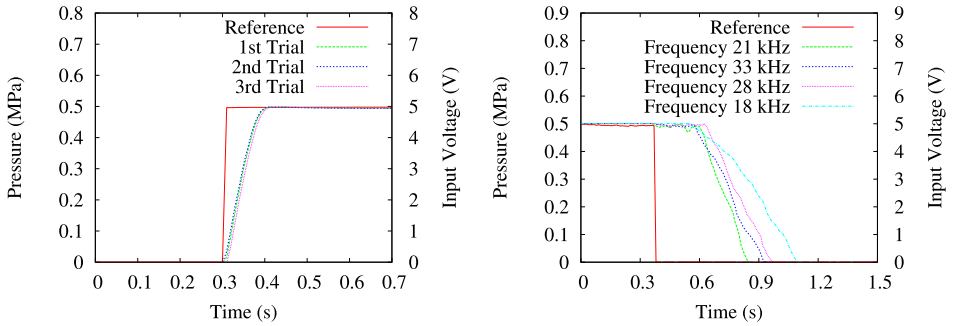

(a) Supply valve (b) Exhaust valve

Figure 6.7: Identification of open-loop semi-speed controller for pneumatic cylinder (FESTO EG-4-20-PK-2) using hybrid solenoid-unconstrained valves. (a) Pressure response at the supply side using solenoid valve, and (b) Pressure response for metering out speed control at the exhaust side using unconstrained valves.

Table 6.2: Switching dead time for metering-out unconstrained valve (unit in second)

	f=21 kHz	f=33 kHz	f=28 kHz	f=18 kHz
1^{st} trial	0.16	0.2	0.25	0.18
2^{nd} trial	0.09	0.31	0.32	0.24
3^{rd} trial	0.24	0.28	0.28	0.14
Average	0.163	0.263	0.283	0.187

cylinder is retracted, which varies for different input frequencies (or flow rates). The observed switching time is not repeated even at the same frequency, which can be implicitly explained by considering the measured switching time as a sum of valve dead-time and valve response time. It can be observed that both the valve dead-time and response time were random. Table 6.2 provides the results for valve switching dead-time at three time trials for metering out valve at frequency 21, 33, 28, and 18 kHz. Comparison was made by changing the unconstrained valves with solenoid on-off valves at the exhaust side, which also has dead-time zone. Fig. 6.9 shows the switching response of exhaust valves using solenoid on-off valves. It can be concluded that the observed dead-time has no relation to the valve, but it is closely caused by the delay at internal spring embedded in a single-acting pneumatic actuator.

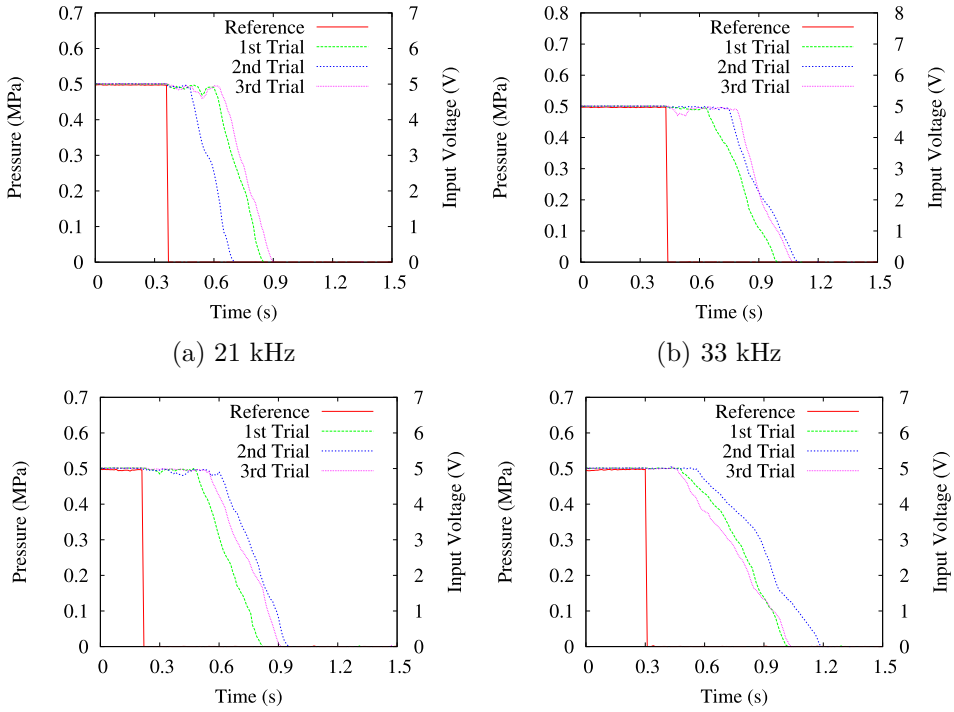

(a) 21 kHz (b) 33 kHz

(c) 28 kHz (d) 18 kHz

Figure 6.8: Repeatability test of the semi-speed control metering out valve for three trials at (a) frequency 21 kHz ($\bar{Q}$ = 4.5 L/min), (b) frequency 33 kHz ($\bar{Q}$ = 3.0 L/min), (c) frequency 28 kHz ($\bar{Q}$ = 1.5 L/min), and (d) frequency 18 kHz ($\bar{Q}$ = 0.8 L/min)

6.6 Performance Assessment

In this section, the performance results are reported for the test of hybrid solenoid-unconstrained valves. Comparative investigation are made with both valves using solenoid on-off valves. The measured result of one cycle motion for the case of all solenoid valves with 10% duty cycle is firstly given in Fig. 6.10. Fig. 6.10(a) is the result measured at the supply valve during traction motion, while Fig. 6.10(b) is for the retraction motion. The results showed that the response started to roll off at a frequency of 15 Hz averagely for the supply and exhaust valves. As shown from the experimental results, increasing the control sampling frequency resulted in slower response of the pneumatic cylinders. It can be noted in Fig. 6.11 that the valve response deteriorated for an increasing frequency and it stops when the control sampling time T is smaller than the valve switching time D . Example from the datasheet of SMC valves shows the time required to open and close the valve is about 3 ms [64], so that the total time required for one on-off cycle is 6 ms. For a PWM control that is switched at 10% duty

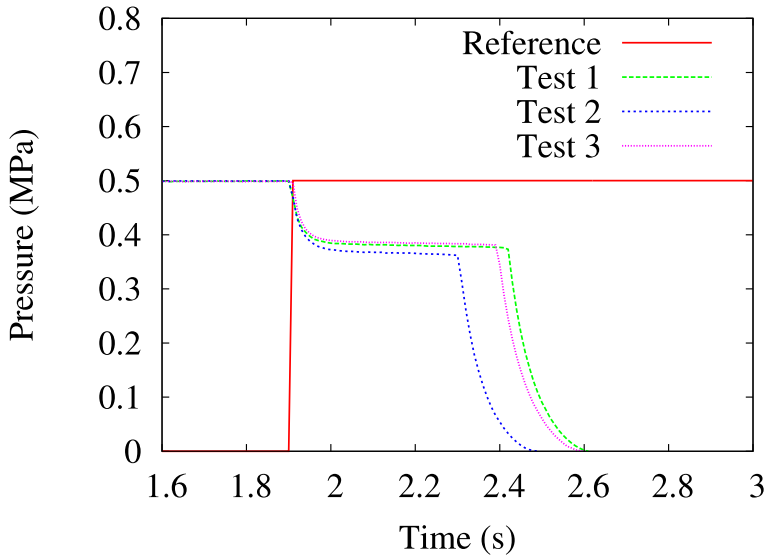

Figure 6.9: Pressure response for retraction of a pneumatic cylinder using solenoid on-off valve.

ratio, theoretical calculation indicates that the control sampling frequency should not exceed 15 Hz. Since it is always desirable to increase the control sampling frequency to maintain a good tracking accuracy, these findings reveal a tradeoff between valve response and tracking accuracy.

The open-loop response using hybrid solenoid-unconstrained valves at different switching frequency and duty cycle is shown in Fig. 6.12(a) & (b) for the PWM-controlled supply valve, where the maximum limit of the PWM switching frequency is 7 Hz. Compared to the result in Fig. 6.10 that has maximum switching frequency of 20 Hz, the open-looped control response for the hybrid valve system was deteriorating. The decreased frequency bandwidth can be considered as the cumulative influence of integration with a pair of unconstrained valve. The unconstrained valves used at the exhaust port is not constrained initially, and it requires a little time to allow a sufficient airflow to close the valve before the charging process takes place. Fig. 6.12(b) indicates a higher flow response at higher duty cycle. As a general rule of thumb, the flow control is done by modulating the pulse width, keeping the sampling frequency constant. Unconstrained valves at the exhaust side was tested to emulate a semi-PCM control, where the unconstrained valve was switched at Q=0.8 L/min and Q=4 L/min. Fig. 6.13 shows the results of PCM-emulated flow control at 2, 5, and 10 Hz, which proves the practicability of unconstrained valves for semi PCM-emulation.

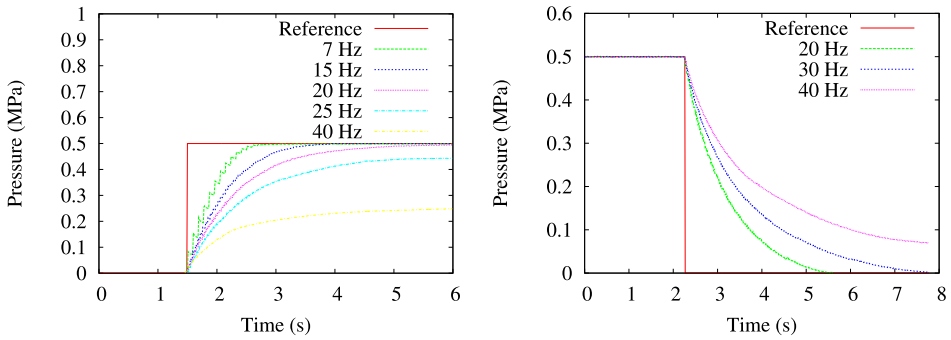

(a) Supply valve (b) Exhaust valve

Figure 6.10: PWM control response test for the case of both solenoid on-off valves. (a) Switching response of the supply valve, and (b) Switching response of the exhaust valve.

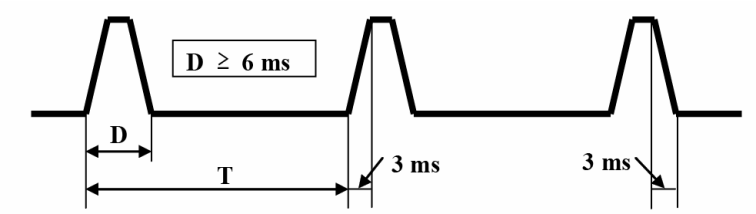

Figure 6.11: Switching response of a solenoid on-off valve SMC S070 series.

6.7 Conclusion

Compared to the PWM and PCM control using the conventional solenoid on-off valves, DFC-controlled unconstrained valves has been proved to be practical for the emulation of PCM control while being much more compact. Despite their demerit of a dummy constraint, an application test of speed control using a hybrid solenoid-unconstrained valve system was proposed to be free from the treats of valve failures that often occurs in PCM control using on-off valves. The performance of unconstrained valves for PCM-emulation was verified through a series of experiments for different frequencies, which shows its practicability for the control of pneumatic cylinders.

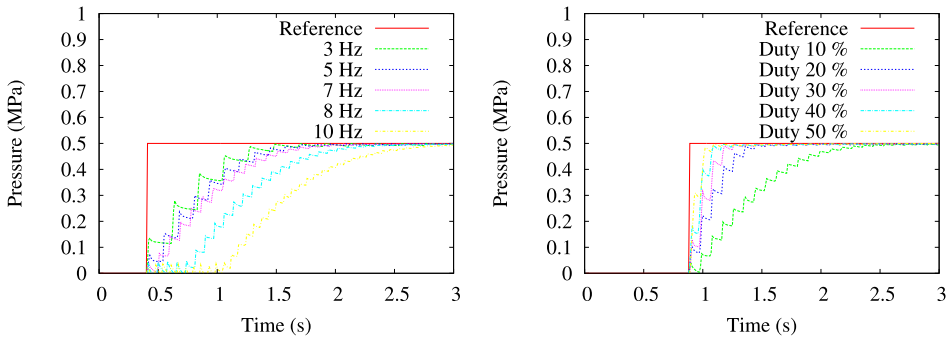

(a) (b)

Figure 6.12: PWM control for supply valve using hybrid solenoid - unconstrained valves. (a) Limitation of switching frequency, and (b) PWM-based flow control at various duty cycle.

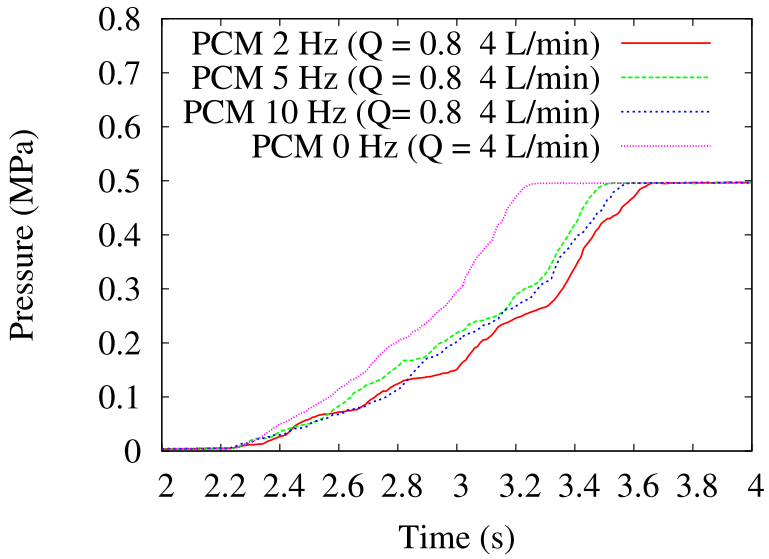

Figure 6.13: Tracking response of PCM control using unconstrained valves for hybrid valves.

Chapter 7

Discussions and Future Works

The technology of pneumatic valves is progressing from large-scale and heavyweight industrial valves to the development of miniaturized valves with less weight. This is because applications for wearable robots require high power-to-weight ratio as they minimize weight restrictions on the users wearing them. The size and weight of valves are no longer problems due to the development of MEMS fabrication processes, however, the limitations of micro valves are their low flow rate and manufacturing complexity. Hindrances for valve miniaturization also comes from the lack of ultra precision assembly and the limited availability of mini solenoid valves.

The work in this dissertation is an on-going research program to miniaturize pneumatic valves used for wearable robots or human assist applications. A radically different principle from that of conventional pneumatic valves is presented, whereby a valve is actuated using vibration modes of a PEA. This control valve has an unconstrained poppet structure and therefore the assembling procedures become much easier for miniaturized valves. Our current achievement of unconstrained valves, measuring ϕ 7 x 9 mm, has been much more compact than the conventional solenoid valves. In practical application, this valve is able to operate at pressure up to 0.5 MPa and has an average flow rate ranging from 3.5 to 29.5 L/min, depending on the valve sizes. The valve is tested with different levels of input voltage, frequency, and supply pressure to observe its peculiar flow characteristics. We have formulated a simulation model of a piezoelectically-driven unconstrained pneumatic ON-OFF poppet valve, considering the mechatronic part of a PEA, and its integration with a pneumatic and mechanical impact system. The modeling of each subsystem was introduced in order to generate an overall valve model based on the dynamics of a bouncing poppet. The simulated and experimental results showed good agreement, thus validating the proposed simulation model. This dynamic model can

be used to calculate the outlet flow rate of an unconstrained valve with an adjustable input voltage and frequency. In addition, this analytical model can be used to estimate the input/output behavior of valves with different parameters.

We have discussed unconstrained valve design focusing on miniaturization, where the individual design parameters are studied in detail referring to experimental results. For unconstrained valves, flow generation drops together with valve miniaturization is concluded, illustrating the tradeoff between power and size limitations. Low power generation of PEAs is also related to energy conversion inefficiency, which is improved by using a second-order LC tuner. Using an LC tuner increased the output flow up to 400% over conventional approaches. Considering its applications for robotic use, valve drivers must also be miniaturized, placing constraints on valve and driver miniaturization. Simply using high voltage input to increase flow is trivial but high-voltage drivers are difficult to miniaturize, making it desirable to limit operating voltage. Maximizing flow requires the following unconstrained-valve design parameters be considered:

- A compact valve with a high flow is designed by appropriately combining the poppet - orifice diameter based on PEA size and a poppet - orifice ratio exceeding 4.
- Base thickness is functionally similar to a diaphragm. A thin base inevitably has a higher flow.
- Experiments confirm that the valve material does not affect the output flow.
- Large accumulator volume (hollow valve space) leads to higher flow but contradicts the purpose of miniaturization.

Integration of PEA driver and an unconstrained valve with an embedded microprocessor allows conversion from harmonic input voltage into direct PWM control switching without requiring an additional interface. It is now easy to control the valve by providing it with a digital input command. A series of tests were performed to evaluate the performance of modulated digital switching valves, and satisfactory results of PWM control were obtained. The flow tendency and valve response time were discussed, showing the experimental results of pulse width and pulse frequency modulation. The behavior and versatility of unconstrained modulated digital switching valve in control systems were presented, with descriptions of the advantages and disadvantages of unconstrained valve. Integration of a PEA driver and

a PWM controller into the valve unit was accomplished, which allowed reduction of the overall size.

Using unconstrained valves for pneumatic cylinder and pressure control for PAM applications has advantage over solenoid on-off valves of compactness made possible by the unconstrained structure and piezoelectric actuator use, enabling inherent PCM-emulation. This dissertation describes the implementation of a pressure-controlled servodrive for PAMs using unconstrained valves, where tracking performance throughout using five control algorithms was verified, *i.e.*, PI control, hysteresis control, multi-level hysteresis control, proportional PWM control, and multimode switching control. We found that multi-level hysteresis control was superior to the other existing pressure control algorithms, which has similar results for both solenoid and unconstrained valves. Unconstrained valves provide a frequency-controllable flow rate function (or discrete frequency control) that is advantageous for use in multi-level hysteresis control, where major and minor flow can be supplied by only one valve. As a result, the proposed pressure-control system utilizes fewer valves compared to the existing solenoid valves. Experimental demonstrations using irregular waveforms in loaded condition and different pressure levels indicate that this system has fairly good tracking performance and robustness against external loads. Although the tracking results showed a hysteresis loop and less accuracy, a miniaturized pressure control valve with unconstrained valves was shown to be much more compact than existing standard pressure control valves. Therefore, pressure control using unconstrained valves are practically effective for wearable robots and human assistance robots that demand a high power-to-weight ratio.

Bang-bang control, which can be assumed as the plant operator's behavior, is one of the most popular methods of time optimal control [118]. It aims at the shortest system transition time when set point changes from a value to another. Bang-bang control holds more eminent dynamic performance than PID control, especially in hurdling the change of set point value and influence of large disturbance. But it is inclined to be vibratory in static state. When the deviation enters into small scope, however, the control quality is not better than PID control. In the contrary, it is usually not easy for PID control to guarantee the control performance in the case of large deviation or large disturbance. But it has better static performance and more powerful capability of eliminating the steady-state error when it's in the scope of small deviation. As a result, it is necessary to combine both advantages of above-mentioned control methods. The idea of bang-bang and PID integrated control is generating under this background,

which means selecting bang-bang control in large deviation and delivering to PID control for eliminating the steady-state error. In [118], it was shown that bang-bang + PID integrated control achieved faster dynamic response than compared to PID controller alone. For future improvement, the unconstrained valves can be controlled to use bang-bang control strategies to track large set point variation or reject large disturbance at first, and then switch to PID control strategies for eliminating small deviation.

In regard to pneumatic cylinders, position and velocity control are more common associated with PWM or PCM control. Position tracking of pneumatic cylinders is mostly controlled by servovalves, however, on-off valves can be an alternative solution for use at a restricted working area. In addition, the use of on-off valves is popular for low-cost application. In regard to PWM and PCM control for on-off valves, DFC-controlled unconstrained valves has been proved to be practical for the emulation of PCM control while being much more compact. Despite their demerit of dummy constraint, an application test of speed control using a hybrid solenoid-unconstrained valve system was proposed to be free from the treats of valve failures that often occurs in PCM control using on-off valves. Chapter 6 describes the application test of unconstrained valves for emulating PCM control that was used for speed control. Its practicability for PWM-emulation was verified from a series of experiments, which offers a compact system for speed control of pneumatic cylinders.

Pneumatic actuators have good force-to-weight ratio and natural compliance, making them suitable candidates for impedance control. However, they are generally unsuitable for precise control due to the limited tracking accuracy. The work in [95] is an exceptional example of using pneumatic actuator for high-precision control made possible by using ultra fast pressure regulator. The implication is an increased valve-actuator size in regard to the bulky high-precision pressure regulator that includes a servo valve, flow sensor, isothermal chamber, pressure sensor, and etc. A new approach of hybrid pneumatic-electric actuation was proposed by Shin, *et. al.*, [10] to generate high force from the pneumatic actuation while an electric motor is coupled to compensate for the low dynamics of the pneumatic actuator allowing the hybrid actuation to achiever higher force and frequency bandwidth. The advantages and disadvantages of pneumatic and electric actuation is summarized in Table 7.1, which gives clues for hybrid actuation. In Table 7.1, hybrid actuation inherits the good properties from both pneumatic and electric actuators, while the good characteristics of electric motors complement the drawback of pneumatic actuators and vice versa. In this way, the accuracy problem of miniaturized unconstrained valves for

Table 7.1: Comparison of actuator drives [54]

Actuators	Advantages	Disadvantages
Electro-mechanical	Good positioning accuracy Highly dynamic Flexible drive concept High overall efficiency Condition can be monitored well	Restricted power density Energy consumption during static operation Restricted thermal range of operation High percentage of moving mechanics
Pneumatic	Good working capacity Good thermal operating range Good power-to-weight ratio High reliability & operating safety Good price-performance ratio One supply line	Conditioning of compressed air necessity To some extend: large dimensions Friction & compressibility complicated control Limited positioning accuracy

pneumatic actuation can be solved by hybrid pneumatic-electric actuation while keeping the force-to-weight ratio high once the unconstrained valves can be miniaturized.

Bibliography

[1] K. Suzumori, "New Pneumatic Actuators Producing Breakthrough in Mechatronics," *Proc. of the 7th JFPS Int. Symp. On Fluid Power*, pp. 197-202, 2008.

[2] J. E. Pratt, B. T. Krupp, C. J. Morse, and S. H. Collins, "The RoboKnee: An Exoskeleton for Enhancing Strength and Endurance During Walking," *Proc. IEEE Int. Conf. on Robotics and Automation*, pp. 2430-2435, 2004.

[3] S. K. Banala, *et. al*, "A Gravity Balancing Leg Orthosis for Robotic Rehabilitation," *Proc. IEEE Int. Conf. on Robotics and Automation*, pp. 2474-2479, 2004.

[4] H. Kobayashi, and K. Hiramatsu, "Development of Muscle Suit for Upper Limb," *Proc. IEEE Int. Conf. on Robotics and Automation*, pp. 2480-2485, 2004.

[5] S. Davis, *et. al*, "Enhanced Dynamic Performance in Pneumatic Muscle Actuators," *Proc. IEEE Int. Conf. on Robotics and Automation*, pp. 2836-2841, 2002.

[6] A. M. Bertetto, and M. Ruggiu, "A Novel Fluidic Bellows Manipulator," *Journal of Robotics and Mechatronics*, vol. 16, No. 6, 2004.

[7] N. Saga, J. Y. Nagase, and Y. Kondo, "Development of a Tendon-Driven System Using Pneumatic Balloon," *Journal of Robotics and Mechatronics*, vol. 18, No. 2, 2006.

[8] T. Shimizu, Y. Hayakawa, and S. Kawamura, "Development of a Hexahedron Rubber Actuator," *Proc. IEEE Int. Conf. on Robotics and Automation*, pp. 2619-2624, 1995.

[9] Y. Zhu, and E. J. Barth, "Impedance Control of a Pneumatic Actuator for Contact Tasks," *Proc. of the 2005 IEEE Int. Conf. on Robotics and Automation*, pp. 987-992, 2005.

[10] D. Shin, I. Sardellitti, and O. Khatib, "A Hybrid Actuation Approach for Human-Friendly Robot Design," *2008 IEEE Int. Conf. on Robotics and Automation*, pp. 1747-1752, 2008.

[11] M. L. Hughes, S. Dewhirst, and R. A. Heron, "A low-cost microprocessor to fluid power interface valve," *Microprocessors in Fluid Power Engineering*, I Mech E Conference Publications, 1984.

[12] T. Akagi, S. Dohta, and S. Katayama, "Development of Small-Sized Flexible Pneumatic Valve Using Vibration Motor and Its Application for Wearable Actuator," *15th Int. Conf. on Mechatronics and Machine Vision in Practice*, pp. 441-446, 2008.

[13] M. C. Birch, et. al., "A Miniature Hybrid Robot Propelled by Legs," *2001 IEEE/RSJ Int. Conf. on Intelligent Robots and Systems*, vol. 2, pp. 845-851, 2001.

[14] Y.K. Lee and I. Shimoyama, "A Multi-Channel Micro Valve for Micro Pneumatic Artificial Muscle," *The 15th IEEE Int. Micro Electro Mechanical Systems (MEMS'02)*, pp. 702-705, Las Vegas, Nevada, USA, 2002.

[15] S. Uehara and S. Hirai, "Unconstrained Vibrational Pneumatic Valves for Miniaturized Proportional Control Devices," *9th Int. Conf. on Mechatronics Technology (ICMT2005)*, Kuala Lumpur, Malaysia, December, 2005.

[16] F. W. Wilson, P. D. Harvey and C. B. Gump, *Pneumatic Controls for Industrial Application*, American Society of Tool and Manufacturing Engineers (ASTME), Manufacturing Data Series, 1965.

[17] T. Miyajima, *et. al.*, "Development of Pneumatic High Precise Position Controllable Servo Valve," *Proc. of the 2004 IEEE Int. Conf. on Control Applications*, Sept. 2004.

[18] K. Ahn, and S. Yokota, "Intelligent Switching Control of Pneumatic Actuator Using On/Off Solenoid Valves," *Mechatronics 15*, pp. 683-702, 2005.

[19] Y. Chen, J. F. Zhang, C. J. Yang, and B. Niu, "Design and Hybrid Control of the Pneumatic Force-Feedback Systems for Arm-Exoskeleton by Using On/Off Valve," *Mechatronics 17*, pp. 325-335, 2007.

[20] http://www.theleeco.com/__85256B740051C08B.nsf/0/F01369CF96E7E8FF852564BC006F1479?Open

[21] K. W. Oh, C. H. Anh, "Review of Micro Valves," *Journal of Micromechanics and Microengineering 16*, pp. R13-R39, 2006.

[22] N. T. Nguyen, S. T. Wereley, *Fundamentals and Applications of Microfluidics*, Artech House Publishers, 2nd Edition.

[23] C. Fu, Z. Rummler, and W. Schomburg, "Magnetically driven micro ball valves fabricated by multilayer adhesive film bonding," *J. Micromech. Microeng. 13*, pp. 96-102, 2003.

[24] P. Shao, Z. Rummler, and W. Schomburg, "Polymer micro piezo valve with a small dead volume," *J. Micromech. Microeng. 14*, pp. 305-309, 2004.

[25] P. W. Barth, "Silicon microvalves for gas flow control," *Proc. 8th Int. Conf. on Solid-State Sensors and Actuators (Transducers'95)*, pp. 276-277, 1995.

[26] C. M. Ho, X. Yang, C. Grosjean, and Y. C. Tai, "A MEMS thermopneumatic silicone rubber membrane valve," *Sensors Actuators A 64*, pp. 101-108, 1998.

[27] M. Kohl, D. Dittmann, E. Quardt, and B. Winzek, "Thin film shape memory microvalves with adjustable operation temperature," *Sensors Actuators A 83*, pp. 214-219, 2000.

[28] G.S. Fischer, I. Iordachita, C. Csoma, J. Tokuda, S.P. DiMaio, C.M. Tempany, N. Hata, and G. Fichtinger, "MRI-Compatible Pneumatic Robot for Transperineal Prostate Needle Placement", *IEEE/ASME Transactions on Mechatronics*, Vol. 13, No. 3, pp. 295-305, June 2008.

[29] R. Lane and B. Craig, "An Introduction to Smart Materials," *Material Ease, The AMPTIAC Quarterly*, Vol. 7, No. 2, pp. 9-14.

[30] X. P. Ouyang, "Piezoelectric Actuation for Screw-in Cartridge Valves," *Proc. of the 2008 IEEE/ASME Int. Conf. on Advanced Intelligent Mechatronics*, pp. 49-55, 2008.

[31] G. S. Chung, and K. B. Han, "Characteristics of a micromachined piezovalve combined with a multilayer ceramic actuator," *Microelectronics Journal 38*, pp. 690-694, 2007.

[32] S. Shoji, B. van der Schoot, N. de Rooij, and M. Esashi, "Smallest Dead Volume Microvalves for Integrated Chemical Analyzing Systems," *Tech. Dig. 6th Int. Conf. on Solid-State Sensors and Actuators*, pp. 1052-1055, 1991.

[33] M. Esashi, S. Shoji, and A. Nakano, "Normally Closed Microvalve and Micropump Fabricated on a Silicon Wafer," *Proc. of MEMS'89, 1st IEEE Int. Workshop Micro Electromechanical System*, pp. 29-34, 1989.

[34] I. Chakraborty, *et. al*, "MEMS micro-valve for space applications," *Sensors and Actuators A*, vol. 83, pp. 188-193, 2000.

[35] D. Hirooka, K. Suzumori, and T. Kanda, "Flow control valve for pneumatic actuators using particle excitation by PZT vibrator," *Sensors and Actuators A 155*, pp. 285-289, 2009.

[36] C.S. Joo, Y.B. Bang, K.I. Lee and Y.B. Shim, "Development of a High-Speed Electrohydraulic Servovalve System Using Stack-Type Piezoelectric Elements", *Int. Journal of the Korean Society of Precision Engineering*, Vol. 4, No. 6, Nov. 2003.

[37] J.E. Lindler and E.H. Anderson, "Piezoelectric Direct Drive Servovalve", *Proc. of SPIE*, Vol. 4698-53, Industrial and Commercial Applications of Smart Structures Technologies 2002.

[38] H.B. Zhao, K. Stanley, Q.M.J. Wu and E. Czyzewka, "Structure and Characterization of a Planar Normally Closed Bulk-micromachined Piezoelectric Valve for Fuel Cell Applications", *Sensors and Actuators*, 120:134-141, 2005.

[39] S.N. Yun, Y.B. Ham, J.H. Park, B.S. Ryu and B.O. Choi, "Pressure Regulator for Pneumatic Valve with a PZT Actuator", *SICE-ICASE Int. Joint Conf. 2006*, pp. 4121-4125, 2006.

[40] A. Doll, M. Wischke, H.J. Schrag, A. Geipel, F. Goldschmidtboeing and P. Woias, "Characterization of active silicon microvalves with piezoelectric membrane actuators", *Microelectronics Engineering*, 84:1202-1206, 2007.

[41] S.B. Choi and J.K. Yoo, "Pressure Control of a Pneumatic Valve System Using a Piezoceramic Flapper", *Proc. of the I MECH E Part C Journal of Mechanical Engineering Science*, Vol. 218, pp. 83-89, 2004.

[42] H. Ohuchi, T. Mita and T. Osada, "Characteristics of Pneumatic On-Off Control Valve Driven by Impulsive Force of a PZT Actuator", *Proc. of 5th Triennial Int. Symposium on Fluid Control, Measurement and Visualization*, pp. 337-342, 1997.

[43] H.J.M.T.A. Adriaens, W.L. de Koning, and R. Banning, "Modeling Piezoelectric Actuators", *IEEE/ASME Transactions on Mechatronics*, Vol. 5, No. 4, pp. 331-341, December 2000.

[44] H.M. Lankarani, P.E. Nikravesh, "Continuous Contact Force Model for Impact Analysis in Multibody Systems", *Nonlinear Dynamics*, pp. 193-207, 1994.

[45] K.L. Johnson, *Contact Mechanics*, Cambridge University Press, Cambridge, 1985.

[46] R.M. Brach, *Mechanical Impact Dynamics: Rigid Body Collisions*, John Wiley & Sons, New York, 1991.

[47] B.M. Kim, S. Aramaki, "Motion of Spherical Particles After Impinging on a Flat Plate", *Reports of Institute of Advanced Material Study*, Vol. 13, No. 1, pp. 1-5, Kyushu University, 1999.

[48] M. Goldfarb, N. Celanovic, "Modeling Piezoelectric Stack Actuators for Control of Micromanipulation", *IEEE Transactions on Control Systems Technology*, Vol. 3, pp. 69-79, June 1997.

[49] B.W. Andersen, *The Analysis and Design of Pneumatic Systems*, John Wiley & Sons, Inc., 1967.

[50] http://www.physikinstrumente.com/en/products/piezo_tutorial.php

[51] http://www.physikinstrumente.com/en/pdf_extra/2009_PI_Piezo_University_Designing_with_Piezo_Actuators_Tutorial.pdf

[52] D.J. Morris, D.F. Bahr, M.J. Anderson, "Displacement amplification in curved piezoelectric diaphragm transducers," *Sensors and Actuators A: Physical*, vol. 141, pp. 262-265, 2008.

[53] J.J. Vlassak and W.D. Nix, "A new bulge test technique for the determination of Young's modulus and Poisson's ratio of thin films," *Journal of Material Research*, vol. 7, pp. 3242-3249, 1992.

[54] R. Isermann, Mechatronic Systems Fundamentals, Springer, (2005).

[55] http://www.physikinstrumente.com/en/products/prdetail.php?sortnr=400600.75

[56] http://www.rosscontrols.com/vresp.htm

[57] A.M. Al-Ibrahim, D.R. Otis, "Transient Air Temperature and Pressure Measurements During the Charging and Discharging Processes of an Actuating Pneumatic Cylinder," *Proc.of the 45th National Conf on Fluid Power*, 1992.

[58] M. Tatsumi, M. Ito, S. Jien, S. Hirai, and K. Honda, "Influence of Shape and Material to Miniaturize Unconstrained Vibration Pneumatic Poppet Valves," *The Proc. on Spring Conf. of Japan Fluid Power System Society 2009*, pp. 125 - 127, 2009 (in Japanese).

[59] K. A. A. Yehia, "A New Approach for Designing Solenoid Valves," *Journal of Applied Science Research 2(12)*, pp. 1099 - 1105, 2006.

[60] T. Kushida, "High Speed Powerful and Simple Solenoid Actuator "DISOLE" and Its Dynamic Analysis Results," *SAE Technical Papers Series*, pp. 127 - 136, 1985.

[61] T. Kajima and Y. Kawamura, "Development of a High-Speed Solenoid Valve: Investigation of Solenoids," *IEEE Transactions on Industrial Electronics*, v. 42, pp. 1 - 8, 1995.

[62] L. C. Passarini and P. R. Nakajima, "Development of a High-Speed Solenoid Valve: an Investigation of the Importance of the Armature Mass on the Dynamic Response," *Journal of the Brazilian Society of Mechanical Sciences and Engineering*, Vol. XXV, No. 4, pp. 329 - 335, 2003.

[63] http://ww1.koganei.co.jp/jp/shop/goods/series.aspx?category=B010050000&series=B010050010

[64] http://www.smcworld.com/2008/webcatalog/docs/directional/direct345/S070.pdf#page=1

[65] S. Yokota and K. Akutu, "Fast-Acting Electrohydraulic Digital Transducer (Poppet-Type On-Off Valve by Making Use of a Multilayered Piezoelectric Device)," *Nihon kikai gakkai ronbun (B)*, vol. 56, No. 524, 1990.

[66] M. J. Guan and W. H. Liao, "Studies on the Circuit Models of Piezoelectric Ceramics," *International Conference on Information Acquisition*, pp. 26 - 31, 2004.

[67] H. W. Katz, *Solid State Magnetic and Dielectric Devices*, London: Wiley, 1959.

[68] D. Campolo, M. Sitti, and R. S. Fearing, "Efficient Charge Recovery Method for Driving Piezoelectric Actuators with Quasi-Square Waves," *IEEE Trans. On Ultrasonics, Ferroelectrics, and Frequency Control*, Vol. 50, No. 3, pp. 237 - 244, 2003.

[69] M. Karpelson, G. Y. Wei, and R. J. Wood, "Milligram-Scale High-Voltage Power Electronics for Piezoelectric Microrobots," *2009 IEEE Int. Conf. on Robotics and Automation*, pp. 2217 - 2224, 2009.

[70] C. Grosjean, X. Yang, and Y. C. Tai, "A Practical Thermopneumatic Valve," *Twelfth IEEE Int. Conf. on MEMS 1999*, pp. 147-152, 1999.

[71] B. Tondu, S. Ippolito, J. Guiochet and A. Daidie, "A Seven-degrees-of-freedom Robot-arm Driven by Pneumatic Artificial Muscles for Humanoid Robots," *The Int. Journal of Robotics Research*, vol. 24, No. 4, pp. 257-274, April 2005.

[72] R.W. Colbrunn, G.M. Nelson and R.D. Quinn, "Design and Control of a Robotic Leg with Braided Pneumatic Actuators," *Proc. IEEE/RSJ Int. Conf. on Intelligent Robots and Systems*, Hawai, 2001.

[73] K. Hosoda and T. Takuma, "Ballistic Control for Biped Walking with Pneumatic Actuators," *2004 Int. Symposium on Nonlinear Theory and its Applications*, pp. 83-86, Fukuoka, Japan, 2004.

[74] J.F. Zhang, et al., "Modeling and control of a curved pneumatic muscle actuator for wearable elbow exoskeleton," *Mechatronics 18*, pp. 448-457, 2008.

[75] E.V. Mangan, D.A. Kingsley, R.D. Quinn and H.J. Chiel, "Development of a Peristaltic Endoscope," *IEEE Int. Conf. on Robotics and Automation (ICRA'02)*, pp. 347-352, USA, May 2002.

[76] S. Nishino, et al., "Development of Robot Hand with Pneumatic Actuator and Construct of Master-Slave System," *Proc. of the 29th Annual Int. Conf. of the IEEE EMBS*, pp. 3027-3030, France, 2007.

[77] A. Kitagawa, et al., "Development of a Portable Pneumatic Power Source Using Phase Transition at the Triple Point," *Trans. of the Japan Fluid Power System Society*, vol. 36, No. 6, pp. 158-164, 2005.

[78] S.C. Terry, J.H. Jerman and J.B. Angell, "A Gas Chromatographic Air Analyzer Fabricated on a Silicon Wafer," *IEEE Trans. on Electron Devices*, vol. ED-26, No. 12, pp. 1880-1886, 1979.

[79] Anonymous "GIGATECO Inc. Solenoid Products" http://www.gigateco.jp/en/index.html.

[80] M.M. Hamdan and Z.Q. Gao, "A Novel PID Controller for Pneumatic Proportional Valves with Hysteresis," *IEEE Industrial Application Society 2000 Annual Meeting and World Conf. on Industrial Applications of Electrical Energy*, 2000.

[81] R. Li, W. Shi and Q. Yang, "Multi-region Fuzzy Tracking Control for a Pneumatic Servo Squeezing Forces System," *Proc. of the 5th World Congress on Intelligent Control and Automation*, pp. 4504-4506, China, 2004.

[82] R.B. van Varseveld and G.M. Bone, "Accurate Position Control of a Pneumatic Actuator Using On/Off Solenoid Valves," *IEEE/ASME Transactionson Mechatronics*, vol. 2, No. 3, pp. 195-204, 1997.

[83] E.J. Barth, J. Zhang and M. Goldfarb, "Control Design for Relative Stability in a PWM-Controlled Pneumatic System," *ASME Journal of Dynamic Systems, Measurement, and Control*, vol. 125, pp. 504-508, 2003.

[84] I. Sardellitti, J. Park, D. Shin and O. Khatib, "Air Muscle Controller Design in the Distributed Macro-Mini (DM^2) Actuation Approach," *Proc. of the 2007 IEEE/RSJ Int. Conf. on Intelligent Robots and Systems*, pp. 1822-1827, USA, 2007.

[85] D. Jutras and P. Bigras, "Control of an Actuator Made of Two Antagonist McKibben Muscles via LMI Optimization," *IEEE Int. Sym. on Industrial Electronics (ISIE 2006)*, pp. 3072-3077, Canada, 2006.

[86] R. Van Ham, B. Verrelst, R. Daerden and D. Lefeber, "Pressure Control with On-Off Valves of Pleated Pneumatic Artificial Muscles in a Modular One-Dimensional Rotational Joint," *Int. Conf. on Humanoid Robots*, 2003.

[87] T. Noritsugu and T. Tanaka, "Application of Rubber Artificial Muscle Manipulator as a Rehabilitation Robot," *IEEE/ASME Transactions on Mechatronics*, vol. 2, No. 4, pp. 259-267, 1997.

[88] D.G. Caldwell, G.A. Medrano-Cedra, M. Goodwin, "Control of Pneumatic Muscle Actuators", IEEE Control Systems Magazine, vol. 15, No. 1, pp. 40-48, 1995.

[89] T. Akagi and S. Dohta, "Development of Small-Sized Multi-port Pressure Control Valve for Wearable Actuator," *Proc. of the 2004 IEEE Int. Workshop on Robot and Human Interactive Communication*, pp. 649-654, Japan, 2004.

[90] T. Noritsugu and T. Tanaka, "Application of Rubber Artificial Muscle Manipulator as a Rehabilitation Robot," *Proc. of the IEEE Int. Workshop on Robot and Human Communication*, pp. 112-117, Tsukuba, Japan, 1996.

[91] J. L. Johnson, P. E., "Understanding pressure control with a varying load," *Hydraulics & Pneumatics*, pp. 22-24, July 2005.

[92] J. R. Leigh, *Control Theory A Guided Tour*, IEE Control Engineering Series 45, 1992.

[93] J. L. Johnson, P. E., "PWM - the unconventional way to regulate pressure," *Hydraulics & Pneumatics*, pp. 22-24, June 2004.

[94] Staff report, "Dealing with the Pressure," *Hydraulics & Pneumatics*, pp. 37-42, May 2006.

[95] K. Kawashima, and T. Kagawa, "Unsteady flow generator for gases using an isothermal chamber," *Measurement*, vol. 33, Issue 4, pp. 333-340, June 2003.

[96] S. Jien, Y. Ogawa, S. Hirai, and K. Honda, "Performance Evaluation of a Miniaturized Unconstrained Digital On-Off Switching Valve," *2008 IEEE/ASME Int. Conf. on Advanced Intelligent Mechatronics*, 2008.

[97] T. Noritsugu and M. Takaiwa, "Robust Positioning Control of Pneumatic Servo System with Pressure Control Loop," *IEEE Int. Conf. on Robotics and Automation*, pp. 2613 - 2618, 1995.

[98] T. Noritsugu and T. Wada, "Adaptive structure control of pneumatically actuated robot," *JHPS Int. Symp. Fluid Power*, pp. 591 - 598, 1989.

[99] J. H. Cocatre-Zilgien, F. Delcomyn, and J. M. Hart, "Performance of a Muscle-like "Leaky" Pneumatic Actuator Powered by Modulated Air Pulses," *Journal of Robotic Systems 13(6)*, pp. 379 - 390, 1996.

[100] S. Jien, S. Hirai, Y. Ogawa, M. Ito and K. Honda, "Pressure Control Valve for McKibben Artificial Muscle Actuators with Miniaturized Pneumatic On/Off Valves," *2009 IEEE/ASME Int. Conf. on Advanced Intelligent Mechatronics*, Singapore, 2009.

[101] N. Gulati, and E. J. Barth, "A Globally Stable, Load-Independent Pressure Observer for the Servo Control of Pneumatic Actuators," *IEEE/ASME Transactions on Mechatronics*, vol. 14, No. 3, June 2009.

[102] G. M. Bone, and S. Ning, "Experimental Comparison of Position Tracking Control Algorithms for Pneumatic Cylinder Actuators," *IEEE/ASME Transactions on Mechatronics*, vol. 12, No. 5, pp. 557-561, 2007.

[103] Z. Situm, J. Petric and M. Crnekovic, "Sliding Mode Control Applied to Pneumatic Servo Drive," *The 11th Mediterranean Conf. on Control and Automation*, 2003.

[104] S. R. Pandian, F. Takemura, Y. Hayakawa, and S. Kawamura, "Pressure Observer-Controller Design for Pneumatic Cylinder Actuators," *IEEE/ASME Transactions on Mechatronics*, vol. 7, No. 4, pp. 490-499, 2002.

[105] L. Ruihua, S. Weixiang, and Y. Qingyu, "Multi-region Fuzzy Tracking Control For a Pneumatic Servo Squeezing Forces System," *Proc. of the 5th World Congress on Intelligent Control and Automation*, pp. 4504-4507, 2004.

[106] T. Nguyen, J. Leavitt, F. Jabbari, and J. E. Bobrow, "Accurate Sliding-Mode Control of Pneumatic Systems Using Low-Cost Solenoid Valves," *IEEE/ASME Transactions on Mechatronics*, vol. 12, No. 2, pp. 16-219, 2007.

[107] X. Shen, J. Zhang, E. J. Barth, and M. Goldfarb, "Nonlinear Averaging Applied to the Control of Pulse Width Modulated (PWM) Pneumatic Systems," *Proc. of the 2004 American Control Conf.*, pp. 4444-4448, 2004.

[108] J. Wang, J. Pu, and P. Moore, "A practical control strategy for servo-pneumatic actuator systems," *Control Engineering Practice*, pp. 1483-1488, 1999.

[109] K. R. Pai and M. C. Shih, "Nanoaccuracy Position Control of a Pneumatic Cylinder Driven Table," *JSME International Journal*, Series C, vol. 46, No. 3, pp. 1062-1067, 2003.

[110] J. J. Mannitje, "Pneumatic servodesign methods improves system bandwidth twenty-fold," *Control Engineering*, pp. 79-83, 1981.

[111] E. Richer and Y. Hurmuzlu, "A high performance pneumatic force actuator system: Part I - Non linear mathematical model," *ASME Journal Dynamic System Measurement Control*, 122, pp. 416-425, 2000.

[112] E. Richer and Y. Hurmuzlu, "A high performance pneumatic force actuator system: Part II - Nonlinear controller design," *ASME Journal Dynamic System Measurement Control*, 122, pp. 426-434, 2000.

[113] G. Belforte, S. Mauro, G. Mattiazzo, "A method for increasing the dynamic performance of pneumatic servosystems with digital valves", *Mechatronics 14*, pp. 1105-1120, 2004.

[114] P. Zhang and J. Gao, "Reliability Analysis of a Novel Pulse Code Modulation Flow Control Valve with Self-compensating Ability," *Quality and Reliability Engineering International 23*, John Wiley & Sons, pp. 431-444, 2006.

[115] K. Kojima, Flowrate control circuit, Japanese Patent Number JP59167702, 1983.

[116] S. Kobayashi, M. Cotsaftis and T. Takamori, "Robust Control of Pneumatic Actuators Based on Dynamic Impedance Matching," *Proc. of IEEE Int. Conf. on Systems, Man & Cybernetics*, pp. 983-987, 1995.

[117] D. Hirooka, K. Suzumori, and T. Kanda, "Flow Control Valve for Pneumatic Actuators Using Particle Excitation by PZT Vibrator - 5th report; Applying to Cylinder control -," *The 27th Annual Conf. of the Robotics Society of Japan*, Sept. 2009 (in Japanese).

[118] S. Chen, J. Zhao, and J. Qian, "A Design Method of Bang-Bang and PID Integrated Controller Based on Rough Set," *4th Int. Conf. on Fuzzy Systems and Knowledge Discovery (FSKD 2007)*, 2007.